Electronic Supplementary Information (ESI) for "**Evaluation of Molecules Based on Electron Donor-Acceptor Architecture as Near-infrared (NIR) *β*-Amyloid-targeting Probes**"

Table of Contents

General Procedures. All chemicals and solvents were commercial products and were used without further purification unless otherwise indicated. Column chromatography was performed on silica gel (Yantai Industry Research Institute, 80-100 Å) packed into glass columns. Synthetic amyloid-β protein (1-42) was obtained from PEPTIDE INSTITUTE, Inc. (Japan), and aggregated for in vitro studies using the previously reported procedure.[1] ^{1}H and ^{13}C NMR spectra were recorded on a Bruker spectrometer in $CDCl_3$ solutions at room temperature at 400 and 100 MHz, respectively. The NMR spectra are reported in ppm downfield from tetramethylsilane (TMS) and the multiplicity is defined by s (singlet), d (doublet), t (triplet), or m (multiplet). Mass spectra were acquired using the Surveyor MSQ Plus (ESI) (Waltham, MA, USA) instrument. UV-visible spectra were recorded on the Shimadzu UV-3600 UV-Vis spectrophotometer (Japan). Fluorescence studies were carried out with a spectrofluorophotometer from Shimadzu (RF-5301PC, Japan). Fluorescence quantum yields were measured using aqueous solution of Rhodamine 6G as a standard (Φ = 0.76).[2] The purities of the resulting compounds were determined on the HPLC system SCL-20 AVP (Shimadzu, Japan) equipped with a SPD-20A UV detector (λ = 254 nm). The HPLC analysis was performed on a Venusil MP C18 column (Agela Technologies, 5μm, 4.6 mm×250 mm) eluted with a binary gradient system at a flow rate of 1.0 mL/min. The mobile phase A was water, while the mobile phase B was acetonitrile. Fluorescent observation was performed on the Axio Observer Z1 (Zeiss, Germany) equipped with DAPI, AF488 and AF546 filter sets. All protocols requiring the use of mice were approved by the animal care committee of Beijing Normal University.

Chemistry.

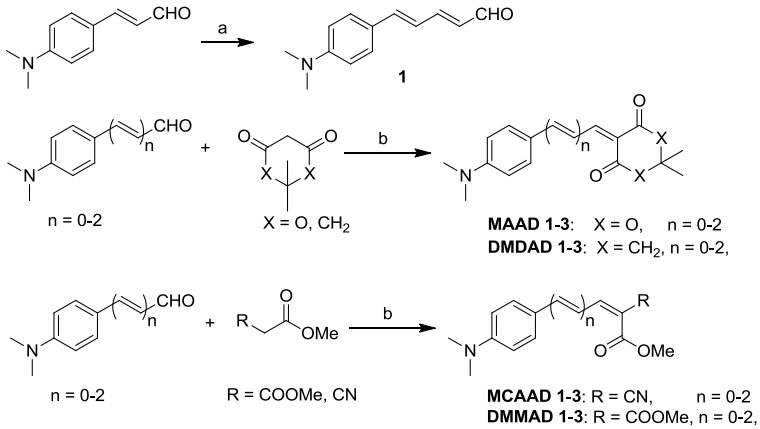

Regents and conditions: (a) (1) ((1,3-Dioxolan-2-yl)methyl)triphenylphosphonium bromide, anhydrous THF, NaH, 18-crown-6, r.t, 24 h; (2) 1 M HCl, H_2O, ammonia water, r.t. (b) For MAAD-1, 2, MCAAD-1, 2, 3 and DMMAD-1, 2, 3, methanol, piperidine, r.t.; for MAAD-3 and DMDAD-2, 3, methanol, r.t or 100 ℃; for DMDAD-1, no solvent, 150 ℃.

(2*E*,4*E*)-5-(4-(dimethylamino)phenyl)penta-2,4-dienal (**1**) To a stirred solution of (*E*)-3-(4-(dimethylamino)phenyl)acrylaldehyde (578 mg, 3.3 mmol) in anhydrous THF (20 mL) was added (1,3-dioxolan-2-ylmethyl)triphenylphosphonium bromide (1.36 g, 3.2 mmol). The reaction mixture was refluxed for 2 h at 70 ℃ and then quenched with an aqueous solution of HCl (1 M), followed by neutralization with ammonia water. The mixture was extracted with CH_2Cl_2 (3×25 mL), and the organic phase was dried over anhydrous magnesium sulfate. The solvent was removed in a vacuum and the residue was purified by flash column chromatography (petroleum ether/ethyl acetate = 4:1, v/v) to yield compound **1** as a yellow solid (139 mg, 46.0%). ^{1}H NMR (400 MHz, $CDCl_3$) δ: 9.56 (d, *J* = 8.1 Hz, 1H), 7.41 (d, *J* = 8.9 Hz, 2H), 7.32 - 7.21 (m, 1H), 6.95 (d, *J* = 15.3 Hz, 1H), 6.82 (dd, *J* = 15.3, 10.9 Hz, 1H), 6.68 (d, *J* = 8.8 Hz, 2H), 6.18 (dd, *J* = 15.0, 8.1 Hz, 1H), 3.03 (s, 6H).

5-(4-(Dimethylamino)benzylidene)-2,2-dimethyl-1,3-dioxane-4,6-dione (**MAAD-1**) 4-(Dimethylamino)benzaldehyde (448.4 mg, 3.0 mmol) and meldrum's acid (432.2 mg, 3.0 mmol) were dissolved separately in 10 mL methanol. Piperidine (50 μL) was added as a catalyst after the two solutions in methanol were mixed together. The reaction mixture was stirred at room temperature for 2 h. The precipitation was collected by filtration. The final products were obtained as a yellow solid after washing with MeOH and petroleum ether (591 mg, 71.6%). M.p.: 165.2-166.3 ℃.

^{1}H NMR (400 MHz, CDCl3) δ: 8.31 (s, 1H), 8.25 (d, *J* = 9.2 Hz, 2H), 6.69 (d, *J* = 9.2 Hz, 2H), 3.16 (s, 6H), 1.76 (s, 6H), 1.39 (s, 9H). MS: m/z calcd for $[C_{15}H_{17}NO_4 + H]^+$ 276.1, found 275.9.

(*E*)-5-(3-(4-(dimethylamino)phenyl)allylidene)-2,2-dimethyl-1,3-dioxane-4,6-dione (**MAAD-2**) The same reaction as described above to prepare MAAD-1 was used, and MAAD-2 was obtained as a purple solid (325 mg, 36.0%). M.p.: 185.5-185.7 ℃. ^{1}H NMR (400 MHz, $CDCl_3$) δ: 8.09 - 8.18 (m, 2H), 7.59 (d, *J* = 8.9 Hz, 2H), 7.37 (dd, *J* = 11.6 Hz, 2.4 Hz, 1H), 6.68 (d, *J* = 8.9 Hz, 2H), 3.11(s, 6H), 1.74 (s, 6H). ^{13}C NMR (100 MHz, $CDCl_3$) δ: 163.9, 161.6, 159.1, 156.9, 153.1, 132.2, 123.2, 120.2, 112.0, 106.0, 104.1, 40.1, 27.5. MS: m/z calcd for $[C_{17}H_{19}NO_4 + H]^+$ 302.1, found 302.0.

5-((2*E*,4*E*)-5-(4-(dimethylamino)phenyl)penta-2,4-dien-1-ylidene)-2,2-dimethyl-1,3-dioxane-4,6-dione (**MAAD-3**) To a solution of (2*E*,4*E*)-5-(4-(dimethylamino)phenyl)penta-2,4-dienal (compound **1**, 45 mg, 0.22 mmol) in methanol was added a solution of meldrum's acid (40 mg, 0.27 mmol) in methanol. The reaction mixture was stirred at room temperature for 1 h. The precipitation was collected by filtration and the product was obtained by flashing column chromatography (petroleum ether/ethyl acetate = 10:1, v/v) as a black solid (40 mg, 55.5%). M.p.: 201.7-202.2 ℃. ^{1}H NMR (400 MHz, $CDCl_3$) δ: 8.08 (d, *J* = 12.5 Hz, 1H), 7.72 - 7.79 (m, 1H), 7.48 (d, *J* = 8.9 Hz, 1H), 7.43 (d, *J* = 8.9 Hz, 2H), 6.96 - 7.05 (m, 2H), 6.69 (d, *J* = 8.9 Hz, 2H), 3.07(s, 6H), 1.74 (s, 6H). ^{13}C NMR (100 MHz, $CDCl_3$) δ: 163.7, 161.4, 158.0, 157.2, 152.0, 146.5, 131.7, 130.9, 130.1, 128.9, 126.3, 123.9, 123.5, 112.1, 107.2, 104.2, 40.1, 27.6. HRMS: m/z calcd for $[C_{19}H_{21}NO_4 + H]^+$ 328.1543, found 328.1549.

2-(4-(Dimethylamino)benzylidene)-5,5-dimethylcyclohexane-1,3-dione (**DMDAD-1**) A mixture of 4-(dimethylamino)benzaldehyde (279 mg, 1.9 mmol) and 5,5-dimethylcyclohexane-1,3-dione (284 mg, 2.0 mmol) was kept at 150 ℃ for 10 min. Subsequently, DMDAD-1 was obtained as a yellow solid by recrystallization from petroleum ether and ethyl acetate (39 mg, 7.7%). M.p.: 143.9-145.4 ℃. ^{1}H NMR (400 MHz, $CDCl_3$) δ: 8.28 (d, *J* = 9.2 Hz, 2H), 8.03 (s, 1H), 6.66 (d, *J* = 9.2 Hz, 2H), 3.12(s, 6H), 2.57 (s, 2H), 2.55 (s, 2H), 1.09 (s, 6H). ^{13}C NMR (100 MHz, $CDCl_3$) δ: 198.6, 197.4, 154.0, 153.4, 138.5, 126.3, 121.5, 111.0, 54.5, 52.5, 40.0, 29.9, 28.6. MS: m/z calcd for $[C_{17}H_{21}NO_2 + H]^+$ 272.2, found 272.1.

(*E*)-2-(3-(4-(dimethylamino)phenyl)allylidene)-5,5-dimethylcyclohexane-1,3-dione (**DMDAD-2**) (*E*)-3-(4-(dimethylamino)phenyl)acrylaldehyde (175.0 mg, 1.0 mmol) and 5,5-dimethylcyclohexane-1,3-dione (140.0 mg, 1.0 mmol) were dissolved in 5 mL methanol, and the reaction mixture was stirred at 100 ℃ for 15 min. The precipitation was collected by filtration and the final product was obtained by flash column chromatography (petroleum ether/ethyl acetate = 4:1 and 2: 1, v/v) as a purple solid (53.5 mg, 18.0%). M.p.: 175.3-176.9 ℃. ^{1}H NMR (400 MHz, $CDCl_3$) δ: 8.31 (dd, *J* = 14.9 Hz, 12.4 Hz), 7.87 (d, *J* = 12.4 Hz, 1H), 7.56 (d, *J* = 8.8 Hz, 2H), 7.36 (d, *J* = 15.0 Hz, 1H), 6.67 (d, *J* = 8.8 Hz, 2H), 3.08(s, 6H), 2.52 (s, 2H), 2.50 (s, 2H), 1.08 (s, 6H). ^{13}C NMR (100 MHz, $CDCl_3$) δ: 198.9, 198.0, 156.6, 153.5, 152.6, 131.6, 125.4, 123.9, 121.2, 111.8, 54.0, 52.3, 40.1, 30.2, 28.6. MS: m/z calcd for $[C_{19}H_{23}NO_2 + H]^+$ 298.2, found 298.1.

2-((2*E*,4*E*)-5-(4-(dimethylamino)phenyl)penta-2,4-dien-1-ylidene)-5,5-dimethylcyclohexane-1,3-dione (**DMDAD-3**) To a solution of (2*E*,4*E*)-5-(4-(dimethylamino)phenyl)penta-2,4-dienal (compound **1**, 24.8 mg, 0.12 mmol) in 2 mL methanol was added dropwise a solution of 5,5-dimethylcyclohexane-1,3-dione (30.6 mg, 0.22 mmol) in 1 mL methanol. The reaction mixture was stirred for 5 h at room temperature. The solvent was removed in a vacuum, and the residue was purified by flash column chromatography (petroleum ether/ethyl acetate = 4:1, v/v) to yield DMDAD-3 as a black solid (12 mg, 30.8%). M.p.: 162.2-164.3 ℃. ^{1}H NMR (400 MHz, $CDCl_3$) δ: 7.87 (dd, *J* = 13.3 Hz, 12.8 Hz), 7.76 (d, *J* = 12.6 Hz, 1H), 7.41 (d, *J* = 8.8 Hz, 2H), 7.22 (dd, *J* = 14.0 Hz, 5.2 Hz), 6.94 (d, *J* = 5.3 Hz, 2H), 6.67 (d, *J* = 8.8 Hz, 2H), 3.05(s, 6H), 2.51 (s, 2H), 2.50 (s, 2H), 1.07 (s, 6H). ^{13}C NMR (100 MHz, $CDCl_3$) δ: 198.8, 198.0, 156.6, 151.9, 151.5, 144.2, 129.6, 127.6, 126.2, 124.2, 112.0, 54.0, 52.3, 40.1, 30.2, 28.6. HRMS: m/z calcd for $[C_{21}H_{25}NO_2 + H]^+$ 324.1958, found 324.1964.

(*E*)-methyl 2-cyano-3-(4-(dimethylamino)phenyl)acrylate (**MCAAD-1**) To a solution of 4-(dimethylamino)benzaldehyde (275.6 mg, 1.8 mmol) in 3 mL methanol was added 2-methoxyacetyl cyanide (210.7 mg, 2.1 mmol), and then piperidine (20 μL) was added as a catalyst. The reaction mixture was stirred for 10 min at room temperature. The final product was obtained after filtration and recrystallization from methanol as a yellow solid (314 mg, 75.8%). M.p.:

138.8-139.1 ℃. ^{1}H NMR (400 MHz, $CDCl_3$) δ: 8.09 (s, 1H), 7.94 (d, *J* = 8.9 Hz, 2H), 6.71 (d, *J* = 9.0 Hz, 2H), 3.88 (s, 3H), 3.12 (s, 6H). MS: m/z calcd for $[C_{13}H_{14}N_2O_2 + H]^+$ 231.1, found 231.1.

(2*E*,4*E*)-methyl 2-cyano-5-(4-(dimethylamino)phenyl)penta-2,4-dienoate (**MCAAD-2**) The same method as described above for the preparation of MCAAD-1 was used, and MCAAD-2 was obtained as a red solid (489 mg, 83.0%). M.p.: 161.6-163.2 ℃. ^{1}H NMR (400 MHz, $CDCl_3$) δ: 7.98 (d, *J* = 11.6 Hz, 1H), 7.49 (d, *J* = 7.4 Hz, 2H), 7.21 (d, *J* = 15.1 Hz, 1H), 7.09 (d, *J* = 13.7 Hz, 1H), 6.69 (d, *J* = 7.4 Hz, 2H), 3.87 (s, 3H), 3.08 (s, 6H). ^{13}C NMR (100 MHz, $CDCl_3$) δ: 163.9, 156.8, 152.5, 150.5, 130.9, 122.7, 118.2, 115.7, 111.9, 98.8, 52.7, 40.1. MS: m/z calcd for $[C_{15}H_{16}N_2O_2 + H]^+$ 257.1, found 257.0.

(2*E*,4*E*,6*E*)-methyl 2-cyano-7-(4-(dimethylamino)phenyl)hepta-2,4,6-trienoate (**MCAAD-3**) The same method as described above for the preparation of MCAAD-1 was used, and the end-product was obtained by flash column chromatography (petroleum ether/CH_2Cl_2 = 1:2, v/v) as a black solid (40 mg, 67.5%). M.p.: 166.8-168.3 ℃. ^{1}H NMR (400 MHz, $CDCl_3$) δ: 7.91 (d, *J* = 12.1 Hz, 1H), 7.41 (d, *J* = 8.8 Hz, 2H), 7.08 (dd, *J* = 14.2 Hz, 10.5 Hz, 1H), 6.71- 6.93 (m, 5H), 3.86 (s, 3H), 3.05 (s, 6H). ^{13}C NMR (100 MHz, $CDCl_3$) δ: 163.6, 155.8, 151.0, 143.9, 131.2, 129.5, 124.2, 122.8, 115.3, 112.1, 100.1, 52.8, 40.2. HRMS: m/z calcd for $[C_{17}H_{18}N_2O_2 + H]^+$ 283.1441, found 283.1447.

Dimethyl 2-(4-(dimethylamino)benzylidene)malonate (**DMMAD-1**) The same method as described above for the preparation of MCAAD-1 was used, and the reaction mixture was stirred at room temperature for 12 h. After the solvent was removed, the product was obtained by flash column chromatography (CH_2Cl_2/ethyl acetate = 40:1, v/v) as a yellow solid (479 mg, 49.7%). M.p.: 85.4-85.7 ℃. ^{1}H NMR (400 MHz, $CDCl_3$) δ: 7.67 (s, 1H), 7.32 (d, *J* = 7.7 Hz, 2H), 6.63 (d, *J* = 7.7 Hz, 2H), 3.88 (s, 3H), 3.81 (s, 3H), 3.02 (s, 6H). MS: m/z calcd for $[C_{14}H_{17}NO_4 + H]^+$ 264.1, found 264.0.

(*E*)-dimethyl 2-(3-(4-(dimethylamino)phenyl)allylidene)malonate (**DMMAD-2**) The same method as described above to prepare DMMAD-1 was used, and the end-product was obtained as a red solid (130 mg, 22.5%). M.p.: 122.0-122.7 ℃. ^{1}H NMR (400 MHz, $CDCl_3$) δ: 7.61 (d, *J* = 11.4 Hz, 1H), 7.42 (d, *J* = 7.1 Hz, 2H), 7.16 (dd, *J* = 13.4 Hz, 13.4 Hz, 1H), 7.01 (d, *J* = 15.0 Hz, 1H), 6.67 (d, *J* = 6.8 Hz, 2H), 3.89 (s, 3H), 3.81 (s, 3H), 3.03 (s, 6H). ^{13}C NMR (100 MHz, $CDCl_3$) δ:

167.2, 166.7, 149.4, 147.7, 132.3, 130.7, 120.9, 119.7, 114.1, 112.8, 53.0, 53.0, 41.1. MS: m/z calcd for $[C_{16}H_{19}NO_4 + H]^+$ 290.1, found 290.8.

Dimethyl 2-((2*E*,4*E*)-5-(4-(dimethylamino)phenyl)penta-2,4-dien-1-ylidene)malonate (**DMMAD-3**) The same method as described above for the preparation of DMMAD-1 was used, and the reaction mixture was stirred at room temperature for 1 h. After the solvent was removed, the product was obtained by flash column chromatography (CH_2Cl_2/ethyl acetate = 60:1, v/v) as a red solid (13 mg, 22.4%). M.p.: 133.9-134.8 ℃. ^{1}H NMR (400 MHz, $CDCl_3$) δ: 7.51 (d, *J* = 11.9 Hz, 1H), 7.35 (d, *J* = 8.8 Hz, 2H), 6.92 - 6.84 (m, 1H), 6.79 - 6.70 (m, 3H), 6.67 (d, *J* = 8.8 Hz, 2H), 3.87 (s, 3H), 3.80 (s, 3H), 3.01 (s, 7H). ^{13}C NMR (100 MHz, $CDCl_3$) δ: 166.1, 165.6, 151.0, 147.2, 147.1, 140.3, 130.8, 128.8, 128.7, 124.8, 52.2, 52.1, 40.3, 40.2. HRMS: m/z calcd for $[C_{18}H_{21}NO_4 + H]^+$ 316.1543, found 316.1549.

The Purity Determination. The purity of the compounds was determined on a HPLC system eluted with acetonitrile/water = 80%: 20% at a flow rate of 1.0 mL/min. As shown in Fig. S1, the retention time increased with the lengthening of the conjugated double bonds, indicating an increasing lipophilicity, which was the primary factor affecting penetration of the blood brain barrier (BBB) along with the molecular weight.

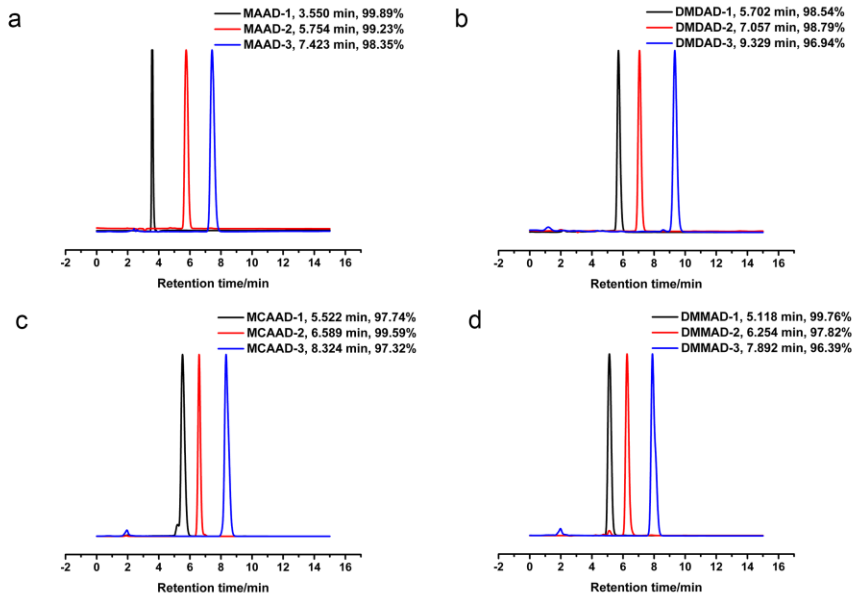

Fig. **S1** HPLC performance of the probes. The peaks were annotated by retention time and purity of the compounds. (a), (b), (c), and (d) showed the data for the MAAD, DMDAD, MCAAD, and DMMAD series, respectively.

Spectroscopic Measurements. The absorption (Figs. S2-S5) and fluorescence (Figs. S6-S9) spectra were determined using UV-Vis (UV-3600, Shimadzu, Japan) and fluorescence spectrophotometers (RF-5301PC, Shimadzu, Japan), respectively. The molar absorption coefficient and quantum yield were measured in dichloromethane, a solvent that mimics the hydrophobic microenvironment of the Aβ fibril "binding pocket".[3] Furthermore, the quantum yields in PBS were also measured.

The spectroscopic data are presented in Table S1. Single absorption/emission maximums and a high quantum yield are prerequisites for high-sensitivity in vivo imaging.[4] For each probe, a single absorption maximum and a single emission maximum were observed. The NIRFs (MAAD-3, DMDAD-3, MCAAD-3 and DMMAD-3) displayed moderate quantum yields (ranging from 0.10% to 4.71%) in dichloromethane. The quantum yield of MAAD-3 in dichloromethane (4.71%) equaled that of NIAD-4 upon binding to the Aβ_{1-40} aggregates (5%)[5]. Conversely, the NIRFs displayed lower quantum yields in PBS, a polar environment, which can lower the energy of the excited states of the ligands and result in lower quantum yields.

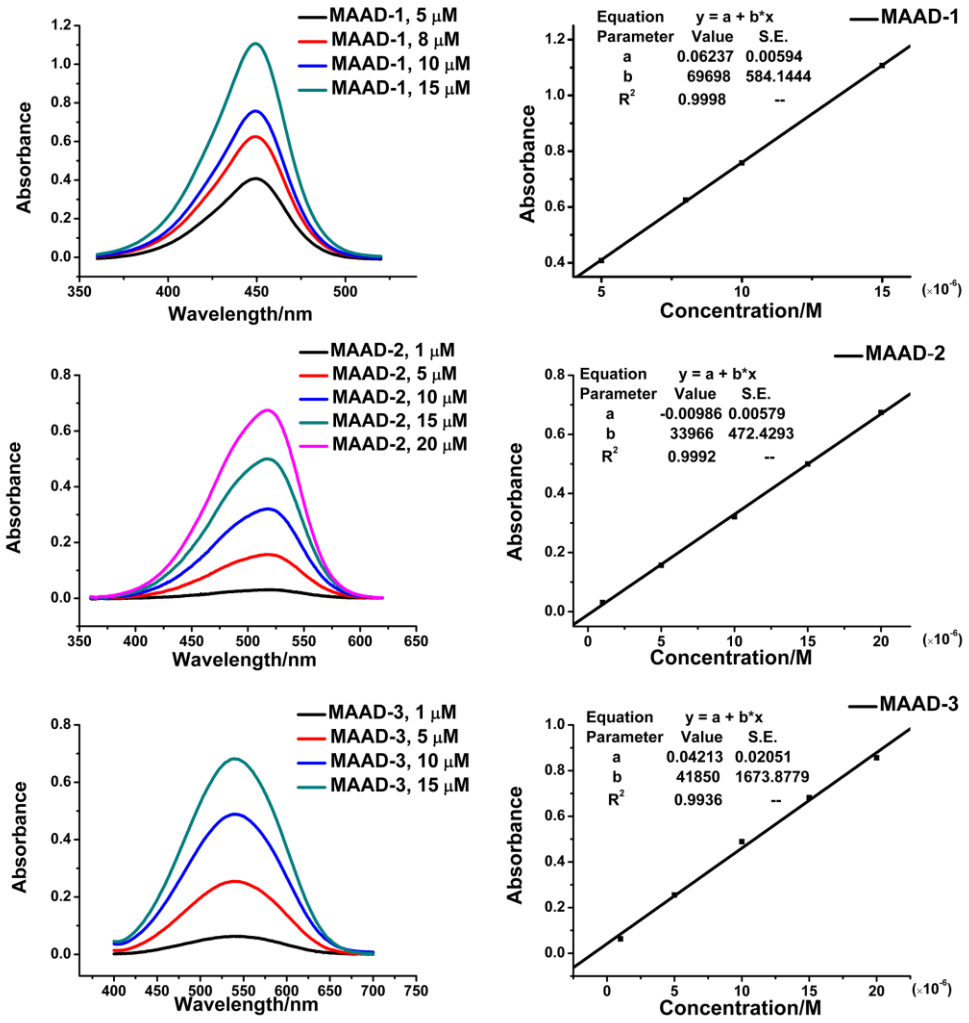

Fig. **S2** Absorption spectra (left panel) and molar absorption coefficients (ε, right panel) of the MAAD probes. The spectra were obtained using dichloromethane as the solvent.

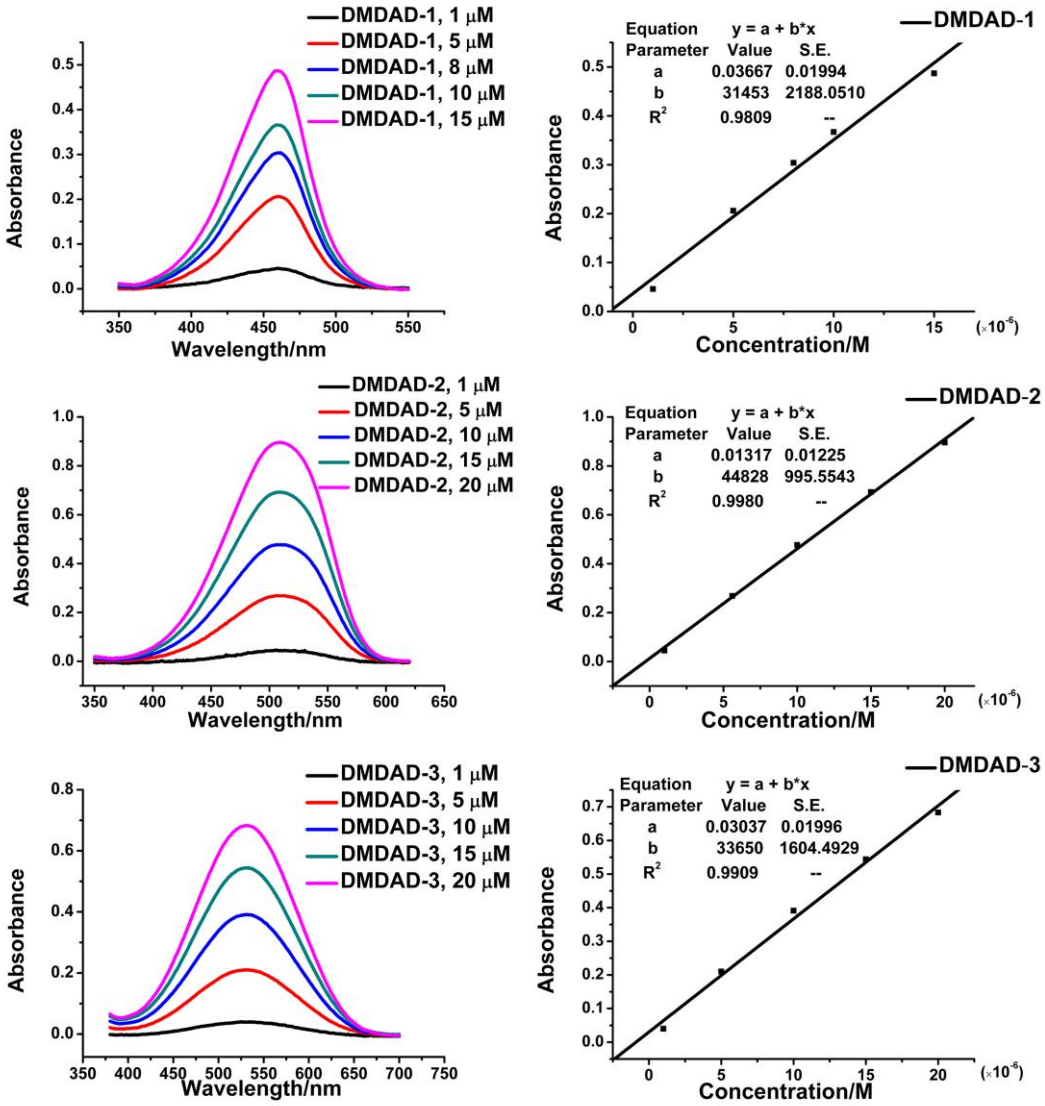

Fig. **S3** Absorption spectra (left panel) and molar absorption coefficients (ε, right panel) of the DMDAD probes. The spectra were obtained using dichloromethane as the solvent.

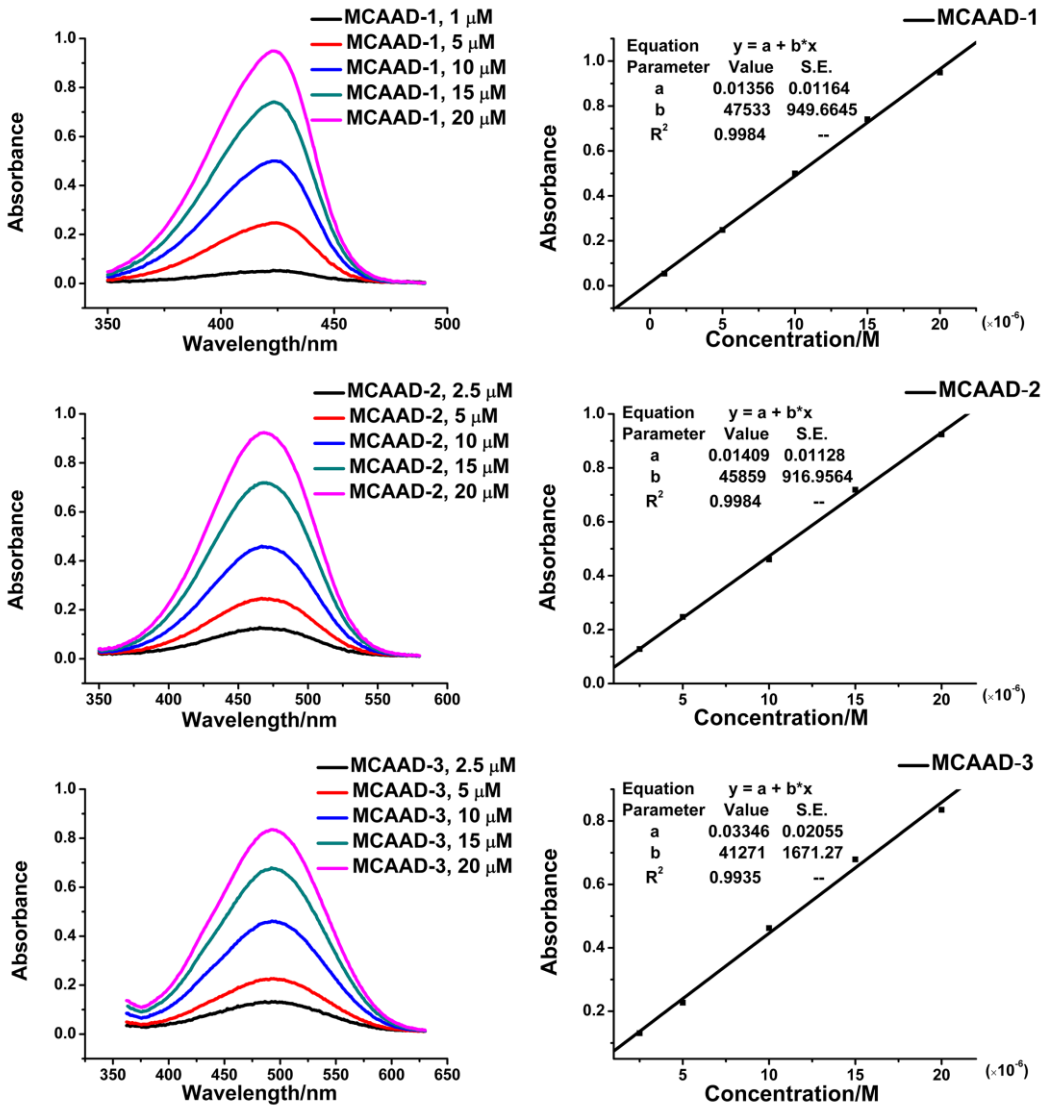

Fig. **S4** Absorption spectra (left panel) and molar absorption coefficients (ε, right panel) of the MCAAD probes. The spectra were obtained using dichloromethane as the solvent.

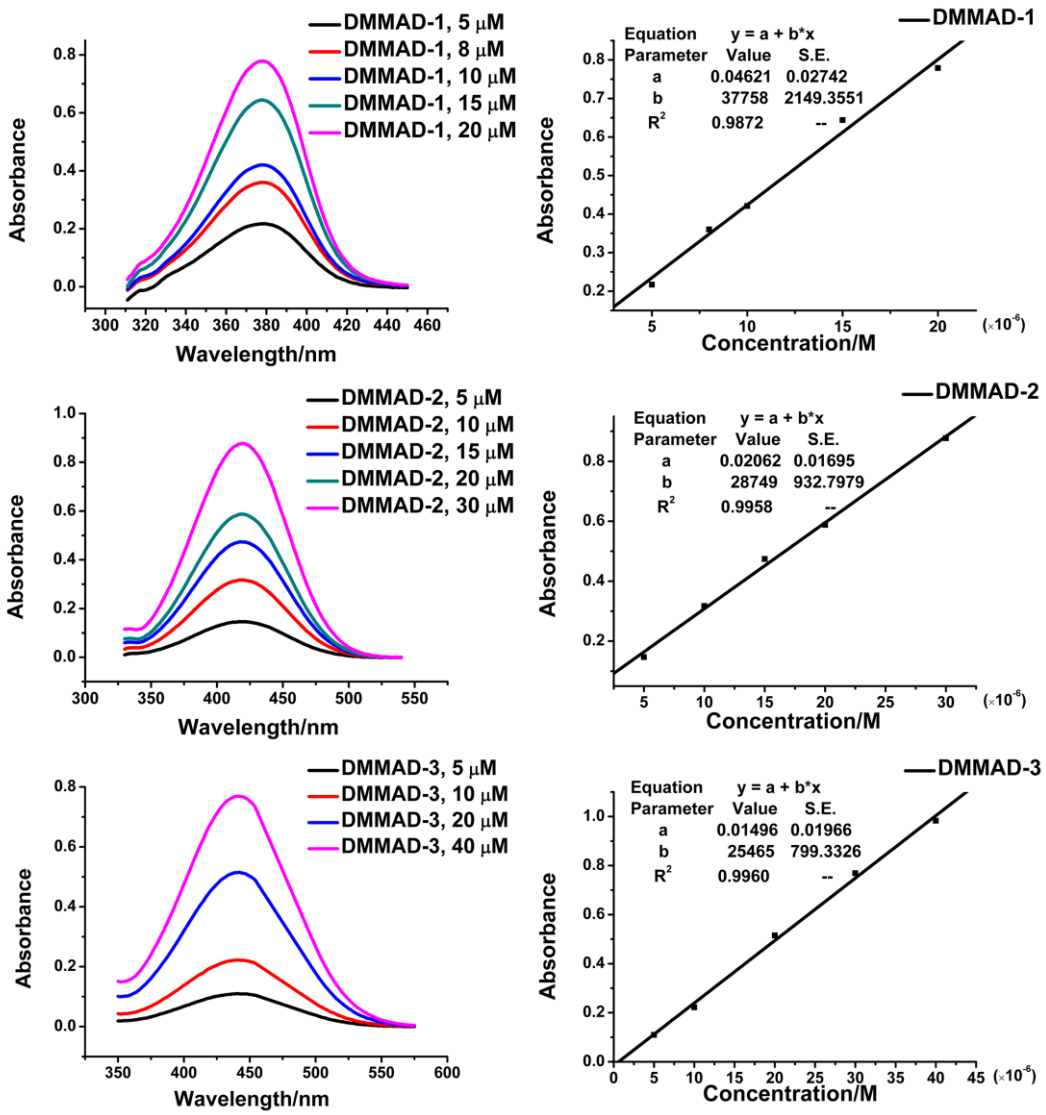

Fig. **S5** Absorption spectra (left panel) and molar absorption coefficients (ε, right panel) of the DMMAD probes. The spectra were obtained using dichloromethane as the solvent.

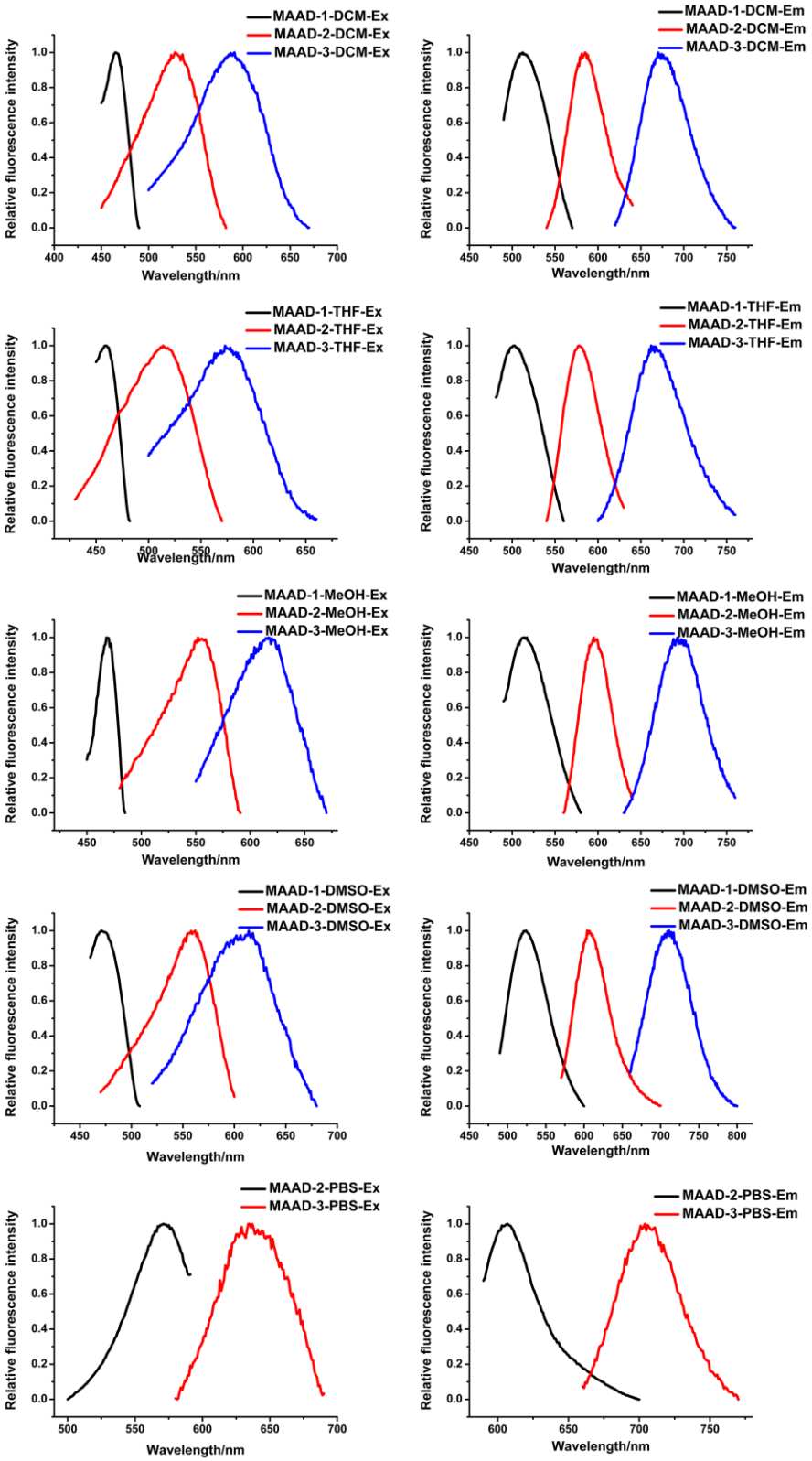

Fig. **S6** The excitation (left panel) and emission (right panel) spectra of the MAAD probes in different solvents: dichloromethane, THF, methanol, DMSO, and phosphate-buffered saline (PBS, 10% ethanol). The emission wavelengths of the solutions were measured at a concentration of 10 μM.

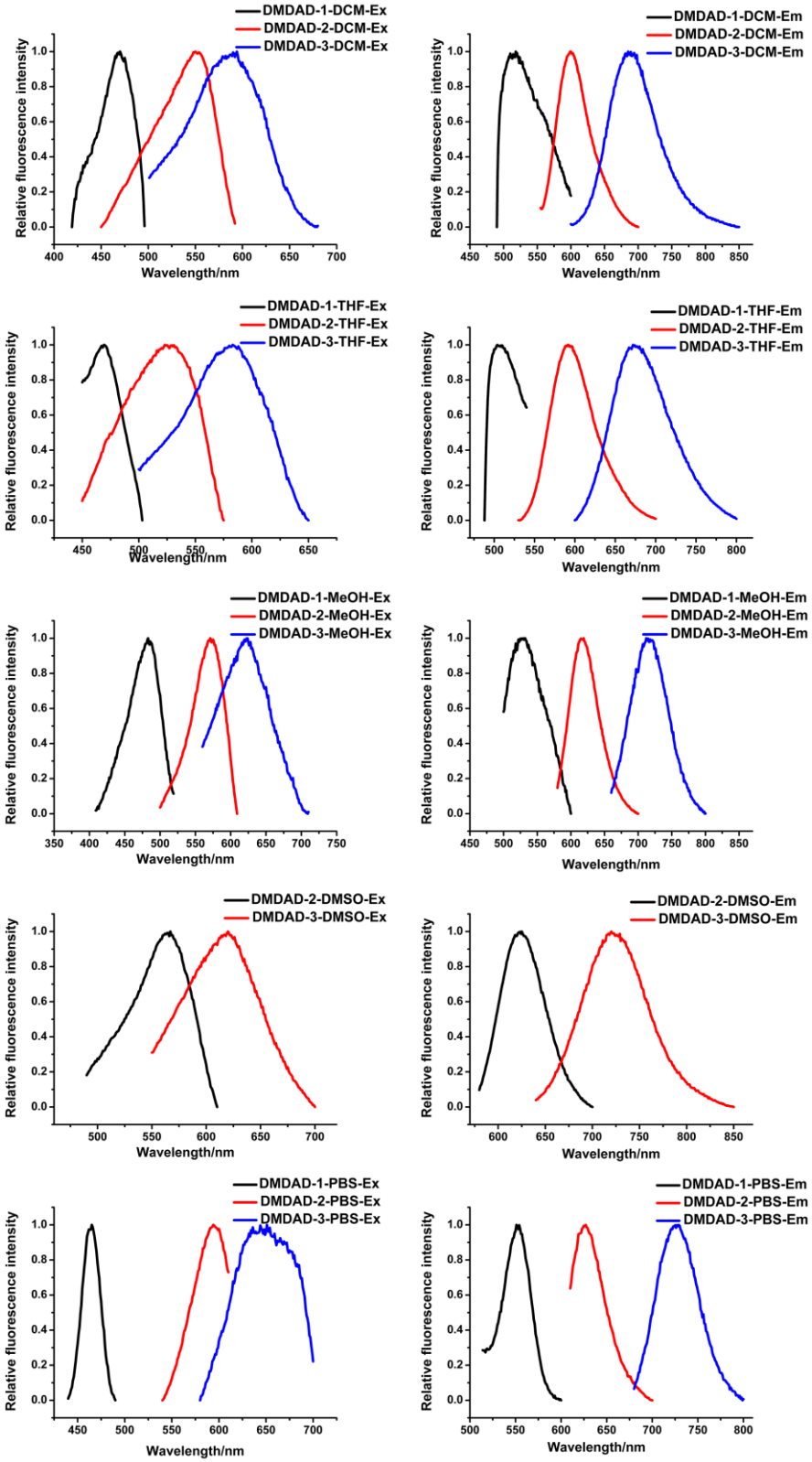

Fig. **S7** The excitation (left panel) and emission (right panel) spectra of the DMDAD probes in different solvents: dichloromethane, THF, methanol, DMSO, and phosphate-buffered saline (PBS, 10% ethanol). The emission wavelengths of the solutions were measured at a concentration of 10 μM.

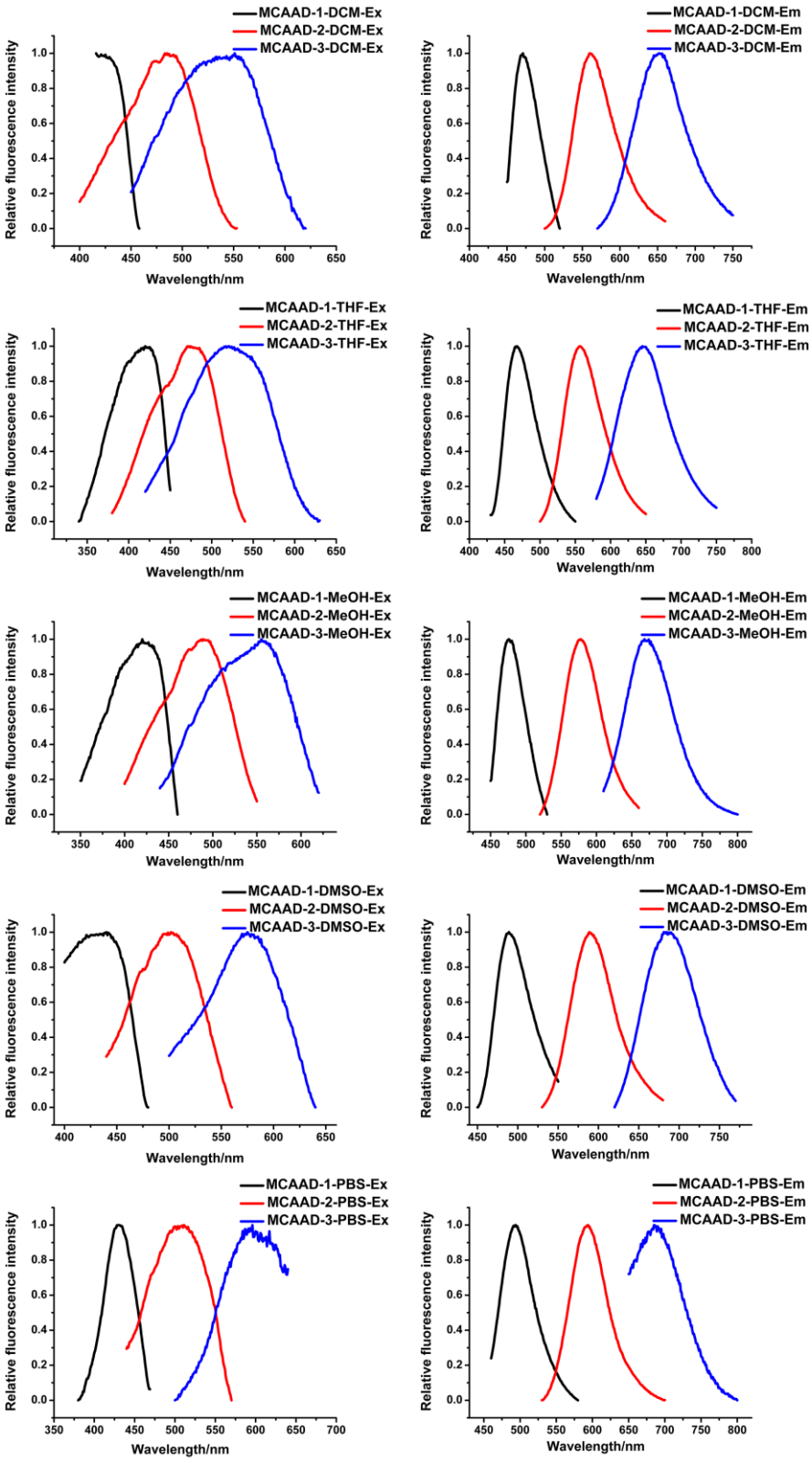

Fig. **S8** The excitation (left panel) and emission (right panel) spectra of the MCAAD probes in different solvents: dichloromethane, THF, methanol, DMSO, and phosphate-buffered saline (PBS, 10% ethanol). The emission wavelengths of the solutions were measured at a concentration of 10 μM.

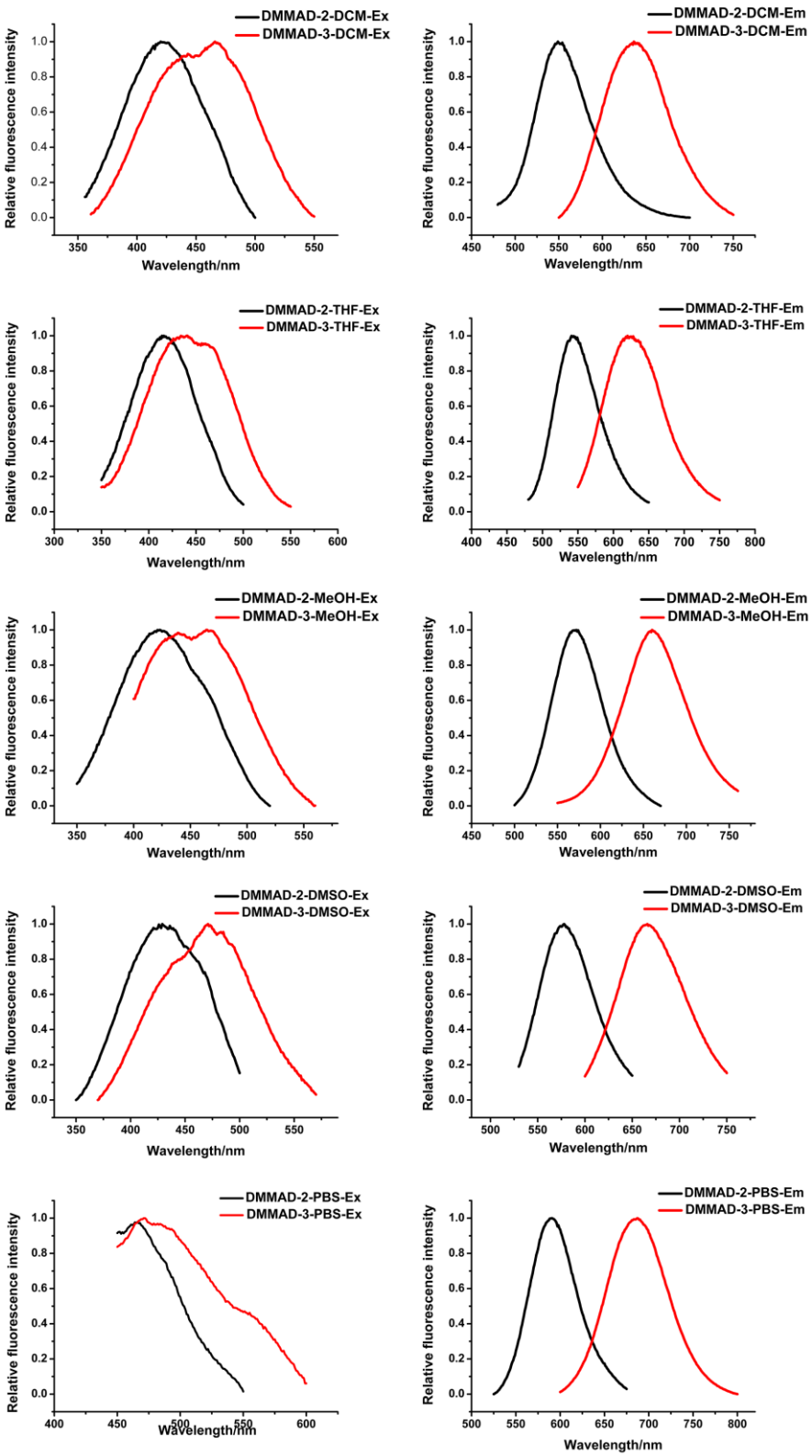

Fig. **S9** The excitation (left panel) and emission (right panel) spectra of the DMMAD probes in different solvents: dichloromethane, THF, methanol, DMSO, and phosphate-buffered saline (PBS). The emission wavelengths of the solutions were measured at a concentration of 10 μM.

Fluorescence Spectral Measurements of NIRFs with A$\beta_{1\text{-}42}$ and BSA. A solution of A$\beta_{1\text{-}42}$ aggregate (10 μg/mL, 0.74 μM in the final test solution) or bovine serum albumin (BSA, 10 μg/mL in the final test solution) in double distilled water was added to a solution of our NIRFs in 2.9 mL PBS (50 nM). The mixture was incubated at 37 ℃ with slight and constant shaking (100 r/min) for 1.5 h. The solutions were then transferred to a quartz sampling cell, and the fluorescent properties (fluorescence excitation/emission wavelength and intensity) were measured by a fluorescence spectrophotometer (RF-396 5301PC, Shimadzu, Japan). The fluorescent properties of the solutions of the NIRFs in PBS (50 nM) were also measured in the same manner as a blank control. The fold increase of the fluorescence intensity after binding to the A$\beta_{1\text{-}42}$ aggregate was calculated by the following equation:

$$\text{Fold increase} = FI_{\text{test}}/(FI_{\text{probe}} - FI_{\text{PBS}})$$

In this equation, FI_{test}, FI_{probe}, and FI_{PBS} represent the fluorescence intensities of the NIRFs upon binding to A$\beta_{1\text{-}42}$ aggregate, the solution of NIRFs in PBS, and PBS alone, respectively.

As shown in Fig. S10, striking increases in the fluorescence intensity and emission blue shifts were observed after our NIRFs bound to the A$\beta_{1\text{-}42}$ aggregate and the fold increase matched the K_{i} values well (Table 1 in the main text). No significant change in fluorescence was detected after incubation with BSA, suggesting that there is little or no interaction between our NIRFs and BSA.

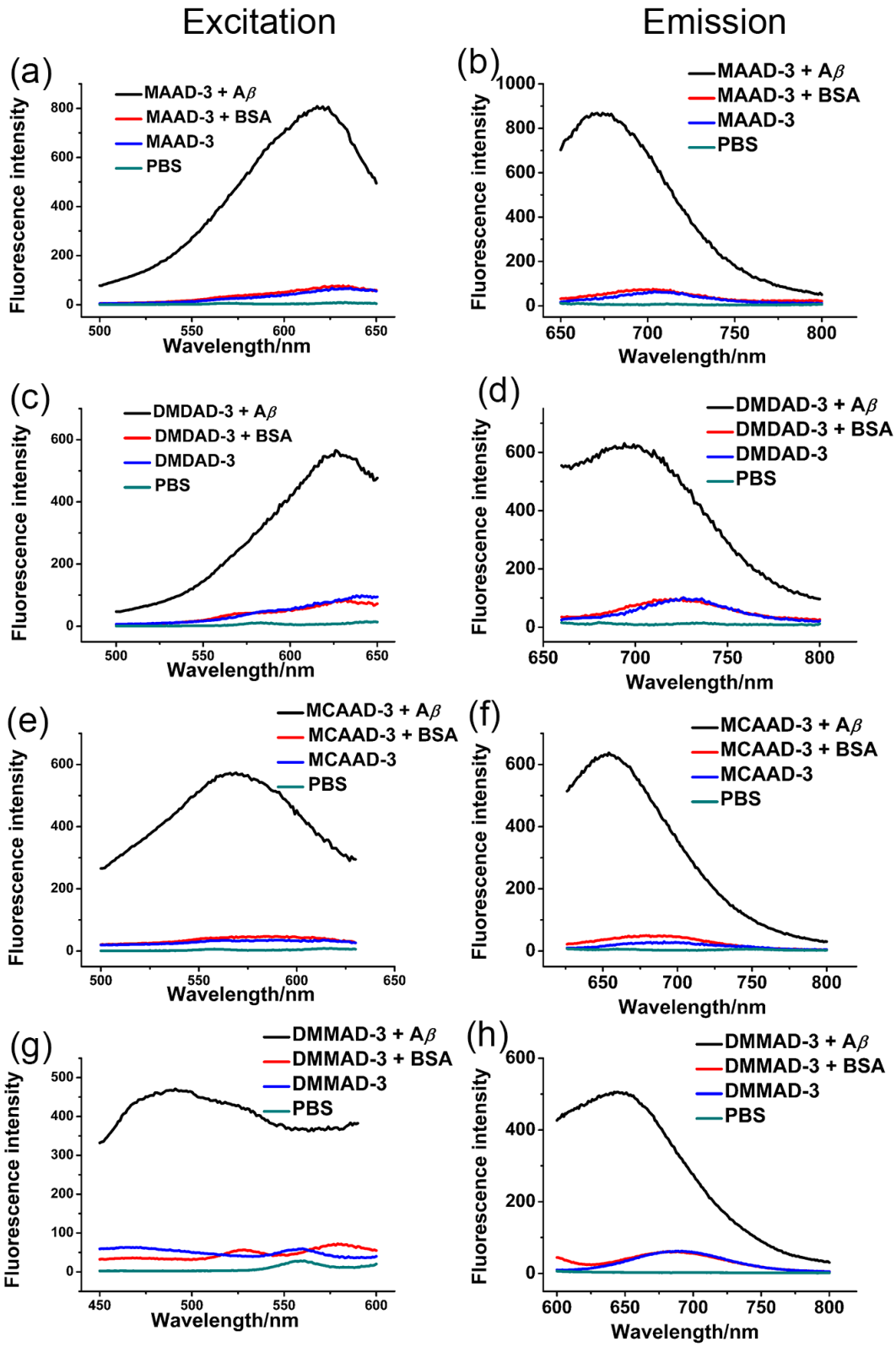

Fig. **S10** The excitation (left panel) and emission (right panel) spectra of the NIRFs upon interaction with Aβ_{1-42} aggregates (black line) or BSA (red line). The spectra of the NIRF solutions in PBS (blue line) and PBS alone (green line) were also measured under the same conditions.

Table S1 The spectroscopic properties (absorption, excitation and emission wavelength, molar absorption coefficients, and fluorescence quantum yields) of the synthesized probes.

Probe	Fluorescence spectrum					UV-vis spectrum	
	Solvent	λ_{ex} nm	λ_{em} nm	Stokes shift nm	Φ^a %	λ_{abs} nm	ε L $mol^{-1}cm^{-1}$
MAAD-1	CH_2Cl_2	465	512	47	n.d.	450	69698
	THF	459	503	44			
	MeOH	468	517	49			
	DMSO	471	524	53			
	PBS		n.d				
MAAD-2	CH_2Cl_2	528	585	57	n.d.	518	33966
	THF	514	580	66			
	MeOH	552	595	43			
	DMSO	562	604	42			
	PBS	571	607	36			
MAAD-3	CH_2Cl_2	591	670	79	4.71/0.048	539	41850
	THF	573	662	89			
	MeOH	617	693	76			
	DMSO	614	711	97			
	PBS	635	704	69			
	with Aβ	618	674	56			
DMDAD-1	CH_2Cl_2	468	518	50	n.d.	460	31453
	THF	469	504	35			
	MeOH	483	531	48			
	DMSO		n.d				
	PBS	465	551	86			
DMDAD-2	CH_2Cl_2	550	599	49	n.d.	508	44828
	THF	523	592	69			
	MeOH	571	619	48			
	DMSO	567	625	58			
	PBS	594	627	33			
DMDAD-3	CH_2Cl_2	594	685	91	2.68/0.033	532	33650
	THF	583	672	89			
	MeOH	623	712	89			
	DMSO	620	720	100			
	PBS	651	725	74			
	with Aβ	626	694	68			
MCAAD-1	CH_2Cl_2	420	471	51	n.d.	423	47533
	THF	420	467	47			
	MeOH	420	476	56			
	DMSO	440	489	49			

	PBS	429	494	65			
MCAAD-2	CH_2Cl_2	485	560	75	n.d.	468	45859
	THF	472	556	84			
	MeOH	489	578	89			
	DMSO	502	589	87			
	PBS	511	594	83			
MCAAD-3	CH_2Cl_2	551	652	101	1.23/0.25	493	41271
	THF	521	645	124			
	MeOH	555	668	113			
	DMSO	575	685	110			
	PBS	596	685	89			
	with Aβ	569	654	85			
DMMAD-1			n.d		n.d.	378	37758
DMMAD-2	CH_2Cl_2	420	549	129	n.d.	419	28749
	THF	414	541	127			
	MeOH	423	572	149			
	DMSO	429	578	149			
	PBS	431	589	158			
DMMAD-3	CH_2Cl_2	455	636	181	0.10/0.068	442	25465
	THF	440	620	180			
	MeOH	450	660	210			
	DMSO	471	666	195			
	PBS	471	687	216			
	with Aβ	493	642	149			

[a] The fluorescence quantum yields were measured in dichloromethane/PBS using rhodamine 6G as a reference.

In Vitro Fluorescent Staining of Aβ Plaques in Transgenic Mouse Brain Sections. Paraffin-embedded brain sections from Tg mice (C57BL6, APPswe/PSEN1, 11 months old, male, 6 μm) were used for the neuropathological staining. After a 15-min immersion (deparaffinization) in xylene, the brain slices were washed with ethanol and then dd water for 5 min each. The brain sections were incubated with solutions of our probes in dd water (1.0 μM, 2.5% DMSO, 10% ethanol) for 10 min. The localization of plaques was confirmed by staining the adjacent sections with thioflavin-S (0.125% in dd water, a common dye for staining Aβ plaques). Finally, the sections were washed with ethanol/water (v: v, 40%: 60%) for 10 min. Fluorescent observation was performed using an Axio Oberver Z1 (Zeiss, Germany) equipped with DAPI, AF488, AF546, and Cy5 filter sets.

Additionally, slices from age-matched normal mice (C57BL6, 11 months, female) were treated following the same procedures as blank controls.

As shown in Figs. 2 (main text) and S11, our probes with longer polyenic chains and higher binding affinities can clearly stain Aβ plaques in brain sections, whereas the probes with the shortest polyenic chains and poor binding affinities barely showed slight fluorescent spots (MAAD-1 and DMDAD-1, Fig. S11 a and e) or no specific signals in the brain sections (MCAAD-1 and DMMAD-1, Fig. S11 i and m). This observation confirmed that the length of the conjugated system was vital for altering the binding affinity of the probes to the Aβ plaques.

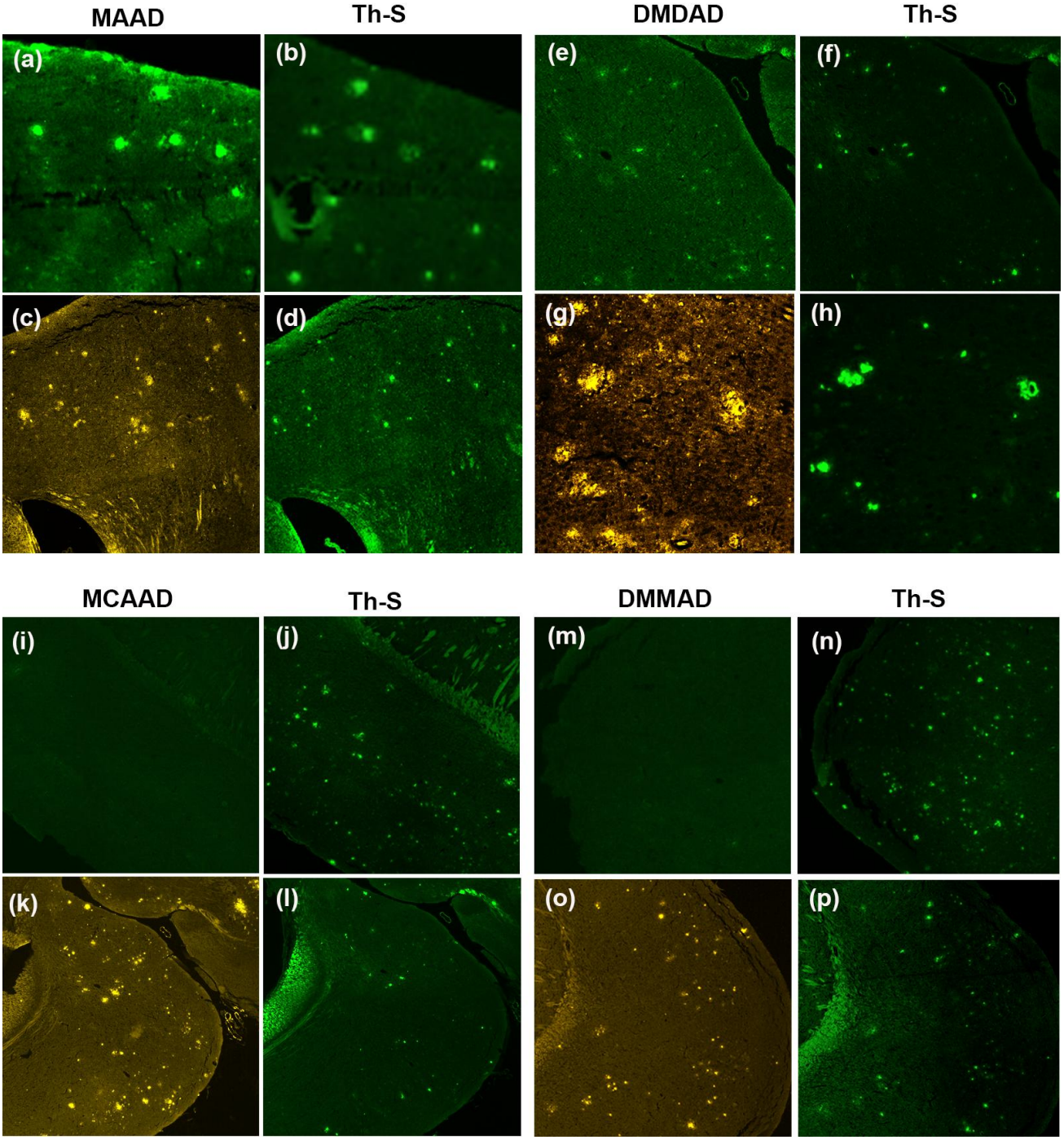

Fig. **S11** In vitro fluorescent staining of Aβ plaques in brain sections of Tg mice by our probes. (a), (c), (e), (g), (i), (k), (m) and (o) were stained by MAAD-1, -2, DMDAD-1, -2, MCAAD-1, -2, and DMM-1, -2, respectively. The presence and distribution of the plaques in the sections were confirmed by fluorescence staining using Thioflavin-S on the adjacent sections (b, d, f, h, j, l, n, and p).

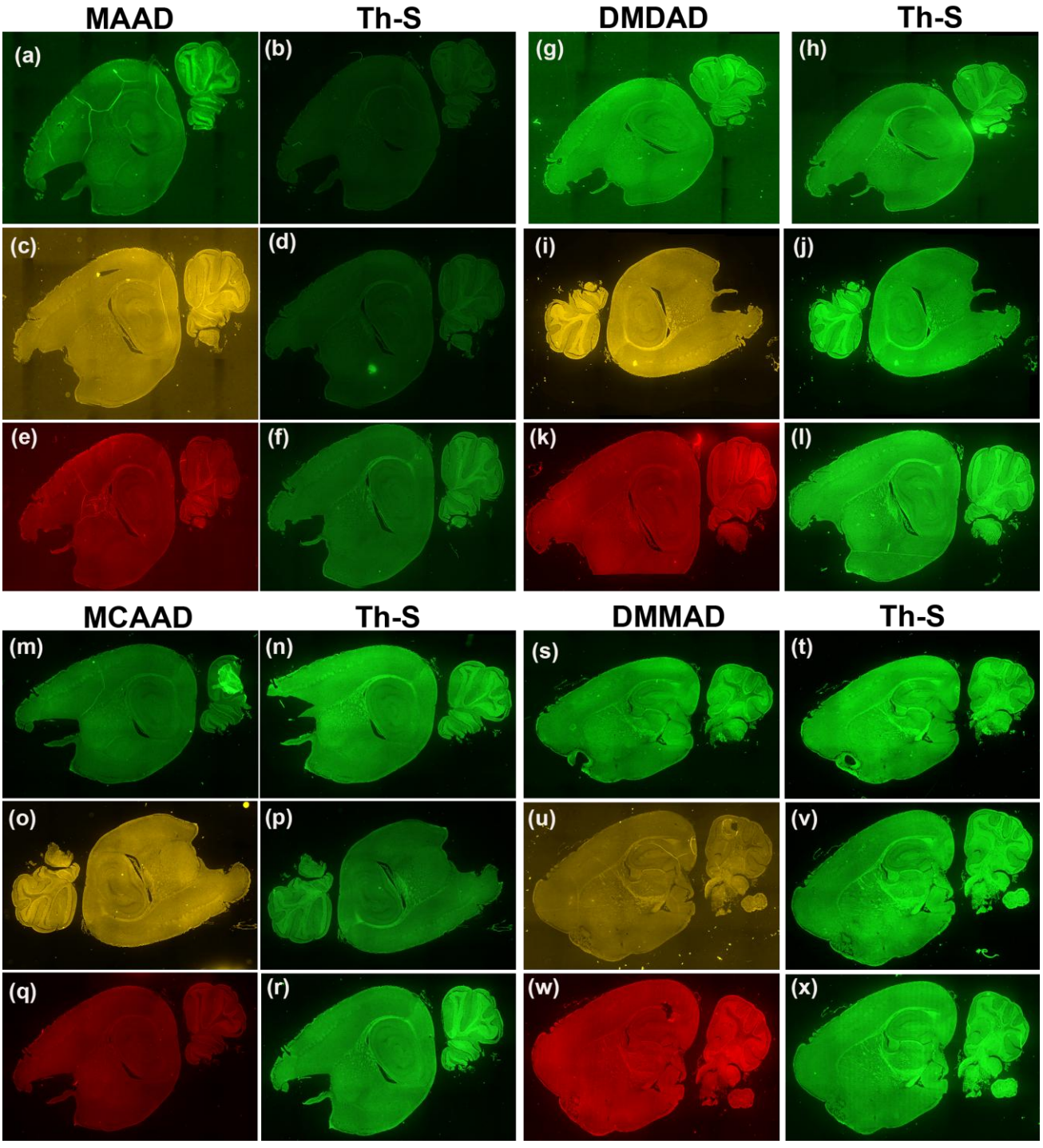

Fig. **S12** In vitro fluorescent staining of Aβ plaques on brain sections of age-matched normal mice by our probes. (a), (c), (e), (g), (i), (k), (m), (o), (q), (s), (u), and (w) were stained by MAAD-1, -2, -3, DMDAD-1, -2, -3, MCAAD-1, -2, -3, and DMM-1, -2, -3, respectively. The adjacent sections were stained by thioflavin-S (b, d, f, h, j, l, n, p, r, t, v, and x).

In vitro Binding Assays Using Aβ_{1-42} Aggregates. The affinities of these probes were assessed by in vitro competitive binding assays using [^{125}I]IMPY as the competitor for binding to Aβ_{1-42} aggregates in solution. The radio-ligand [^{125}I]IMPY was prepared according to procedures described previously.[6] The inhibition experiments were conducted in 12×75 mm borosilicate glass tubes with a reaction mixture containing 100 μL of aggregated Aβ_{1-42} fibrils, 100 μL of radioligand [^{125}I]IMPY (80,000 cpm/100 μL), 100 μL of inhibitors (10^{-4} to $10^{-8.5}$ M in ethanol) and 700 μL of 0.05% BSA aqueous solution in a total volume of 1.0 mL. Nonspecific binding was defined in the presence of 1μM cold IMPY. The mixture was incubated at room temperature for 3 h before it was transferred to borosilicate glass fibril filters (Whatman GF/B) using a Brandel Mp-48T cell harvester. After the bound and free [^{125}I]IMPY were separated, filters containing the bound [^{125}I]IMPY were measured by gamma counter (WALLAC/Wizard 1470, USA) with 70% counting efficiency. The half maximal inhibitory concentration (IC_{50}) was determined from the displacement curves of three independent experiments using GraphPad Prism 4.0 and the inhibition constant (K_i) was calculated using the Cheng-Prusoff equation:[7] $K_i = IC_{50}/(1 + [L]/K_d)$, where [L] is the concentration of [^{125}I]IMPY used in the assay and K_d is the dissociation constant of IMPY. The K_i value of IMPY was also assessed under the same conditions as a control.

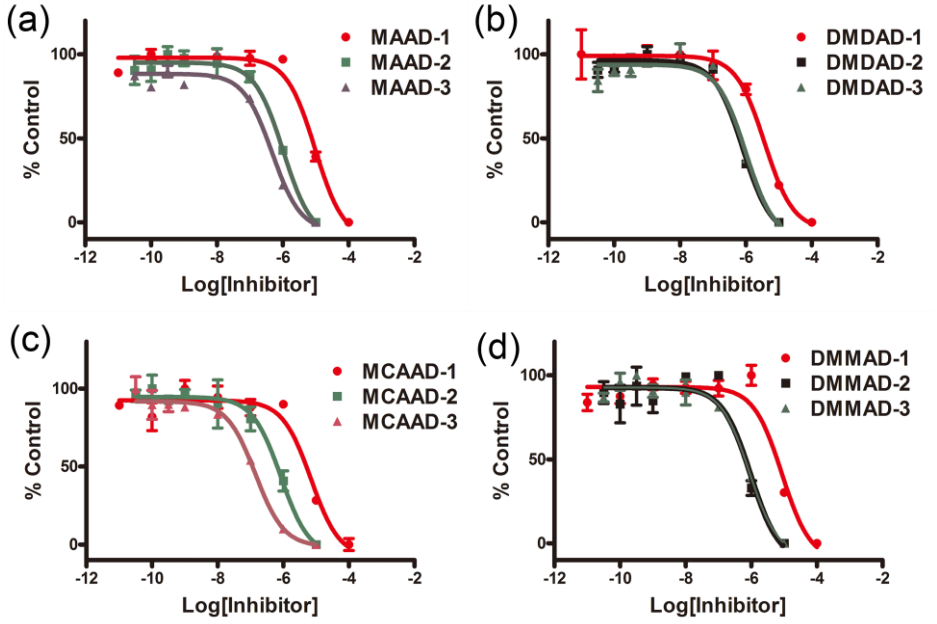

Fig. **S13** Inhibition curves for the binding of [^{125}I]IMPY to Aβ_{1-42} aggregates.

Table S2 The molecular weight, binding data and calculated log *P* values of the synthesized probes.

Probe	M.W.	K_i[a]	Log *P*[b]
MAAD-1	275.30	8007.46 ± 462.69	3.12
MAAD-2	301.13	767.16 ± 109.98	3.77
MAAD-3	327.37	354.25 ± 43.54	4.33
DMDAD-1	271.35	2775.75 ± 1.12	2.89
DMDAD-2	297.39	592.09 ± 108.97	3.51
DMDAD-3	323.43	645.22 ± 77.16	4.12
MCAAD-1	230.26	5221.64 ± 723.35	2.33
MCAAD-2	256.30	544.37 ± 71.60	2.94
MCAAD-3	282.34	105.97 ± 29.77	3.56
DMMAD-1	263.29	7989.18 ± 592.91	2.23
DMMAD-2	289.33	712.46 ± 156.52	2.91
DMMAD-3	315.36	652.61 ± 143.07	3.48
IMPY	--	25.37 ± 11.82	--

[a] Measured in triplicate with results given as the mean ± SD.

[b] Log *P* values were calculated using the online ALOGPS 2.1 program.

Table S3 The molecular weight, binding data, calculated log *P* values and fluorescent properties of the reported probes.

Probe	M.W.	K_d (nM)	Log *P*[a]	λ_{ex} (nm)	λ_{em} (nm)	Stokes shift (nm)
DANIR 2c	249.31	36.9 ± 6.8	3.37	597	665	68
BAP-1	351.20	44.1	3.52	614	648	34
CRANAD-2	410.26	38.69 ± 2.77	6.16	640	805	165
NIAD-4	334.41	10	4.91	450	625	175
AOI987	411.16	220 ± 130	0.90	650	670	20
2C40	477.62	--	1.84	430	570	140
SAD1	306.38	17	5.25	362	497	135

[a] The values were calculated with online ALOGPS 2.1 program.

Blood-Brain Barrier (BBB) Penetrating Test of NIRFs. A solutions of one of our NIRFs (45% DMSO and 55% propylene glycol, 50 μL, 2 mg/Kg) was injected via tail vein of ICR mice (22-24 g, male). The mice were sacrificed at different time points of 2, 10, 30 and 60 min (n = 3-4 for each time point). Brain samples were removed and was homogenized with 1.0 mL acetonitrile and then the leftover homogenate was extracted with 1.0 mL acetonitrile for twice. The extracts were filtered by flashing nylon membrane (0.22 μm) and dried over anhydrous sodium sulfate. After that, 100 μL of the combined acetonitrile were analyzed by HPLC (the conditions used for HPLC analyses were presented in Table S4). To determine the wastage of the compound during homogenate, filtration and desiccation, the recovery rate was measured by the following procedure: ICR mice were sacrificed and the brains were removed; 10 μL of the inject solution of our NIRFs was directly injected into the brains (n = 2) and incubated for 1 h, and then treated by the previous procedures. The blank control was obtained by analyzing the solution of each NIRFs (10 μL diluted to 3.0 mL acetonitrile). Quantitative analysis was derived from peak area and the brain uptake was presented by % injected dose per gram (%ID/g). An Agilent 1260 Infinity Quaternary LC (Agilent Technologies) system was used and the HPLC analyses were performed on a Cosmosil packed column ($5C_{18}$-AR-II, 4.6 × 150 mm, nacalai tesque) with a binary gradient elution system, while the mobile phase A and B were water and acetonitrile, respectively. BAP-1[8], a dipyrromethane (BODIPY) derivative developed as Aβ plaque-specific probe, was used as control.

Table S4 The conditions used in HPLC analyses.

Probe	HPLC analyses			Recovery rate
	Eluent H_2O: CH_3CN	Retention time min	UV detector nm	
MCAAD-3	40: 60	9.93	490	0.95 ± 0.012
DMMAD-3	40: 60	9.21	440	1.00
BAP-1	35: 65	9.46	600	0.95 ± 0.0021

Table S5 Biodistribution of MCAAD-3, DMMAD-3 and BAP-1 in brains of ICR mice.

Probe	Time after injection (min)				$Brain_{2\ min}/brain_{60\ min}$
	2	10	30	60	
MCAAD-3	8.66 ± 1.45	3.53 ± 0.18	1.00 ± 0.10	0.24 ± 0.055	36.1
DMMAD-3	8.02 ± 0.91	3.67 ± 0.81	0.40 ± 0.13	0.11 ± 0.0066	72.9
BAP-1	2.23 ± 0.29	2.37 ± 0.42	1.00 ± 0.15	0.43 ± 0.075	5.2

As shown in Table S5, MCAAD-3 and DMMAD-3 with arborescent moieties (MCA and DMM) could readily penetrate the BBB with high initial brain uptake and fast brain egress (Fig. S14d), while the probes MAAD-3 and DMDAD-3 with explanate hexatomic rings (MA and DMD) couldn't permeate the BBB in this experimental conditions. Meanwhile, BAP-1 displayed poor brain uptake and slow brain egress (Fig. S14d and Table S5). What is more, BAP-1 was obviously metabolized in living brain at the earliest time point of 10 min (Fig. S14c), which is very detrimental for in vivo imaging. These results confirmed that our probes MCAAD-3 and DMMAD-3 could efficiently diffusible across the BBB, which is a prerequisite for an excellent performance in in vivo imaging along with fast washout from the brain. Notably, as suggested by our results, the geometries of the acceptor moieties (arborescent or circinate) acted important in brain uptake and this may provide a meaningful guideline in the design of molecules capable of penetrating the BBB.

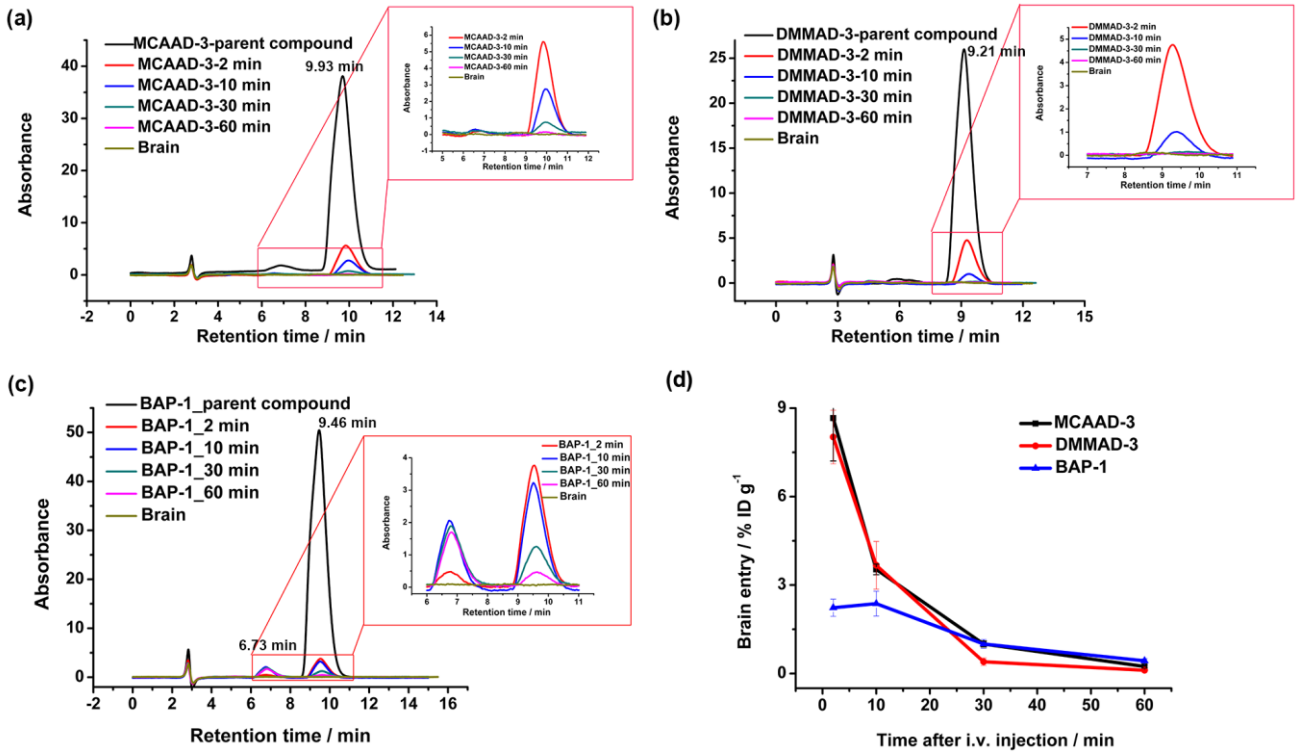

Fig. S14 The HPLC patterns of MCAAD-3 (a), DMMAD-3 (b) and BAP-1 (c). (d) The clearance curves of MCAAD-3 (black line), DMMAD-3 (red line) and BAP-1 (blue line) in the mice brain.

In Vivo Near-Infrared Imaging. In vivo NIR imaging was performed on a IVIS Lumina III system. Double transgenic mouse (n = 3, C57BL6, APPsw/PSEN1, 14 months old, male) and an age-matched control mouse (n = 3, C57BL6, 14-months-old, male) were shaved before background imaging and were i.v. injected with MCAAD-3 (0.1 mg/kg, 20% DMSO, 80% propylene glycol, 50μL). Fluorescence signals from the brain were recorded at different time points after i.v. injection of MCAAD-3. For the measurement, a filter set (ex. at 560 nm and em. at 670 nm) was used. During the imaging process, the mice were kept on the imaging stage under anesthesia with 2.5% isoflurane gas in an oxygen flow (0.8 L/min). Imaging data was analyzed by Living Image Software, and an ROI was drawn around the brain region. Intensity of brain fluorescence was calculated from the radiant efficiency. The data were analyzed in the following method: for each mouse, the fluorescence signal at any given time point [*F*(t),] minus the fluorescence signal before the injection [*F*(pre)] divided by the fluorescence signal of the highest value [*F*(4 min)]. This calculated parameter can reliably eliminate the unavoidable differences and injection capacities among individual animals.

$$\text{Relative fluorescence intensity} = [F(t) - F(pre)]/[F(t`) - F(pre)] \quad \text{(equation 1)}$$

Where the $t \neq 0$, $t` = 4$ min for this probe (MCAAD-3), respectively.

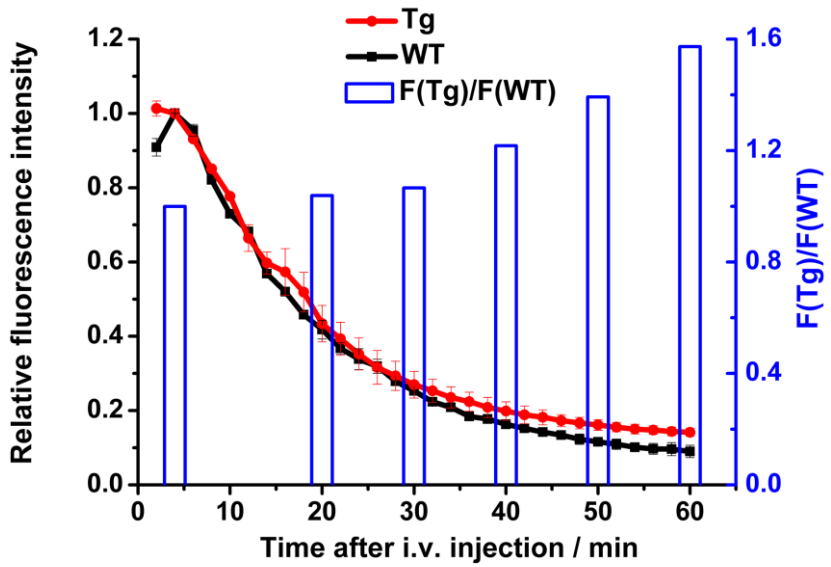

Fig. S15 Brain kinetic curves of MCAAD-3 (left Y axis) and the values of *F*(Tg)/*F*(WT) at selected time points (right Y axis).

Ex Vivo Fluorescent Staining of MCAAD-3 to Aβ Plaques in Transgenic Mouse Brain. A double transgenic mouse (C57BL6, APPsw/PSEN1, 22 months old, male) and an age-matched control mouse (C57BL6, 22 months old, male) were iv injected with MCAAD-3 (0.1 mg/kg, 20% DMSO, 80% propylene glycol, 50μL) and sacrificed at 40 min after injection. The brains were excised, embedded in optimum cutting temperature compound (OCT). Frozen sections of 20 μm were cut, and fluorescent observation was performed by OLYMPUS IXTI system equipped with a GFP filter sets. In addition, the Aβ plaques were further confirmed by the staining of the same section with Thioflavin-S (0.125%) using an AF488 filter set.

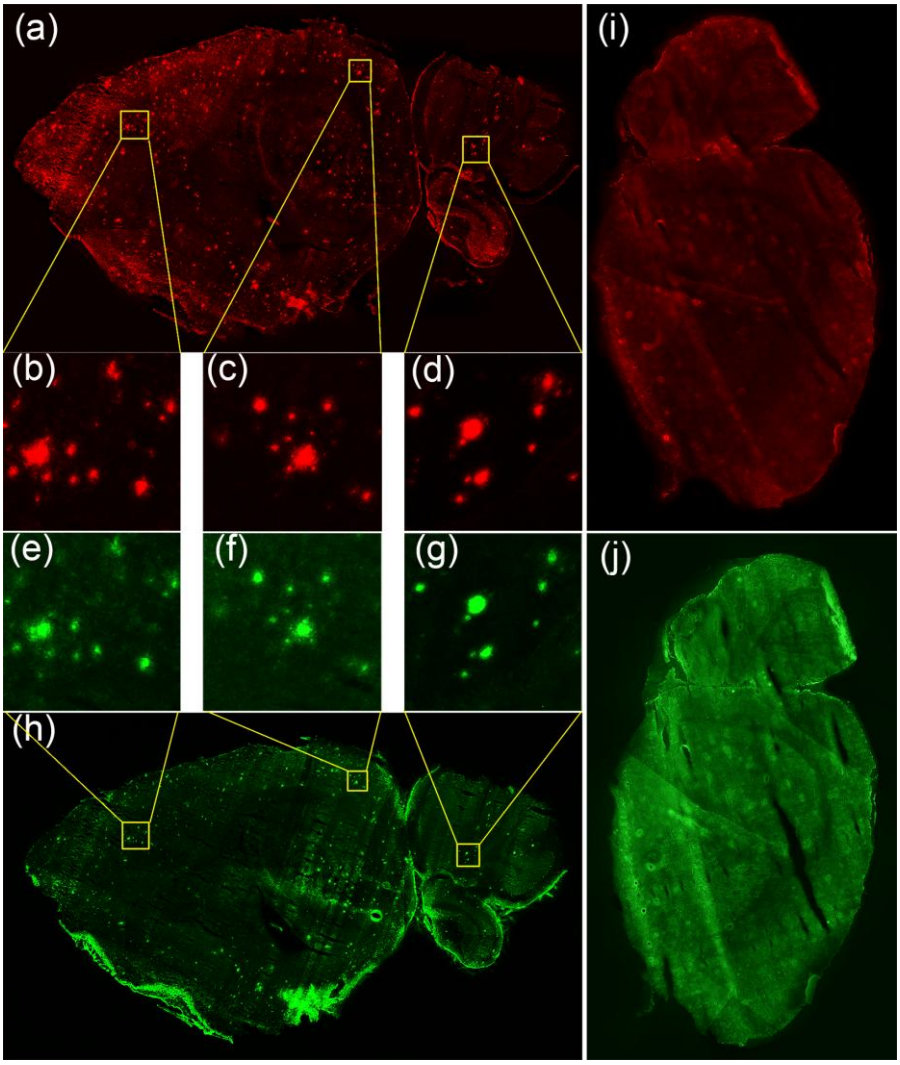

Fig. S16 Ex vivo fluorescence observation (GFP filter set) of brain slices from a Tg mouse (a and h) and WT control mouse (i and j) after injection of MCAAD-3. (b), (c), (d), (e), (f) and (g) were partial enlarged view (20 ×) of the brain slices. The Aβ plaques were further confirmed by staining the same sections with Thioflavin-S (AF488 filter set, h and j).

Computational Studies. All of the molecules were constructed with GaussView 5.0 and optimized ground-state geometries (Fig. S14) were performed in gas phase[3, 5] at B3LYP/6-31G(d)[9] level of theory in Gaussian 09[10]. All of the docking process was achieved using the Lamarckian genetic algorithm method[11] in AutoDock 4.2[12] software on 2-fold Aβ_{1-40} fibrils (PDB ID: 2LMO) downloaded from the protein data bank (www.rcsb.org/pdb). AutoDock Tools 1.5.6[12c, 13] was used in the preparation of the ligand and receptor coordinate files, and therefore, the rigid protein was used as the macromolecule receptor and our probes were set as flexible ligands with all torsions defined to be rotatable. Residues 16-KLVFFA-21 of the Aβ_{1-40} fibril were deemed the most valid binding site for the interaction of small molecules with the fibrils;[14] thus a grid of 36, 60, and 80 points in x, y, and z directions centered on this site was built with a grid spacing of 0.375 Å. The number of GA runs, population size, maximum number of evaluations, and maximum number of generations were set to 100, 300, 2.5×10^7, and 27000, respectively, and default settings were used for all other parameters. After docking, the 100 dock conformations were grouped by the root mean square deviation (RMSD) values within 2 Å. The best poses (lowest-energy/top-ranked) were analyzed for hydrogen bonding or hydrophobic interactions of the ligands with the Aβ fibrils using AutoDock Tools 1.5.6 and Visual Molecular Dynamics 1.8.4 (VMD 1.8.4, University of Illinois)[15].

The docking results are presented in Fig. 4 (main text), Figs. S18-S21 and Table S6. Figs. S18-S20 were charted using VMD 1.8.4. The β-strands of the fibrils were depicted using the NewCartoon method and colored by structure (yellow), while the corresponding residues (LYS16, VAL18, and PHE20) and ligands were represented in Licorice style and colored by residue name. The binding channels were also illustrated vividly by molecular surface coloring of white, blue, red, and green, which represent nonpolar, basic, acid, and polar surfaces, respectively.

Extended Discussion about Molecular Docking. The dock simulations were carried out on 2-fold Aβ_{1-40} fibrils, which dominate the overall population of Aβ fibrils. Two major binding sites, the "IMPY site" and "non-IMPY site", were found to be right at the surface of the fibril and were easily accessible to small molecules ligands.

Based on the results of the dock simulations, we concluded that 1) IMPY and molecules of the MAAD and DMDAD series shared the same hydrophobic binding pocket in the "IMPY site" (Fig. 4,

S18, and S19); 2) molecules of the MCAAD and DMMAD series preferentially bound to the "non-IMPY site" (Fig. 4, and S19) and had secondary preference for the "IMPY site" with higher binding energies (Fig. S20 and Table S6); 3) the experimental pK_i values correlated well with the calculated binding energies at the "IMPY site" (Fig. 4 i and j in the main text) and the dipole moments (R^2 = 0.4895, graph was not given); 4) the binding energy diminished with the lengthening of the conjugated double bonds (Table S6); and 5) the increase in the binding energy was not directly proportional to the extension of the conjugated double bonds; in other words, significant discrepancies were observed between the binding affinities and the calculated binding energies when the number of conjugated double bonds went from one to two, while no such hop arose when the number increased from two to three (Table S2 and S6).

We elucidated these conclusions based on several observations as follows. First, the backbones of all of the probes are very similar, with the primary difference between them being the electron-withdrawing moieties (Fig. 1 in the main text). The extreme differences were their geometries, including nearly explanate hexatomic rings (MA and DMD) and arborescent moieties (MCA and DMM) and the potential to form hydrogen bonds. Compared with probes of the MCAAD and DMMAD series, those probes of the MAAD and DMDAD series arise minor steric clashes, which makes them easier to insert into the "IMPY site", and thus a smaller binding energy (Fig. 4, S17, S19 and Table S6). Conversely, larger stereo-hindrance and H-bonds connecting the hydrogen atoms of LYS16 and the oxygen atoms of the MCA and DMM moieties drive the binding of the MCAAD and DMMAD series probes to the "non-IMPY site" (Fig. 4, S17, S19 and Table S6). Second, it is important to note that hydrophobic interactions dominate in the binding process of ligands with Aβ fibrils as evidenced by the fact that the "IMPY site" and "non-IMPY site" share the same channel formed by the nonpolar residues VAL18 and PHE20 (Fig. 4 and S18-21, marked by a white molecule surface). The greatest number of carbons and a linear carbon chain within the molecules can produce the strongest hydrophobic interactions,[16] which was confirmed by a striking improvement in the binding affinities when the conjugated polyenic chain was slightly lengthened. However, no reliable relationship was observed between the number of the H-bonds and binding affinity or binding energy (Fig. S21 and Table S6). Additionally, hydrophobic interactions are

relatively stronger than other weak intermolecular forces such as Van der Waals interactions or hydrogen bonds.[16] As a result, when the probes were completely or partially buried into the VAL18_PHE20 channel, which is a lower dielectric constant environment,[5] a prominent increase in fluorescence intensity and emission blue shift were observed (Fig. 2 and Table 1 in main text). Third, with the extension of the conjugated polyenic chain, an increase in the distortion energy and steric hindrance during the docking process counterbalanced the enhancement of hydrophobic interactions, thus the increase in binding energy was not directly proportional to the lengthening of the conjugated double bonds.

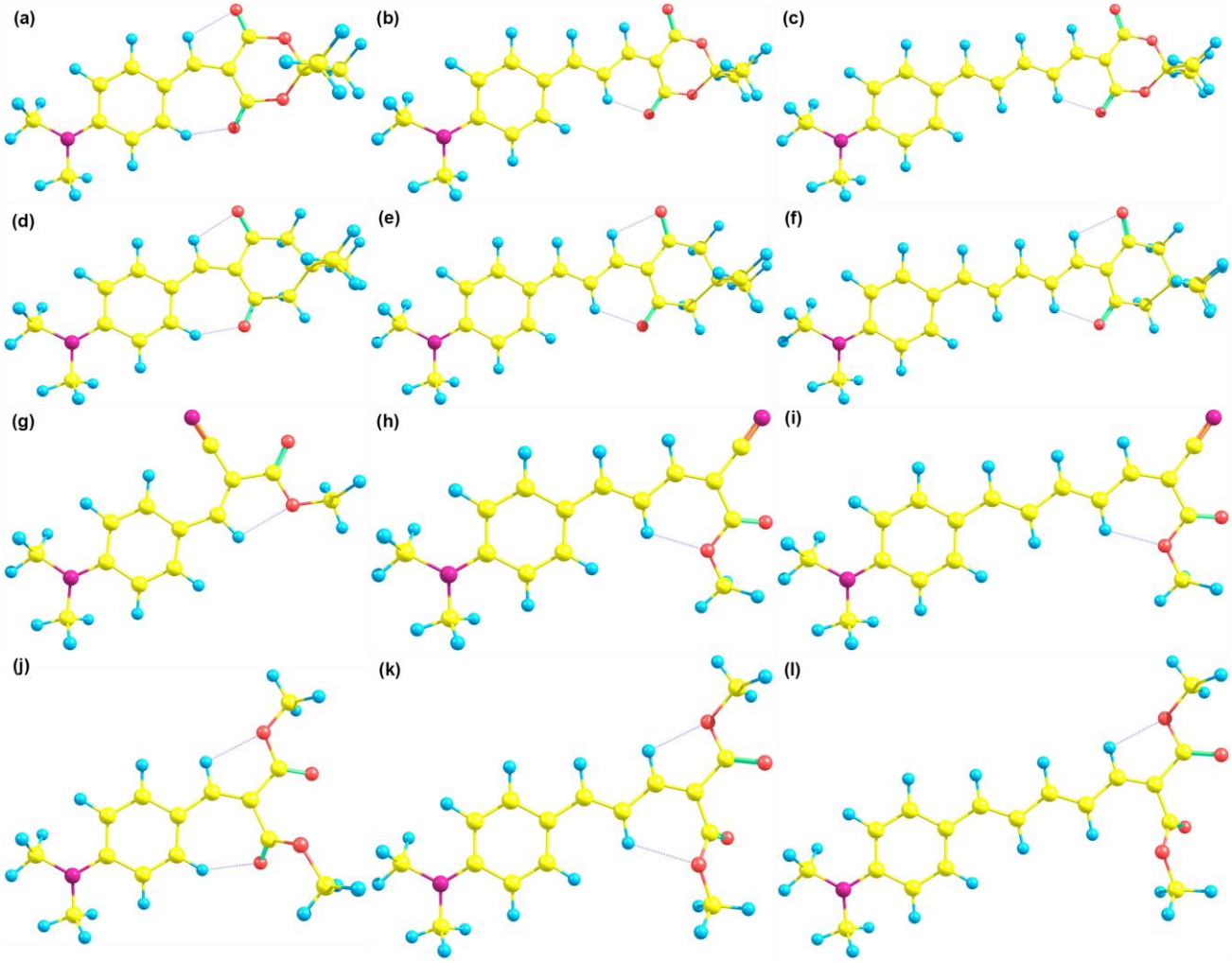

Fig. **S17** The optimized ground-state geometries. (a), (b), (c), (d), (e), (f), (g), (h), (i), (j), (k), and (l) show the optimized ground-state geometries for MAAD-1, -2, -3, DMDAD-1, -2, -3, MCAAD-1, -2, -3, and DMMAD-1, -2, -3, respectively.

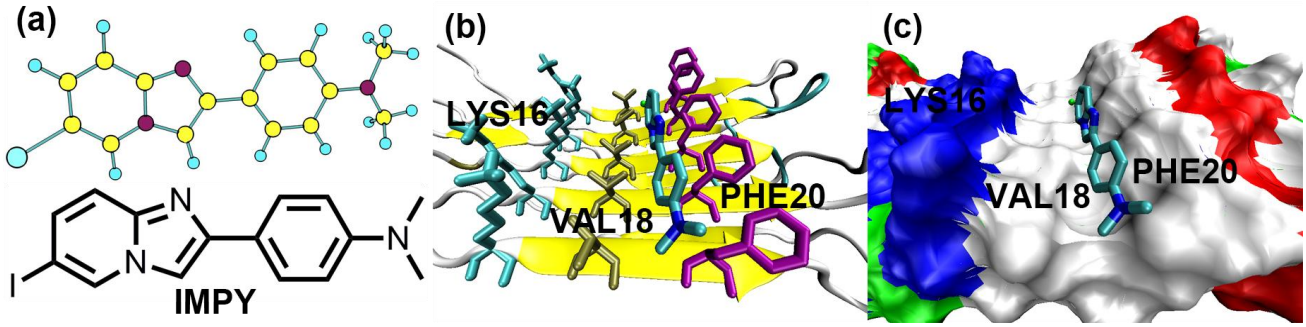

Fig. **S18** (a) The optimized ground-state geometry (upper) and chemical structure of IMPY (below). (b)(c) The binding site of IMPY on 2-fold Aβ fibrils based on molecular docking simulations presented in Licorice style (b) and as a molecular surface representation(c).

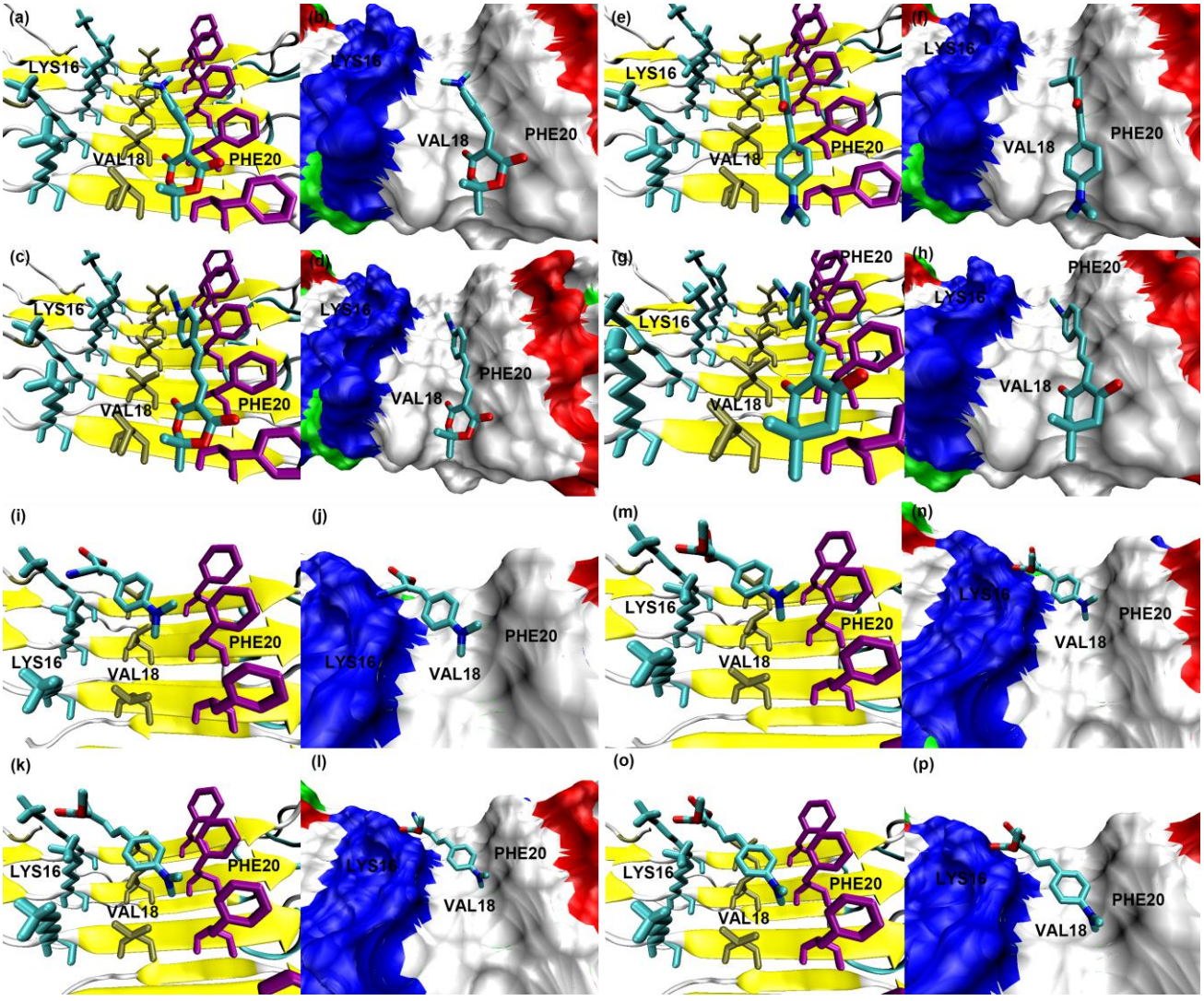

Fig. **S19** The lowest energy/top ranked dock conformations of the probes on Aβ fibrils. (a) & (b), (c) & (d), (e) & (f), (g) & (h), (i) & (j), (k) & (l), (m) & (n), and (o) & (p) represent MAAD-1, -2, DMDAD-1, -2, MCAAD-1, -2, and DMMAD-1, -2, respectively.

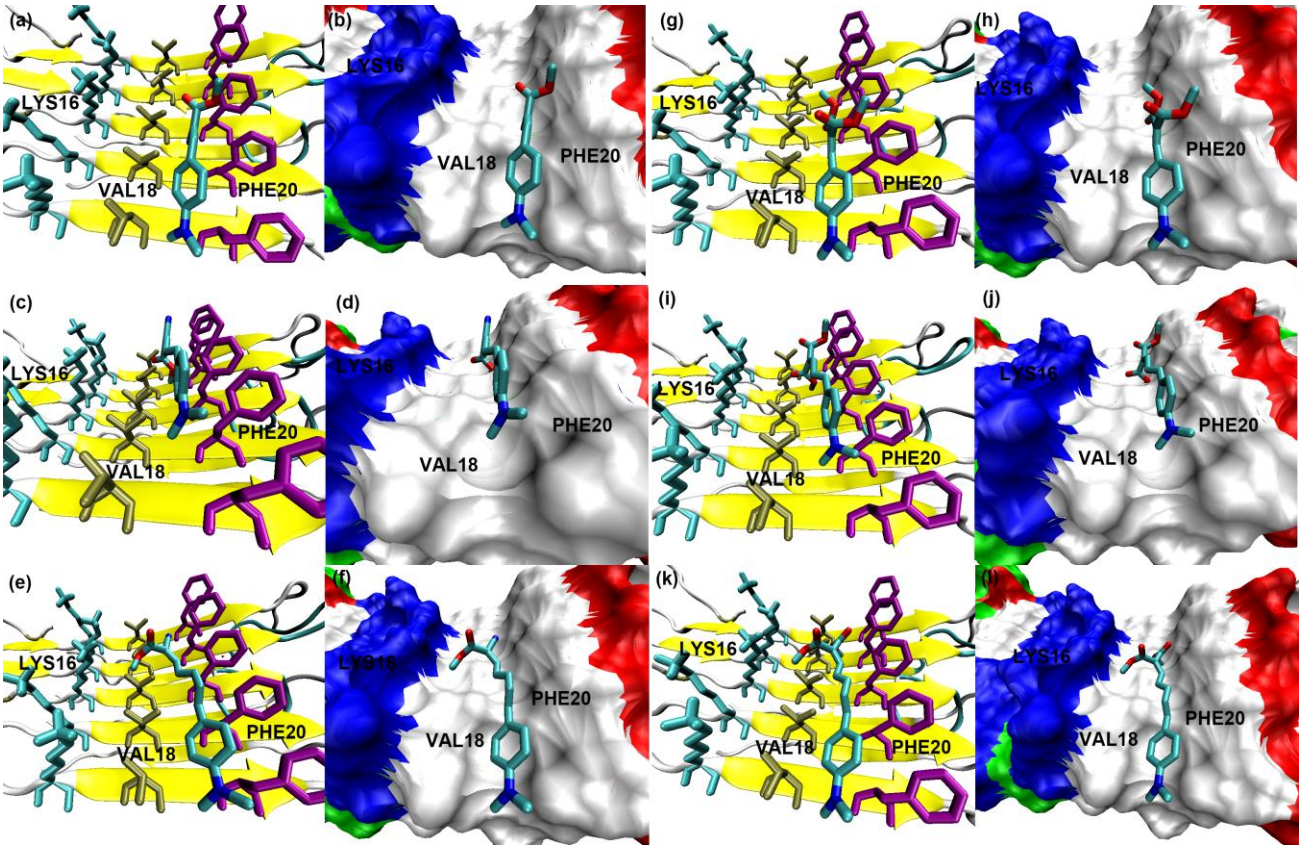

Fig. **S20** The probes of the MCAAD and DMMAD series also possessed an "IMPY site". (a) & (b), (c) & (d), (e) & (f), (g) & (h), (i) & (j) and (k) & (l) represent MCAAD-1, -2, -3, and DMMAD-1, -2, -3, respectively.

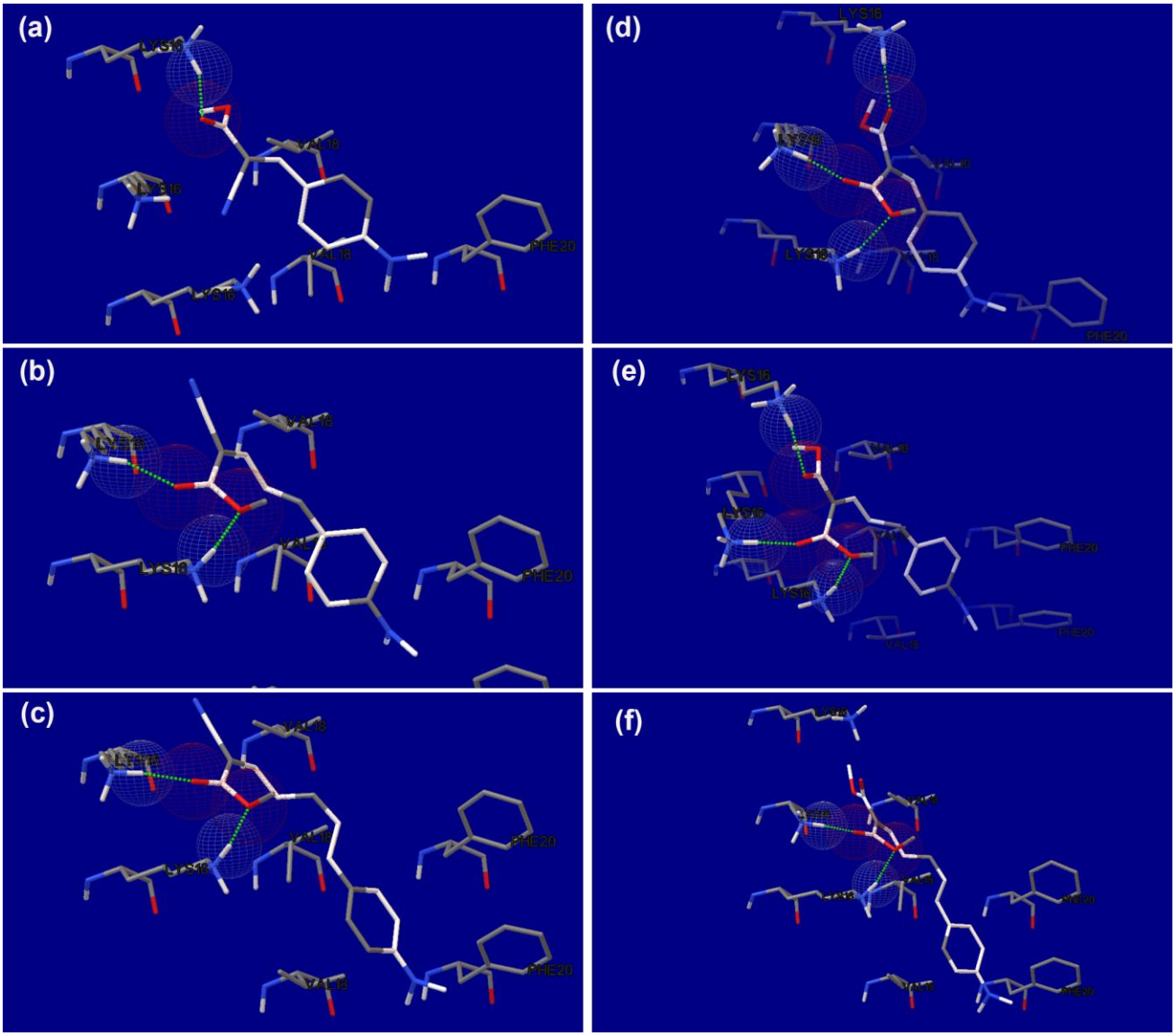

Fig. **S21** Hydrogen bonds played an important role in the dock conformations of the probes of the MCAAD and DMMAD series. The ligands and the binding pocket residues are shown as balls and sticks, and the dashed green lines indicate H-bonds. (a), (b), (c), (d), (e), and (f) represent MCAAD-1, -2, -3, and DMMAD-1, -2, -3, respectively. This figure was produced by AutoDock Tools 1.5.6.

Table S6 Dipole moments and HOMO-LUMO energy gaps along with the binding energies, torsion energies, and occupation percentages of the "IMPY site" and "non-IMPY site" for each probe.

Probe	Dipole moment (Debye)	HOMO-LUMO energy gap (a.u.)	IMPY site			Non-IMPY site		
			Binding energy (kcal mol^{-1})	Torsion energy (kcal mol^{-1})	Occupation percentage (%)	Binding energy (kcal $mol^{-1)}$	Torsion energy (kcal $mol^{-1)}$	Occupation percentage (%)
MAAD-1	6.8997	0.0524	-5.48	0.60	98			
MAAD-2	8.5005	0.0463	-5.94	0.89	100			
MAAD-3	10.0627	0.0473	-6.23	1.19	34		--	
DMDAD-1	5.1431	0.0611	-5.57	0.60	99			
DMDAD-2	6.9144	0.0531	-5.85	0.89	99			
DMDAD-3	8.3047	0.0509	-6.30	1.19	89			
MCAAD-1	9.0570	0.1421	-4.07	1.19	65	-4.01	1.19	14
MCAAD-2	13.3572	0.1405	-4.61	1.49	7	-5.20	1.49	85
MCAAD-3	14.8186	0.1201	-4.87	1.79	35	-5.06	1.79	38
DMMAD-1	5.7847	0.1323	-3.72	1.79	16	-4.53	1.79	59
DMMAD-2	9.2949	0.1453	-4.40	2.09	4	-5.21	2.09	87
DMMAD-3	10.4497	0.1219	-4.85	2.39	47	-5.22	2.39	29

Appendixes: ^{1}H-NMR, ^{13}C-NMR, MS, and HRMS of the Synthesized Probes

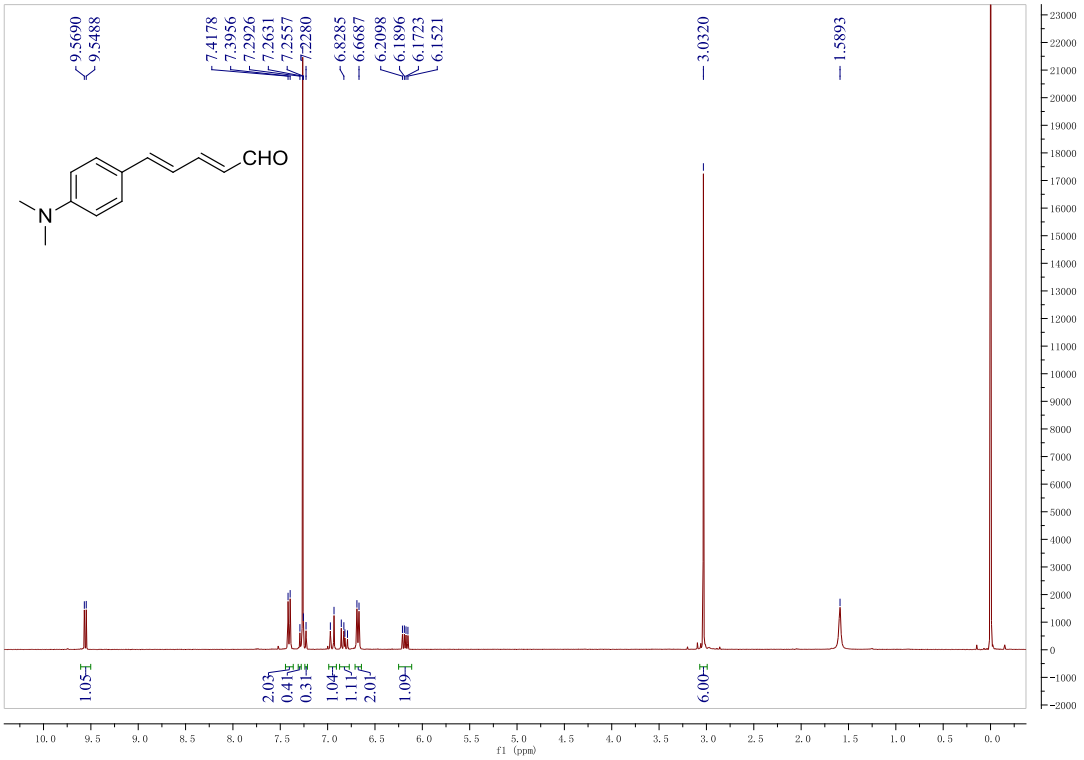

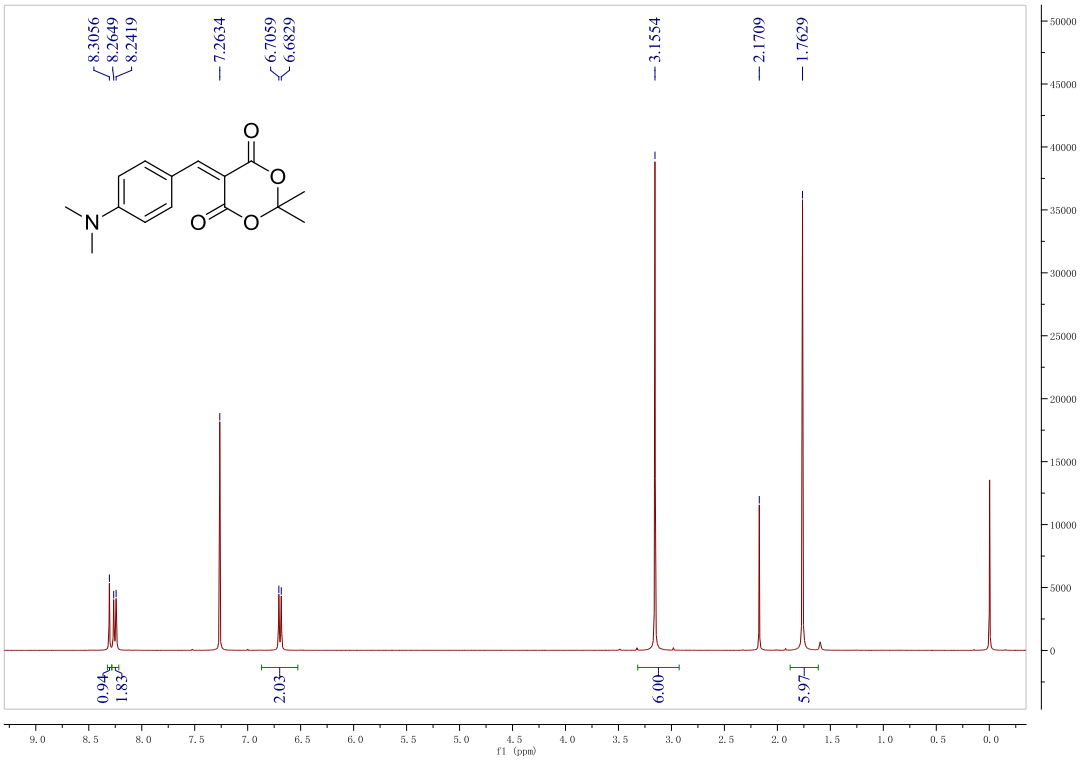

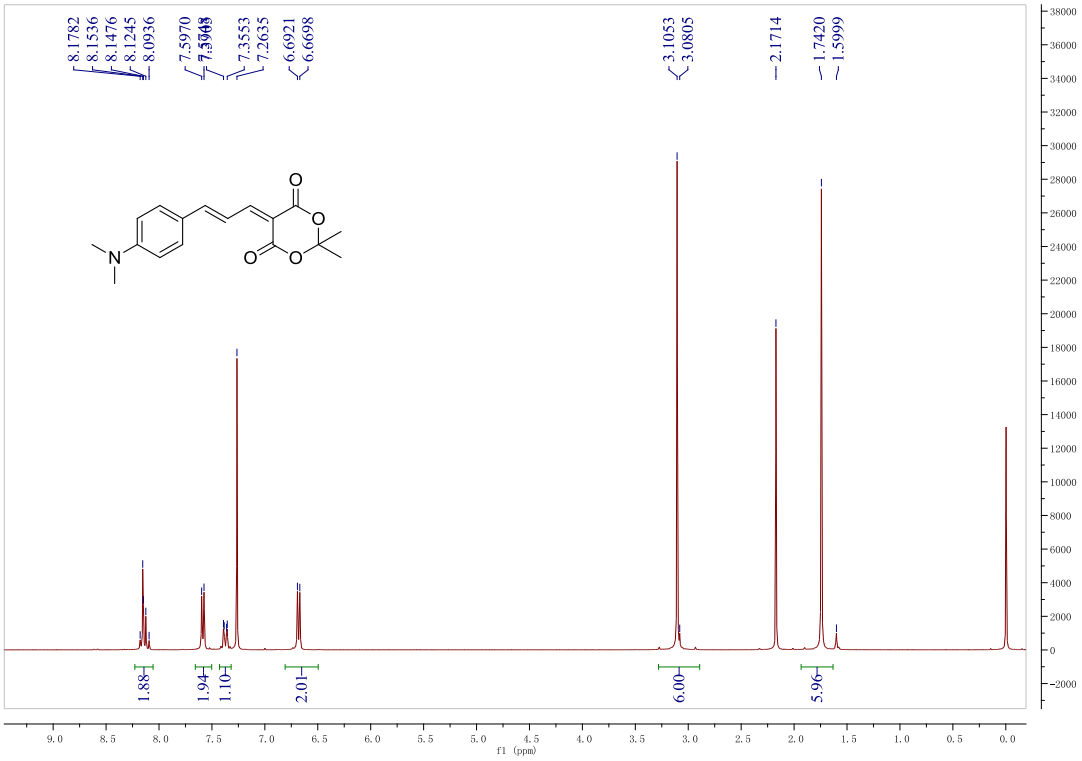
8.1782
8.1536
8.1476
8.1245
8.0936
7.5970
7.3553
7.2635
6.6921
6.6698
3.1053
3.0805
2.1714
1.7420
1.5999
1.88
1.94
1.10
2.01
6.00
5.96
f1 (ppm)

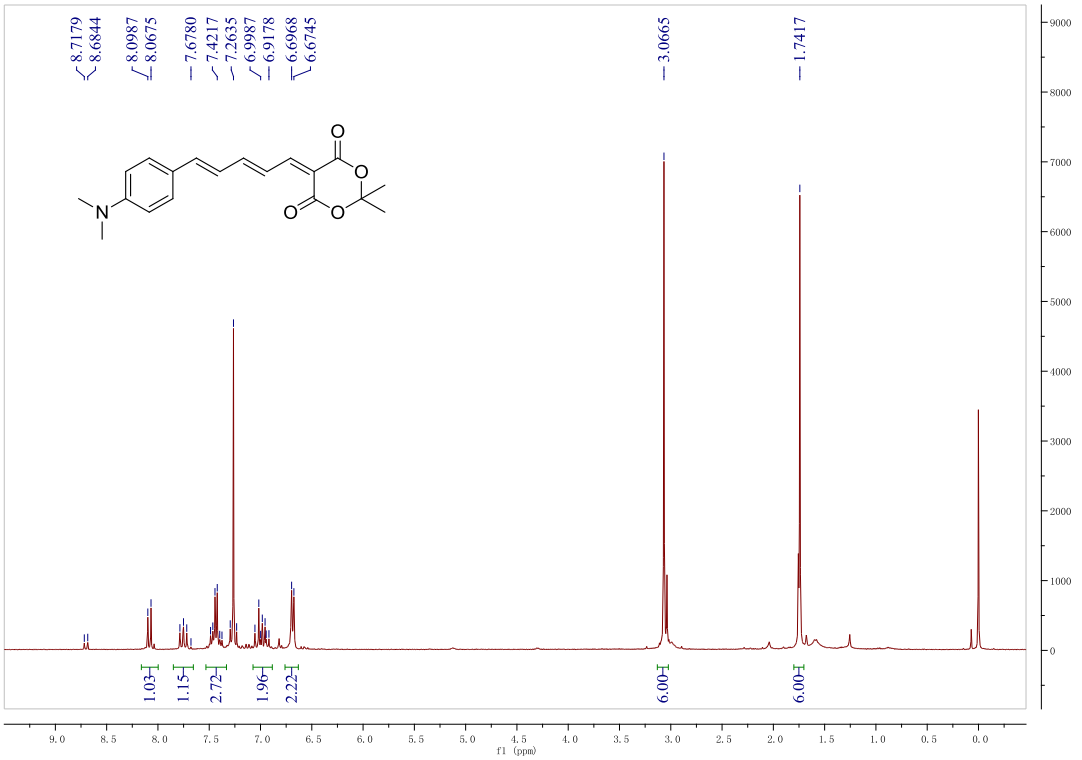
8.7179
8.6844
8.0987
8.0675
7.6780
7.4217
7.2635
6.9987
6.9178
6.6968
6.6745
3.0665
1.7417
1.03
1.15
2.72
1.96
2.22
6.00
6.00
f1 (ppm)

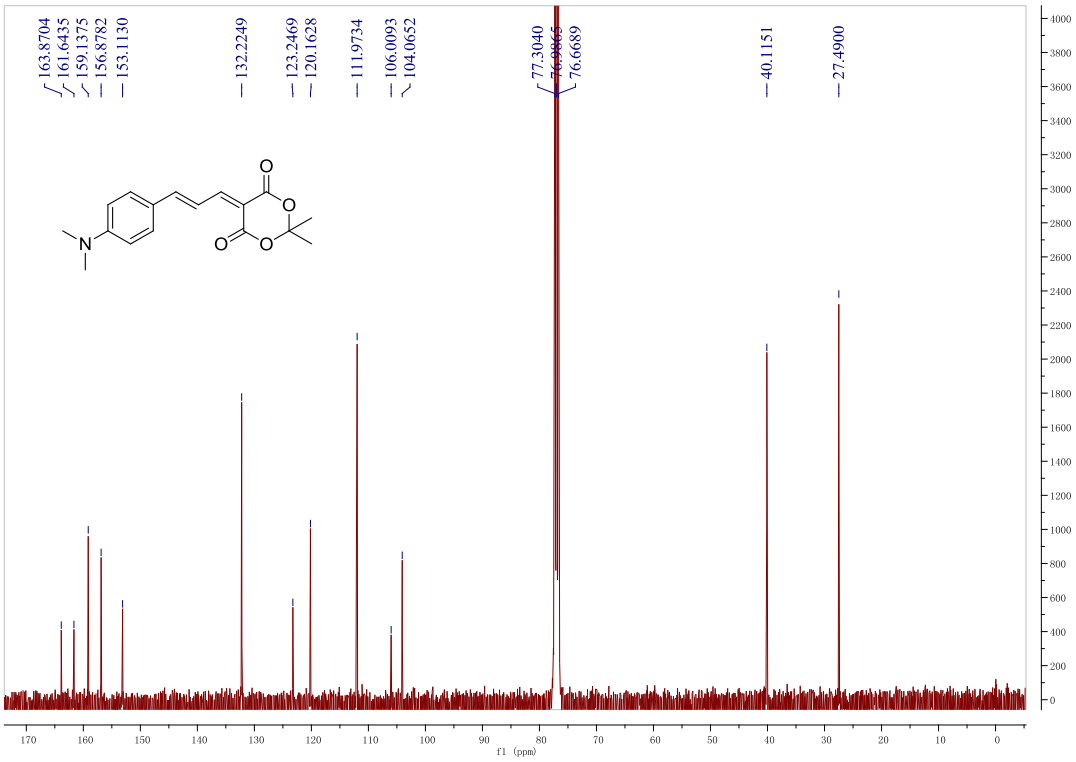
163.8704
161.6435
159.1375
156.8782
153.1130
132.2249
123.2469
120.1628
111.9734
106.0093
104.0652
77.3040
76.9865
76.6689
40.1151
27.4900
f1 (ppm)

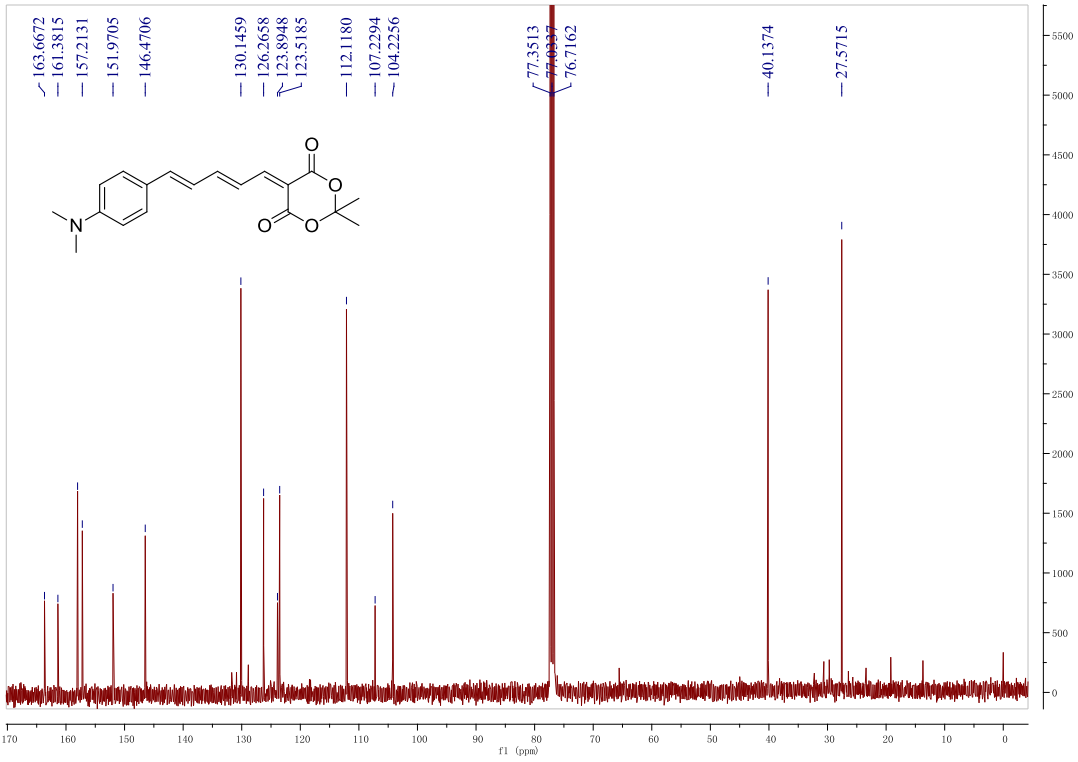
163.6672
161.3815
157.2131
151.9705
146.4706
130.1459
126.2658
123.8948
123.5185
112.1180
107.2294
104.2256
77.3513
77.0337
76.7162
40.1374
27.5715
f1 (ppm)

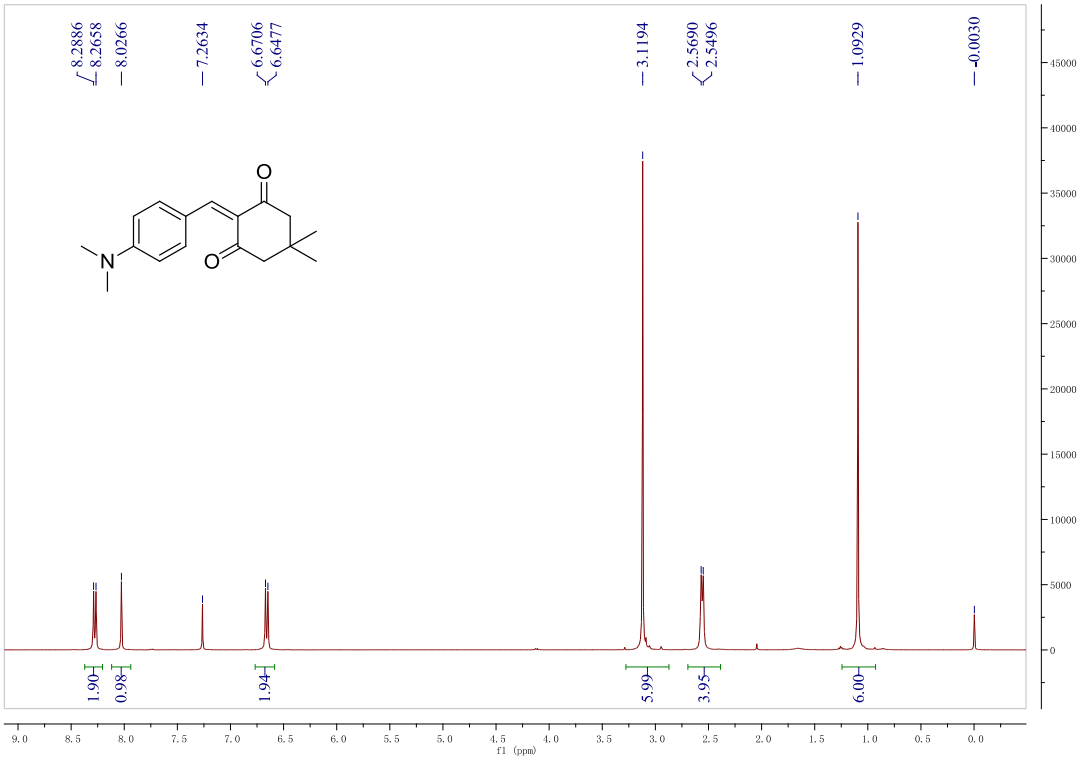
8.2886
8.2658
8.0266
7.2634
6.6706
6.6477
3.1194
2.5690
2.5496
1.0929
-0.0030
1.90
0.98
1.94
5.99
3.95
6.00
f1 (ppm)

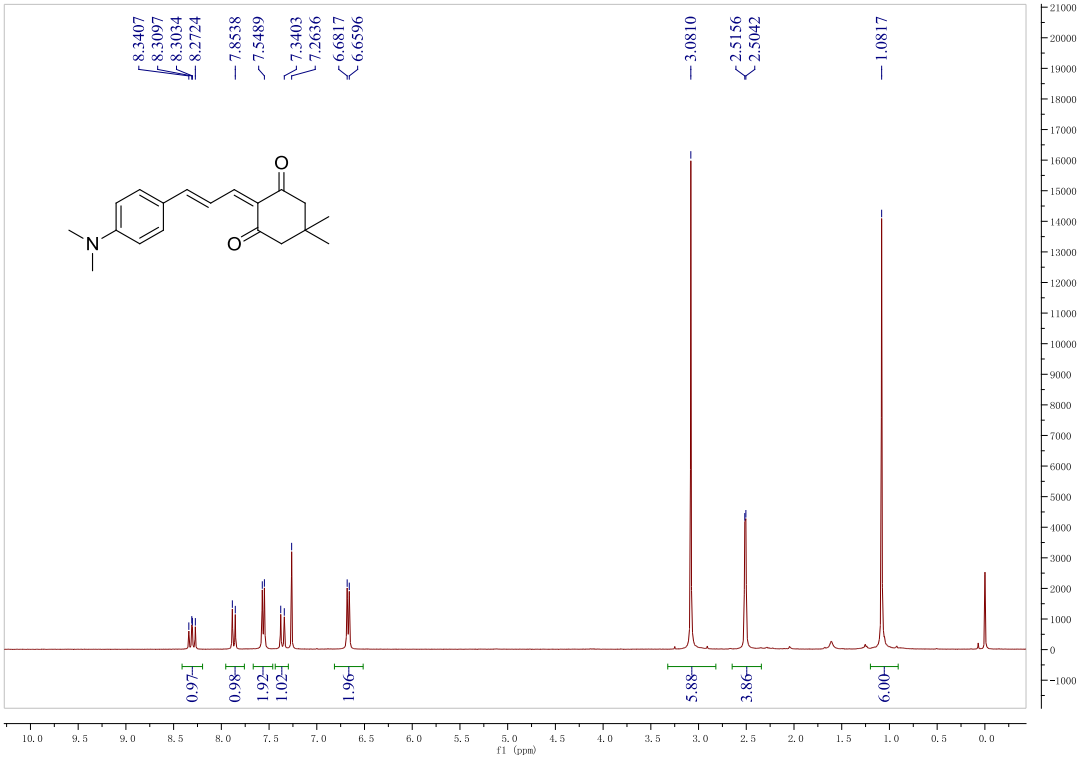
8.3407
8.3097
8.3034
8.2724
7.8538
7.5489
7.3403
7.2636
6.6817
6.6596
3.0810
2.5156
2.5042
1.0817
0.97
0.98
1.92
1.02
1.96
5.88
3.86
6.00
f1 (ppm)

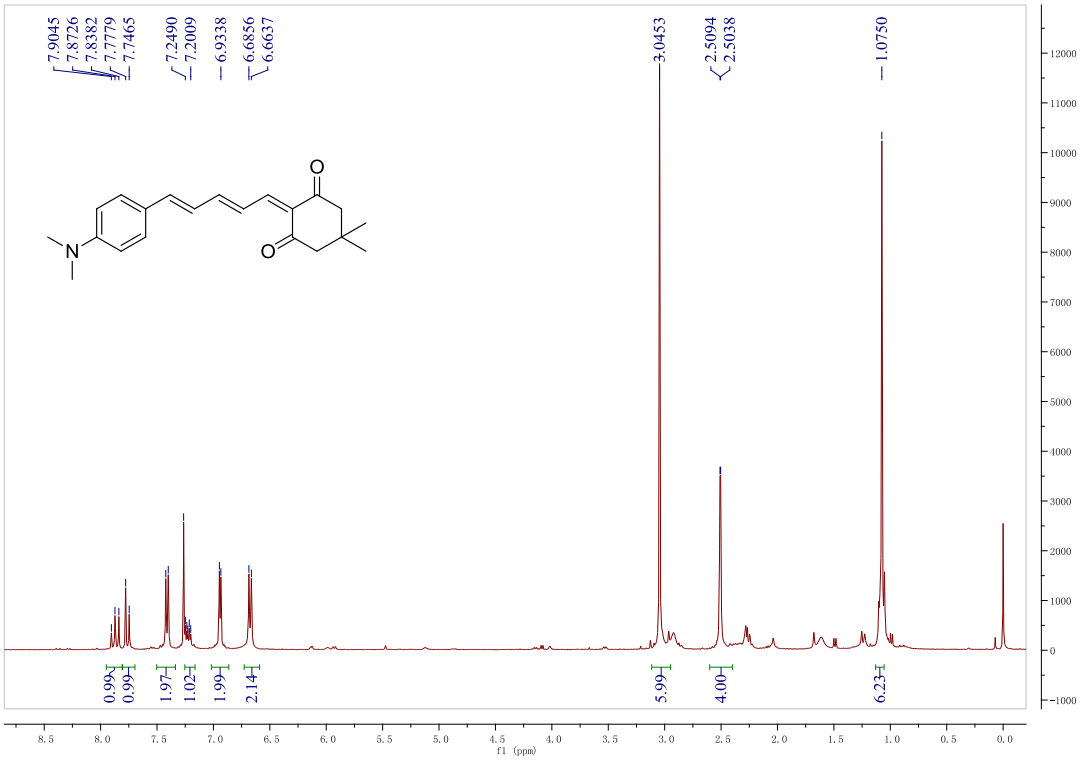
7.9045
7.8726
7.8382
7.7779
7.7465
7.2490
7.2009
6.9338
6.6856
6.6637
3.0453
2.5094
2.5038
1.0750
0.99
0.99
1.97
1.02
1.99
2.14
5.99
4.00
6.23
f1 (ppm)

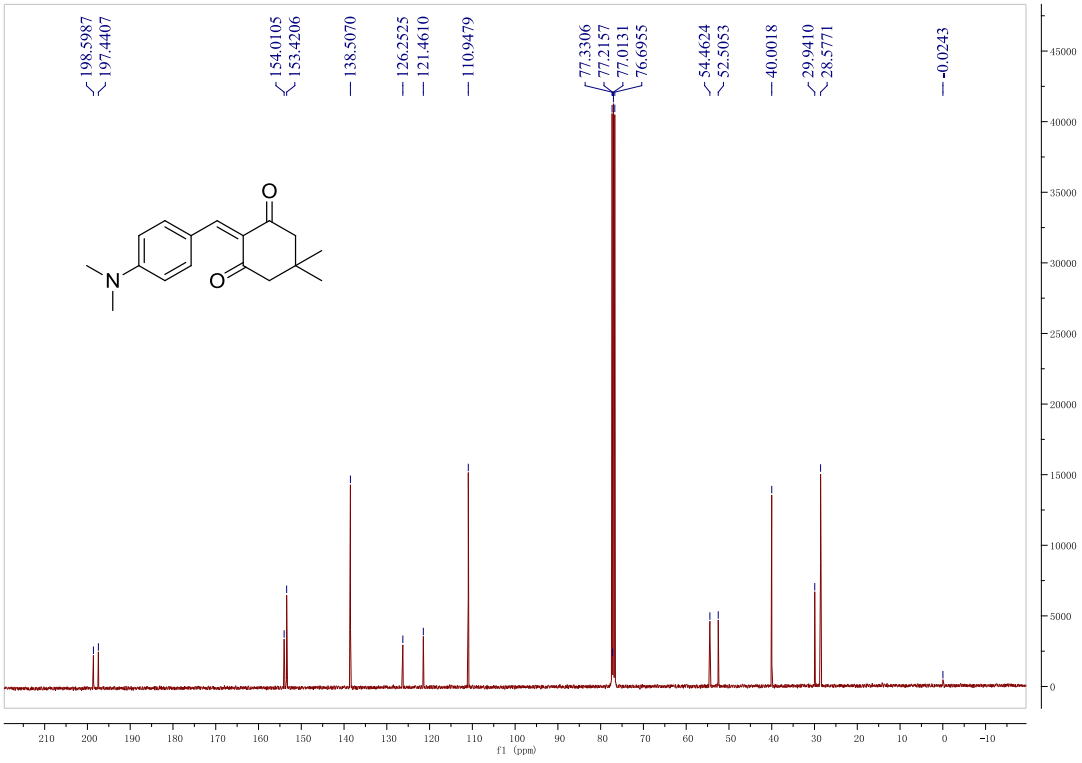
198.5987
197.4407
154.0105
153.4206
138.5070
126.2525
121.4610
110.9479
77.3306
77.2157
77.0131
76.6955
54.4624
52.5053
40.0018
29.9410
28.5771
-0.0243
f1 (ppm)

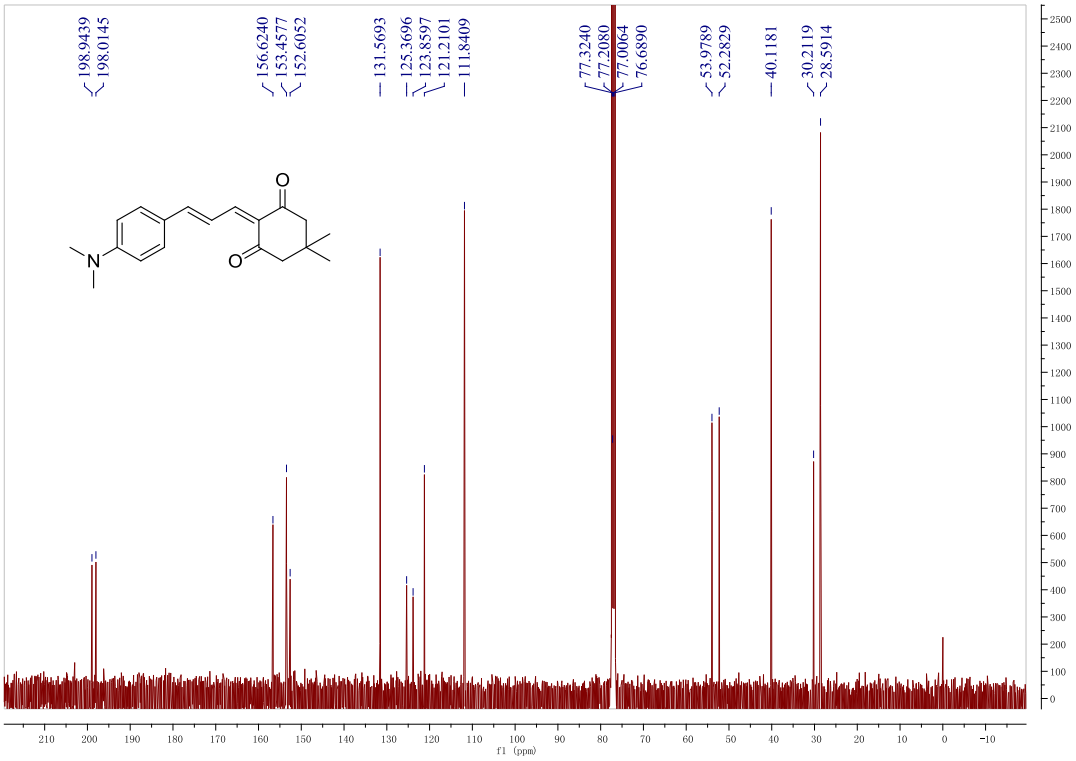
198.9439
198.0145
156.6240
153.4577
152.6052
131.5693
125.3696
123.8597
121.2101
111.8409
77.3240
77.2080
77.0064
76.6890
53.9789
52.2829
40.1181
30.2119
28.5914
O
O
N
f1 (ppm)

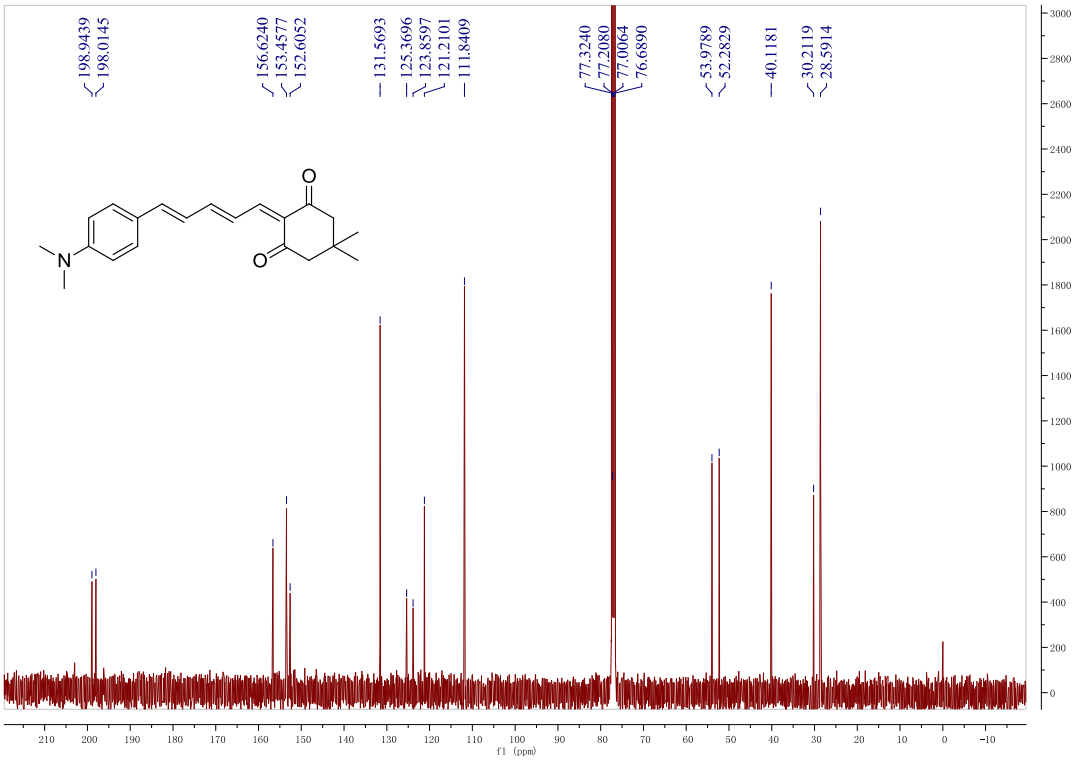
198.9439
198.0145
156.6240
153.4577
152.6052
131.5693
125.3696
123.8597
121.2101
111.8409
77.3240
77.2080
77.0064
76.6890
53.9789
52.2829
40.1181
30.2119
28.5914
O
O
N
f1 (ppm)

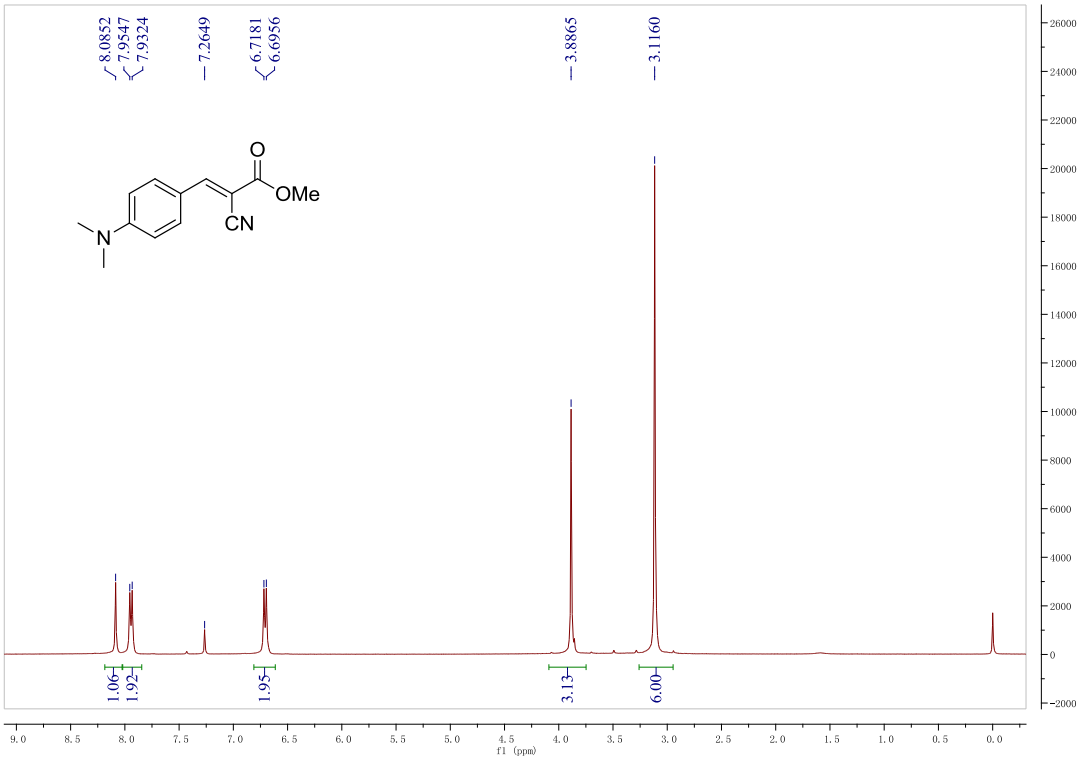
8.0852
7.9547
7.9324
7.2649
6.7181
6.6956
3.8865
3.1160
O
OMe
CN
N
1.06
1.92
1.95
3.13
6.00
f1 (ppm)

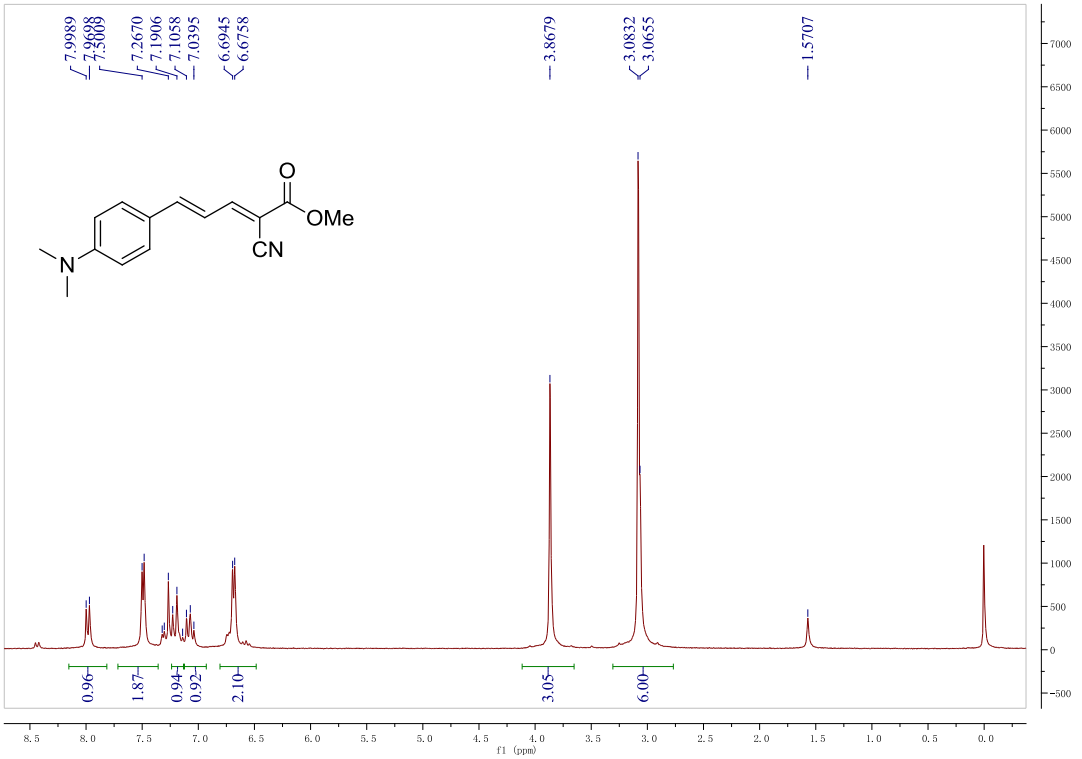
7.9989
7.9698
7.9608
7.5009
7.2670
7.1906
7.1058
7.0395
6.6945
6.6758
3.8679
3.0832
3.0655
1.5707
O
OMe
CN
N
0.96
1.87
0.94
0.92
2.10
3.05
6.00
f1 (ppm)

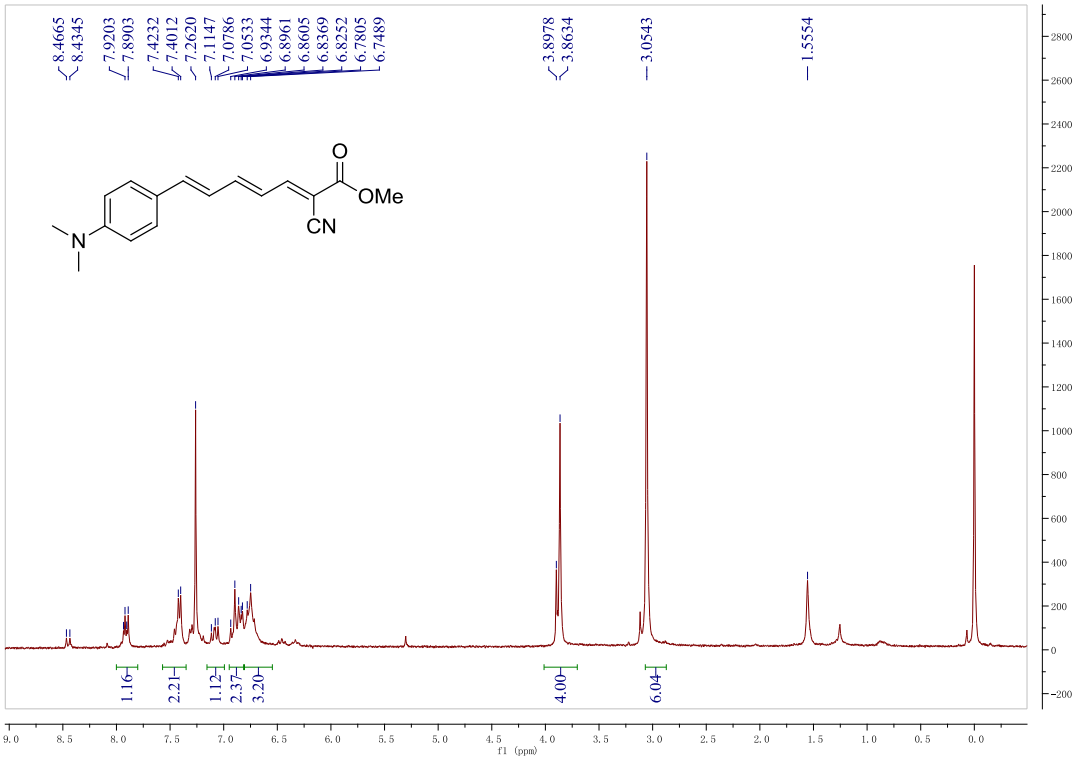
8.4665
8.4345
7.9203
7.8903
7.4232
7.4012
7.2620
7.1147
7.0786
7.0533
6.9344
6.8961
6.8605
6.8369
6.8252
6.7805
6.7489
3.8978
3.8634
3.0543
1.5554
O
OMe
CN
N
1.16
2.21
1.12
2.37
3.20
4.00
6.04
f1 (ppm)

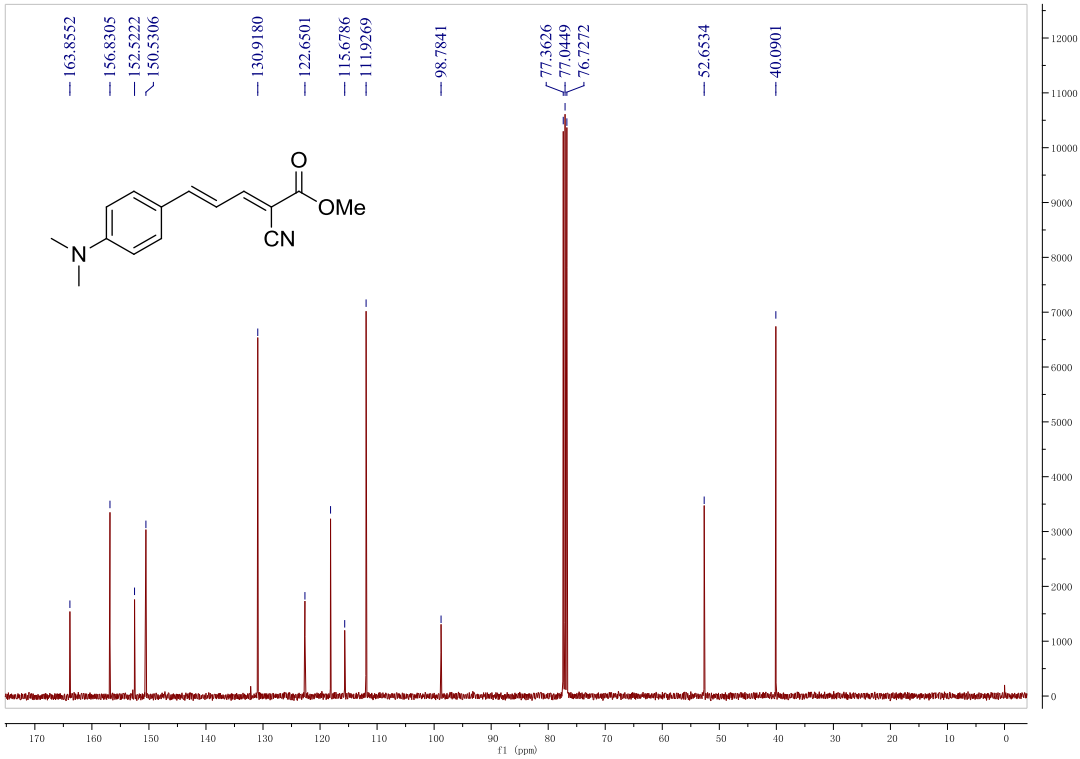
163.8552
156.8305
152.5222
150.5306
130.9180
122.6501
115.6786
111.9269
98.7841
77.3626
77.0449
76.7272
52.6534
40.0901
O
OMe
CN
N
f1 (ppm)

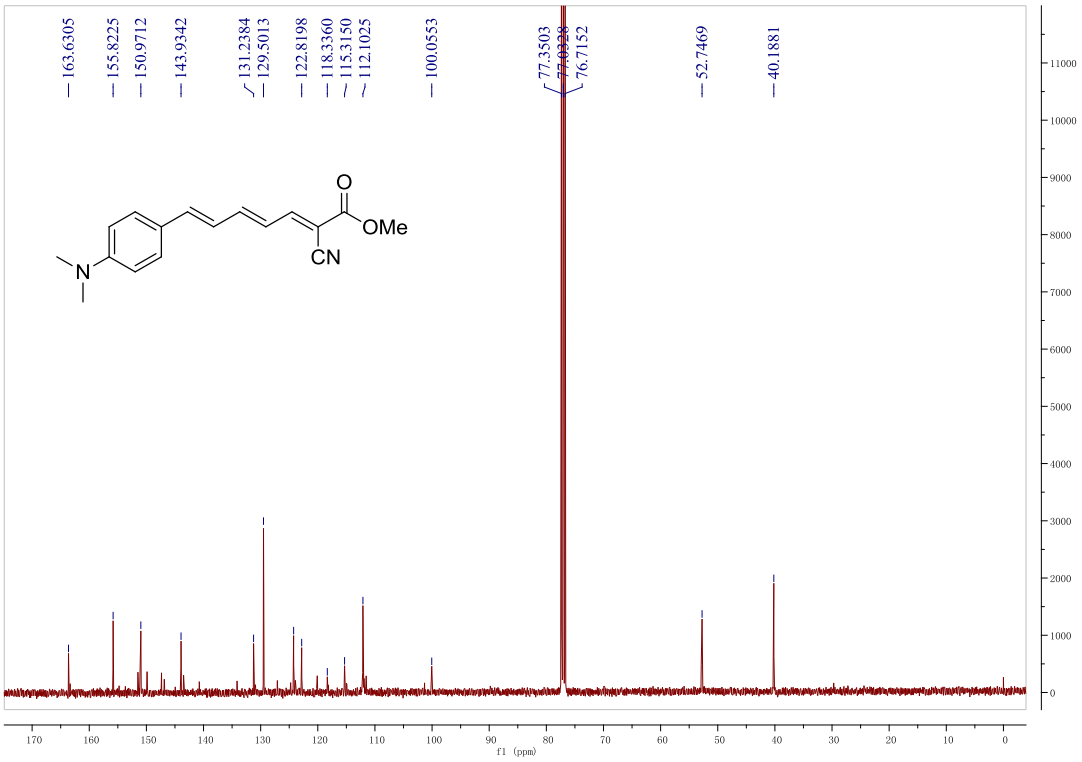
163.6305
155.8225
150.9712
143.9342
131.2384
129.5013
122.8198
118.3360
115.3150
112.1025
100.0553
77.3503
77.0328
76.7152
52.7469
40.1881
O
OMe
CN
N
f1 (ppm)

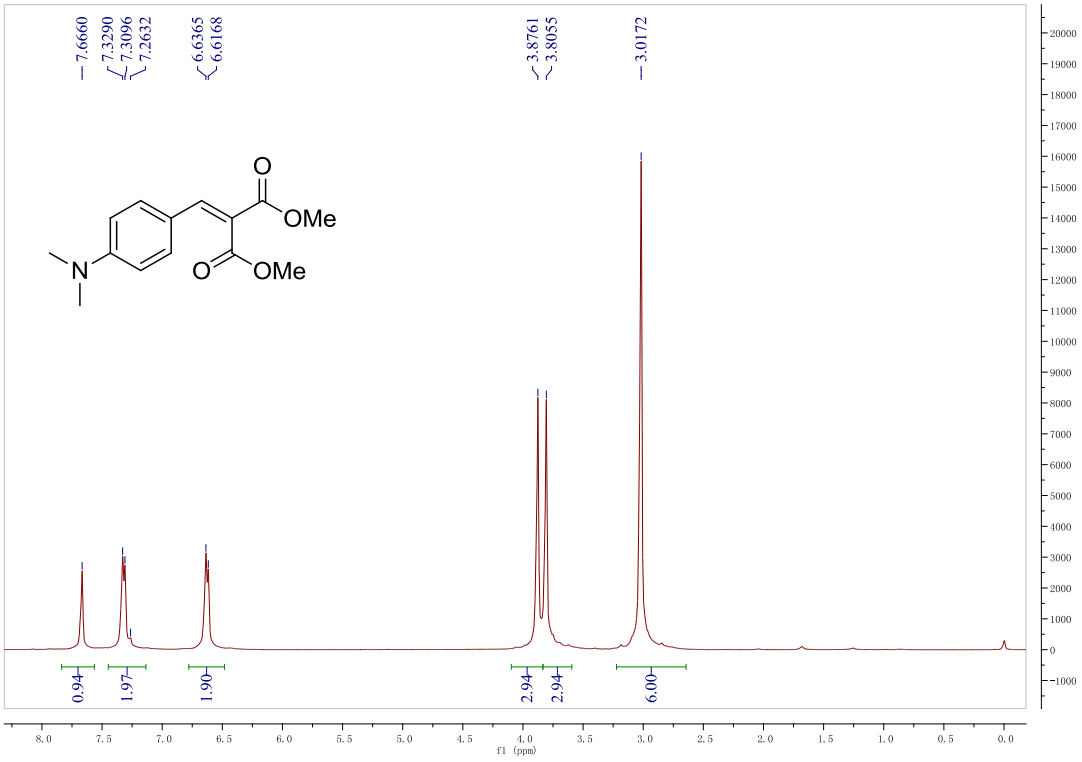
7.6660
7.3290
7.3096
7.2632
6.6365
6.6168
3.8761
3.8055
3.0172
O
OMe
O
OMe
N
0.94
1.97
1.90
2.94
2.94
6.00
f1 (ppm)

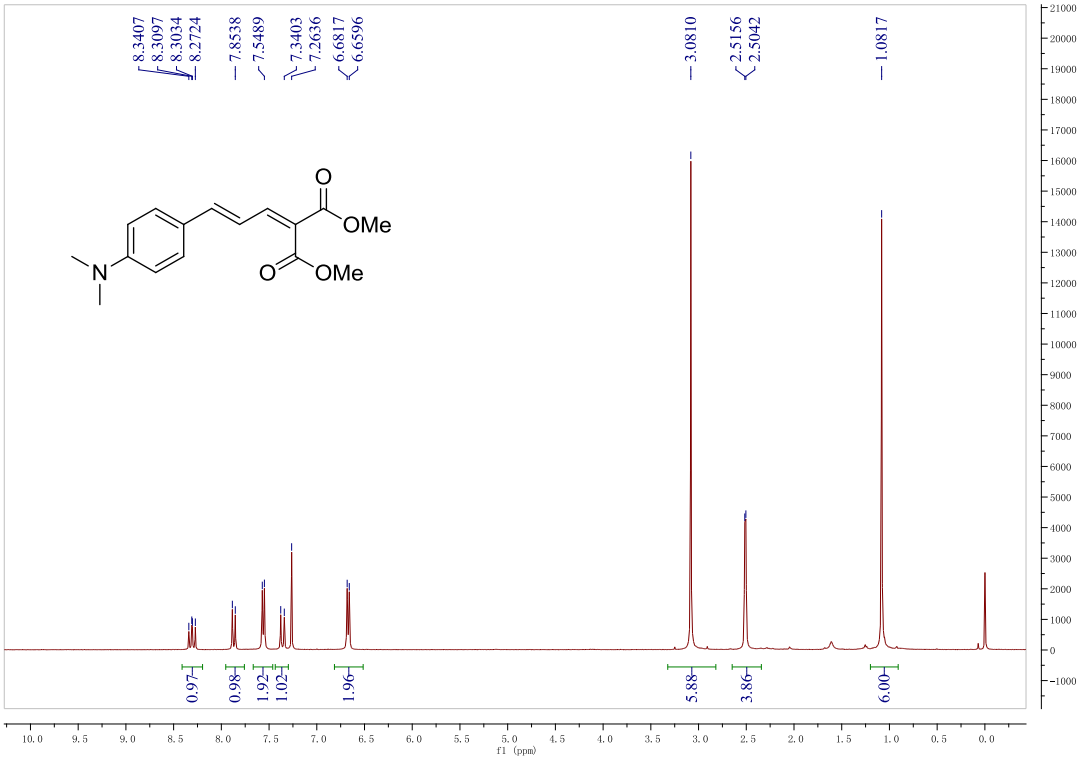
8.3407
8.3097
8.3034
8.2724
7.8538
7.5489
7.3403
7.2636
6.6817
6.6596
3.0810
2.5156
2.5042
1.0817
O
OMe
O
OMe
N
0.97
0.98
1.92
1.02
1.96
5.88
3.86
6.00
f1 (ppm)

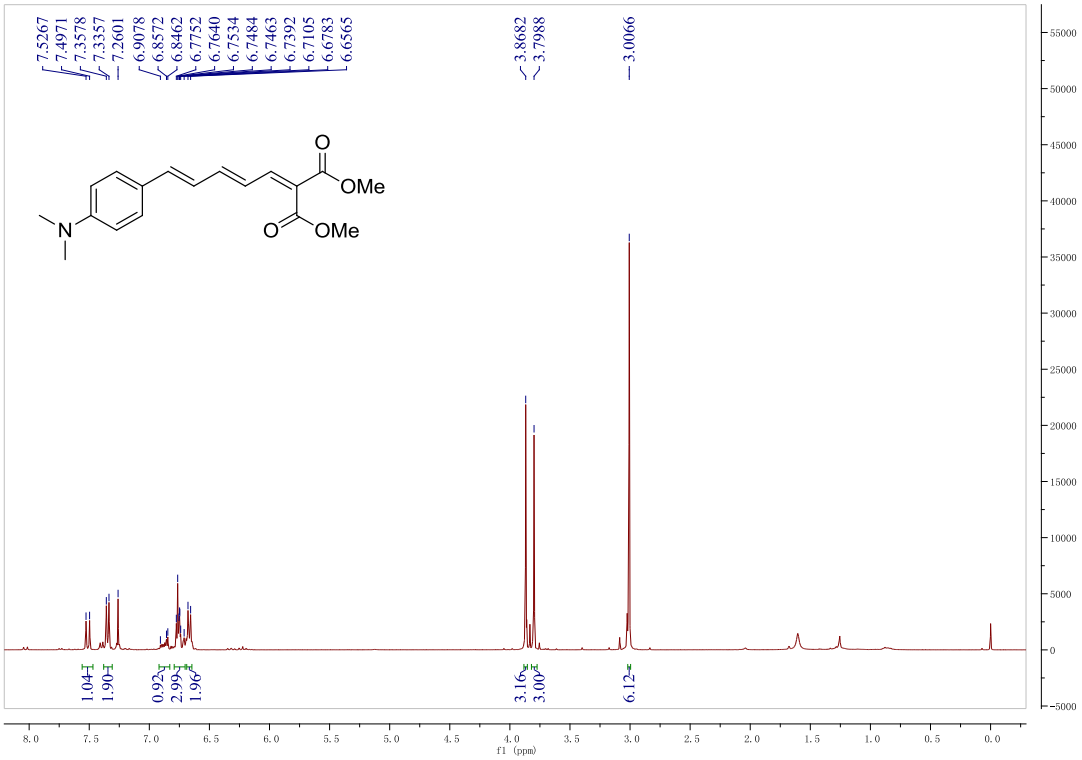
7.5267
7.4971
7.3578
7.3357
7.2601
6.9078
6.8572
6.8462
6.7752
6.7640
6.7534
6.7484
6.7463
6.7392
6.7105
6.6783
6.6565
3.8682
3.7988
3.0066
O
OMe
O
OMe
N
1.04
1.90
0.92
2.99
1.96
3.16
3.00
6.12
f1 (ppm)

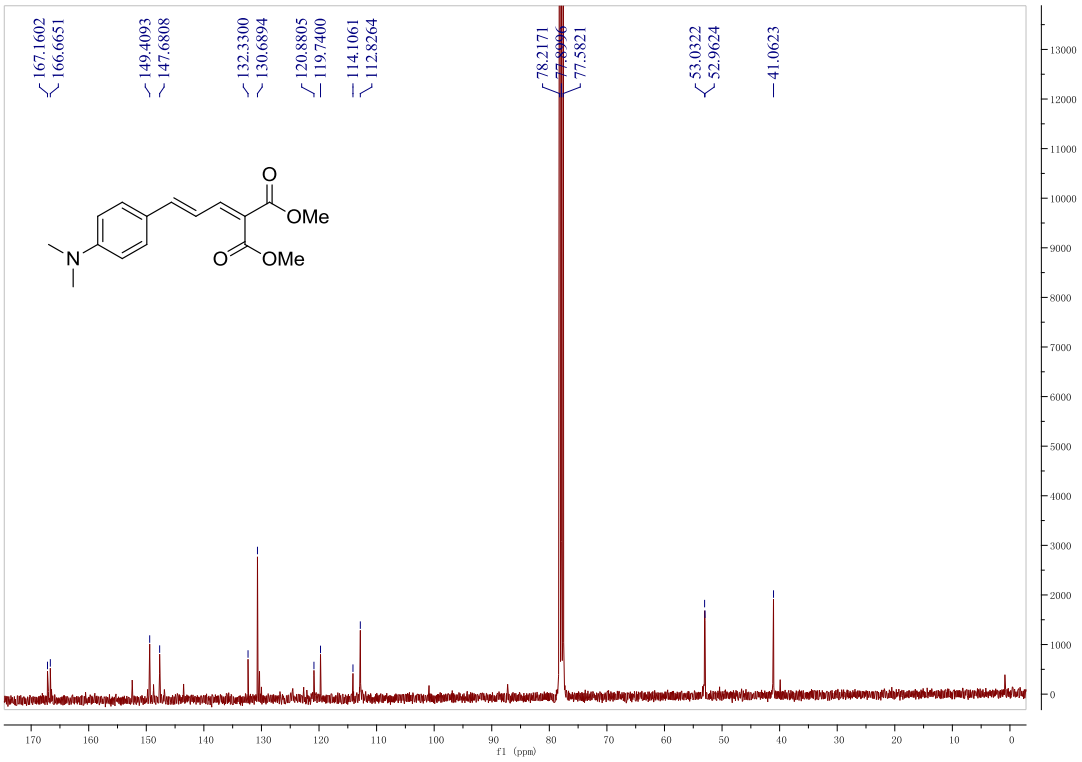
167.1602
166.6651
149.4093
147.6808
132.3300
130.6894
120.8805
119.7400
114.1061
112.8264
78.2171
77.8996
77.5821
53.0322
52.9624
41.0623
OMe
OMe
O
O
N
f1 (ppm)

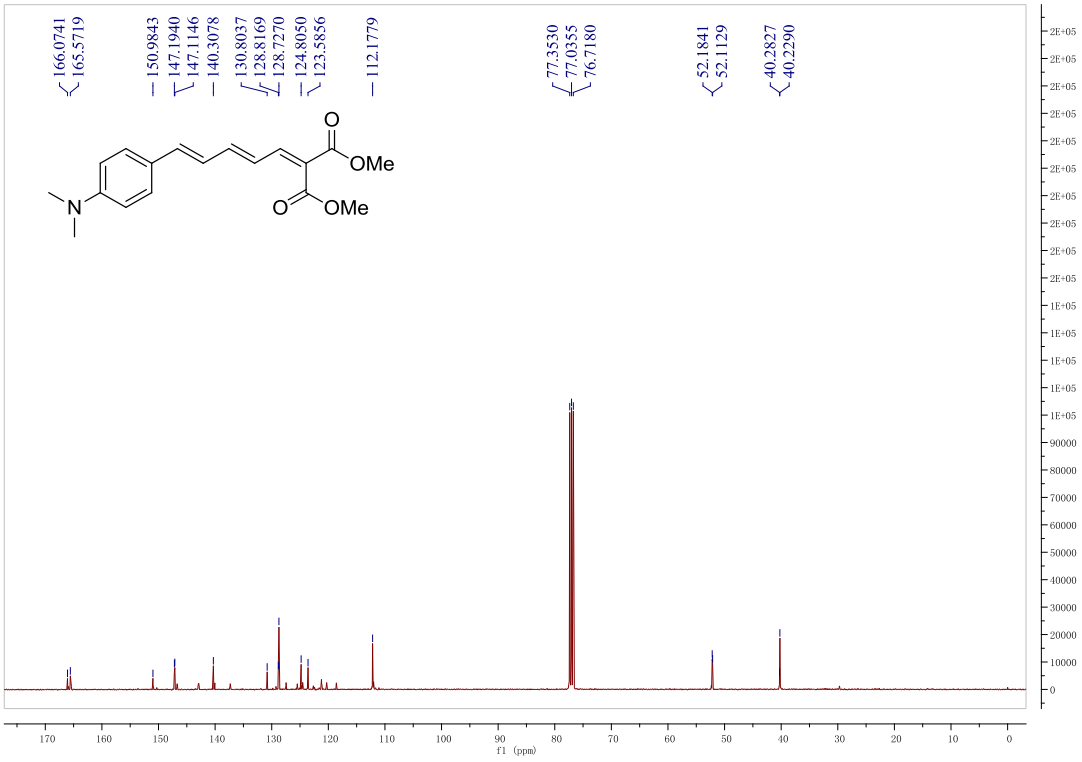
166.0741
165.5719
150.9843
147.1940
147.1146
140.3078
130.8037
128.8169
128.7270
124.8050
123.5856
112.1779
77.3530
77.0355
76.7180
52.1841
52.1129
40.2827
40.2290
OMe
OMe
O
O
N
f1 (ppm)

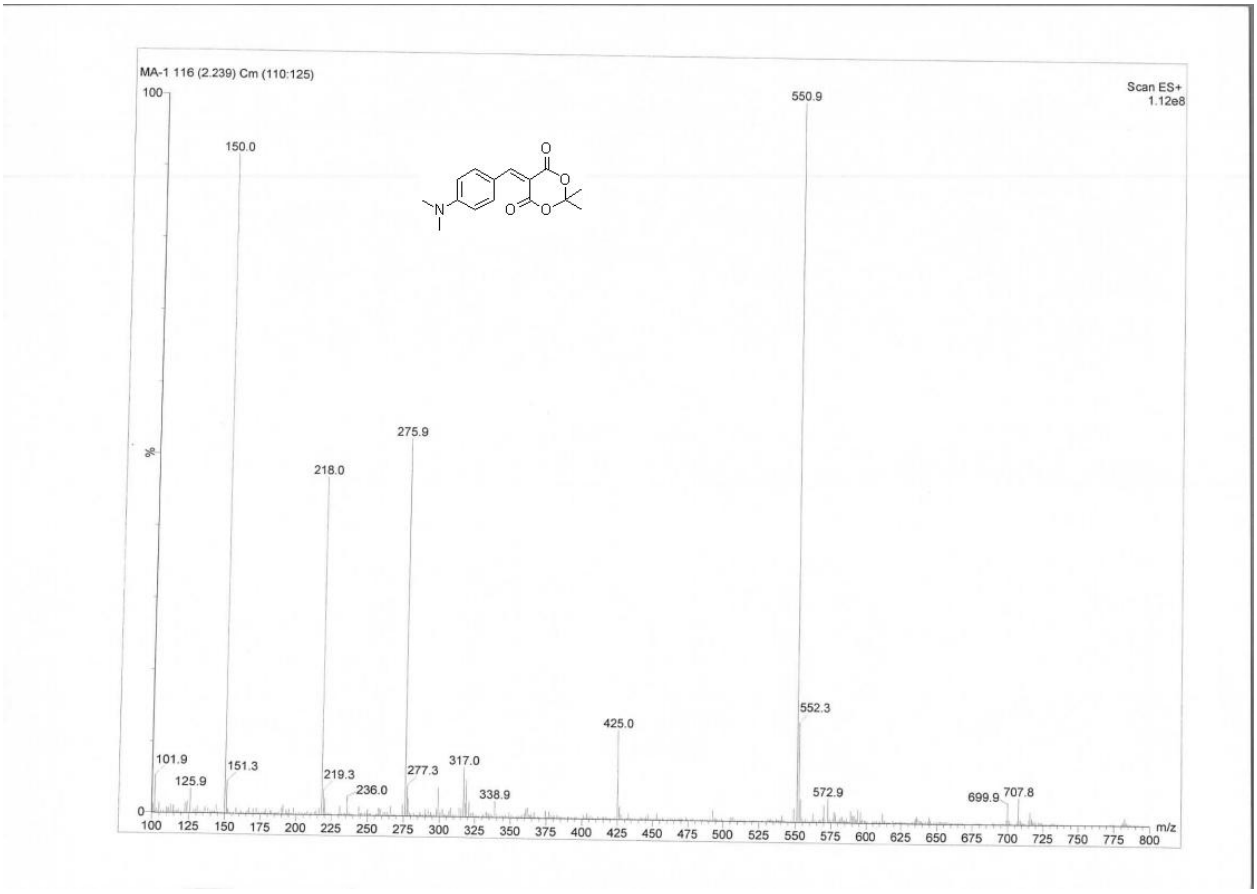
MA-1 116 (2.239) Cm (110:125)
Scan ES+
1.12e8
100
%
0
150.0
550.9
275.9
218.0
552.3
425.0
101.9
125.9
151.3
219.3
236.0
277.3
317.0
338.9
572.9
699.9
707.8
m/z
100 125 150 175 200 225 250 275 300 325 350 375 400 425 450 475 500 525 550 575 600 625 650 675 700 725 750 775 800

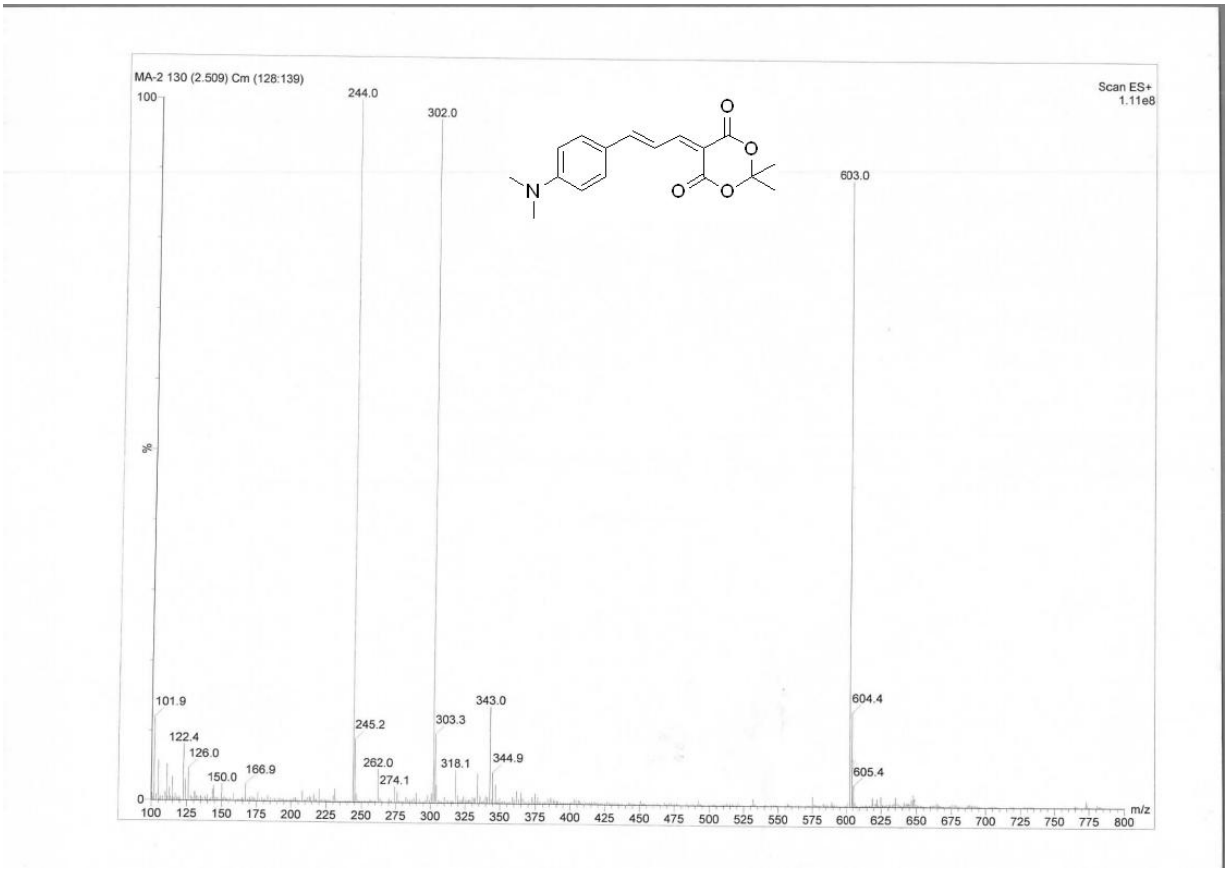
MA-2 130 (2.509) Cm (128:139)
Scan ES+
1.11e8
100
%
0
244.0
302.0
603.0
101.9
122.4
126.0
150.0
166.9
245.2
262.0
274.1
303.3
318.1
343.0
344.9
604.4
605.4
m/z
100 125 150 175 200 225 250 275 300 325 350 375 400 425 450 475 500 525 550 575 600 625 650 675 700 725 750 775 800

Elemental Composition Report

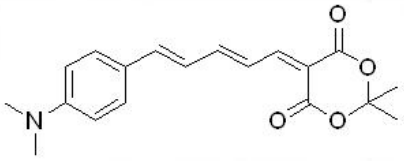

Single Mass Analysis
Tolerance = 5.0 PPM / DBE: min = -1.5, max = 50.0
Element prediction: Off
Number of isotope peaks used for i-FIT = 3

Monoisotopic Mass, Even Electron Ions
96 formula(e) evaluated with 2 results within limits (up to 50 closest results for each mass)
Elements Used:
C: 0-30 H: 0-30 N: 0-5 O: 0-5
FHL-MA-3 91 (1.550)
TOF MS ES+ 2.09e+003

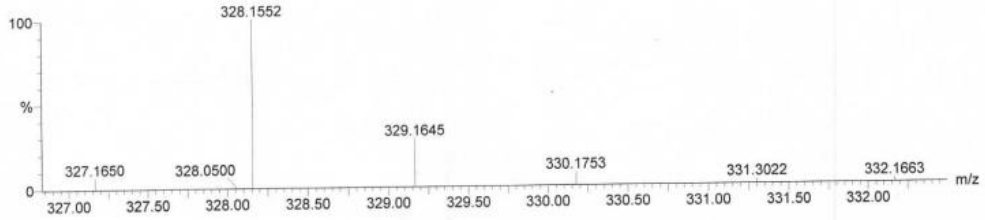

Minimum:				-1.5		
Maximum:		5.0	5.0	50.0		
Mass	Calc. Mass	mDa	PPM	DBE	i-FIT	Formula
328.1552	328.1549	0.3	0.9	9.5	36.5	C19 H22 N O4
	328.1562	-1.0	-3.0	14.5	32.9	C20 H18 N5

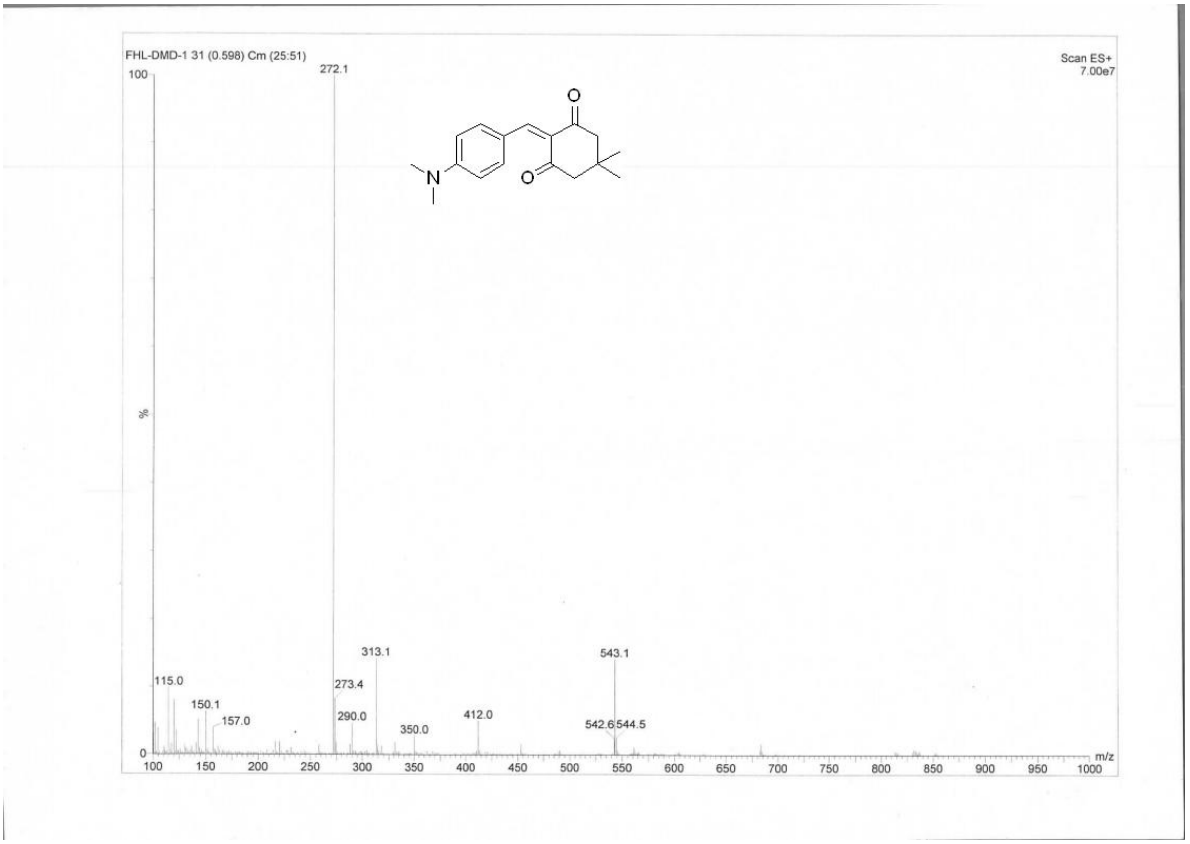

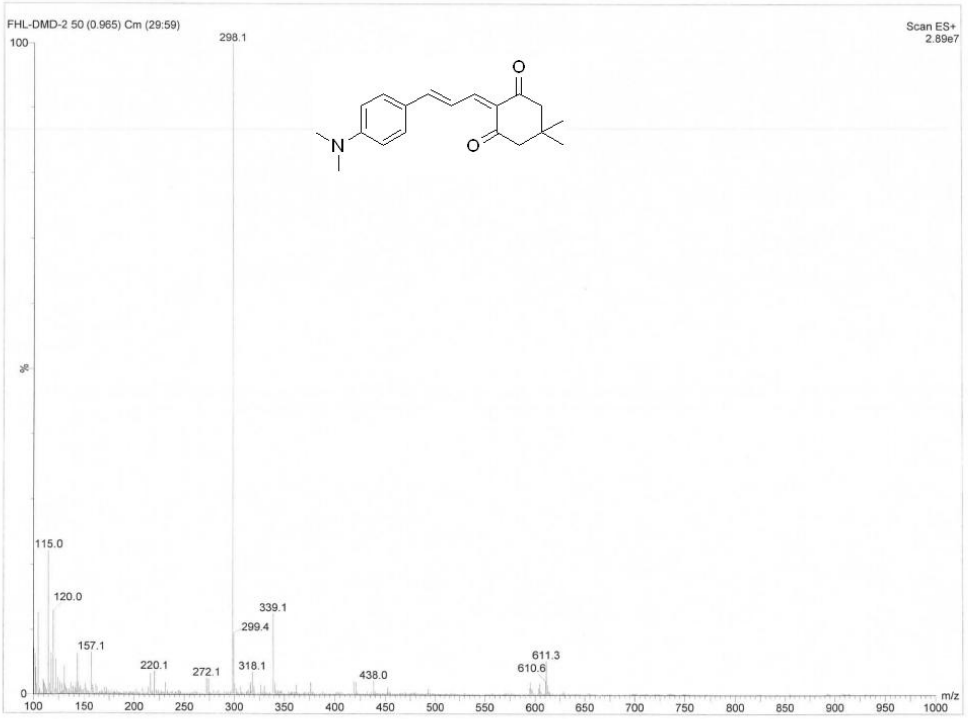

Elemental Composition Report

Single Mass Analysis
Tolerance = 5.0 PPM / DBE: min = -1.5, max = 50.0
Element prediction: Off
Number of isotope peaks used for i-FIT = 3

Monoisotopic Mass, Even Electron Ions
96 formula(e) evaluated with 1 results within limits (up to 50 closest results for each mass)
Elements Used:
C: 0-30 H: 0-30 N: 0-5 O: 0-5
FHL-DMD-3 73 (1.245)
TOF MS ES+
2.34e+003

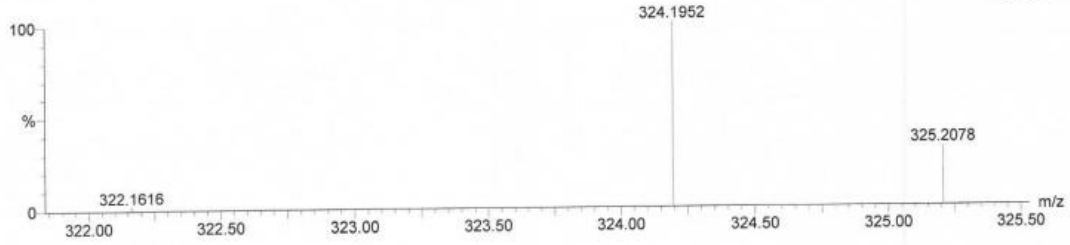

Minimum:				-1.5		
Maximum:		5.0	5.0	50.0		
Mass	Calc. Mass	mDa	PPM	DBE	i-FIT	Formula
324.1952	324.1964	-1.2	-3.7	9.5	n/a	C21 H26 N O2

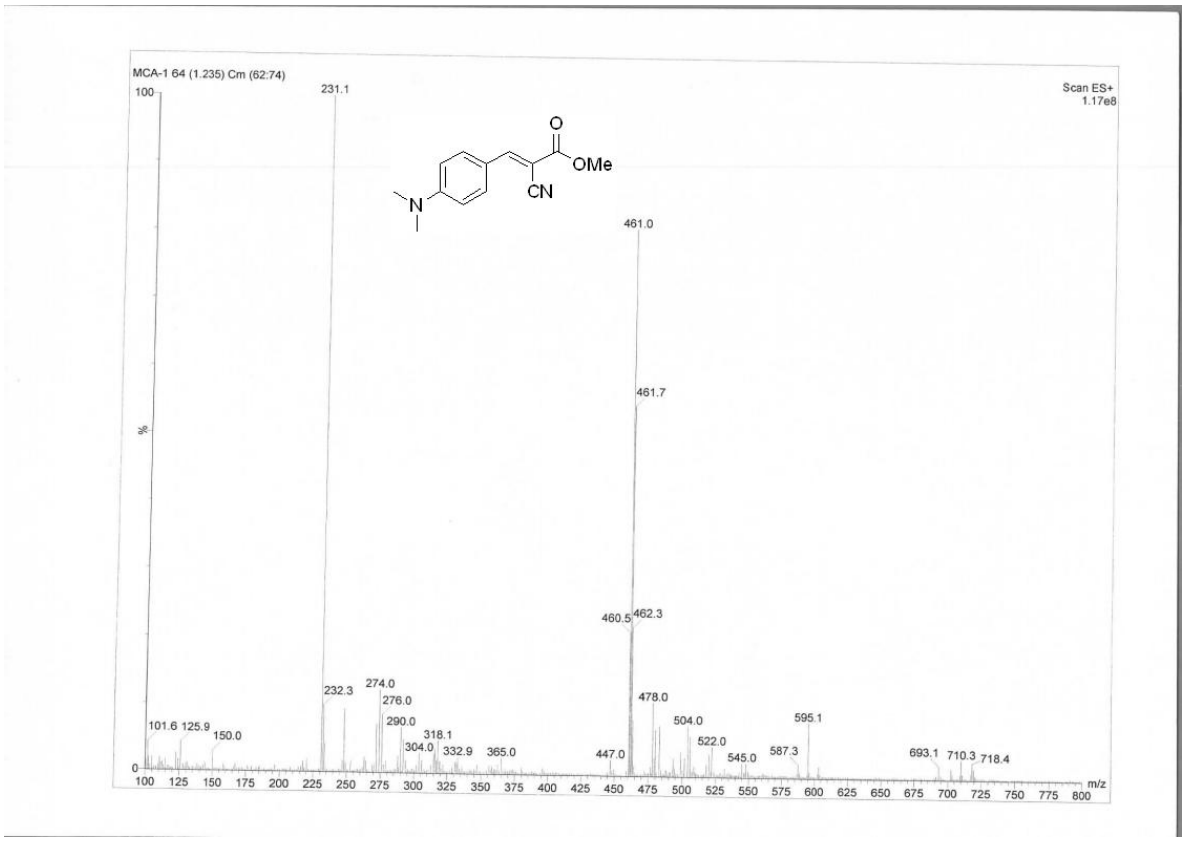
MCA-1 64 (1.235) Cm (62:74)
Scan ES+
1.17e8
100
%
0
231.1
461.0
461.7
460.5
462.3
232.3
274.0
276.0
290.0
318.1
304.0
332.9
365.0
447.0
478.0
504.0
522.0
545.0
587.3
595.1
693.1
710.3
718.4
101.6
125.9
150.0
O
OMe
CN
N
100 125 150 175 200 225 250 275 300 325 350 375 400 425 450 475 500 525 550 575 600 625 650 675 700 725 750 775 800
m/z

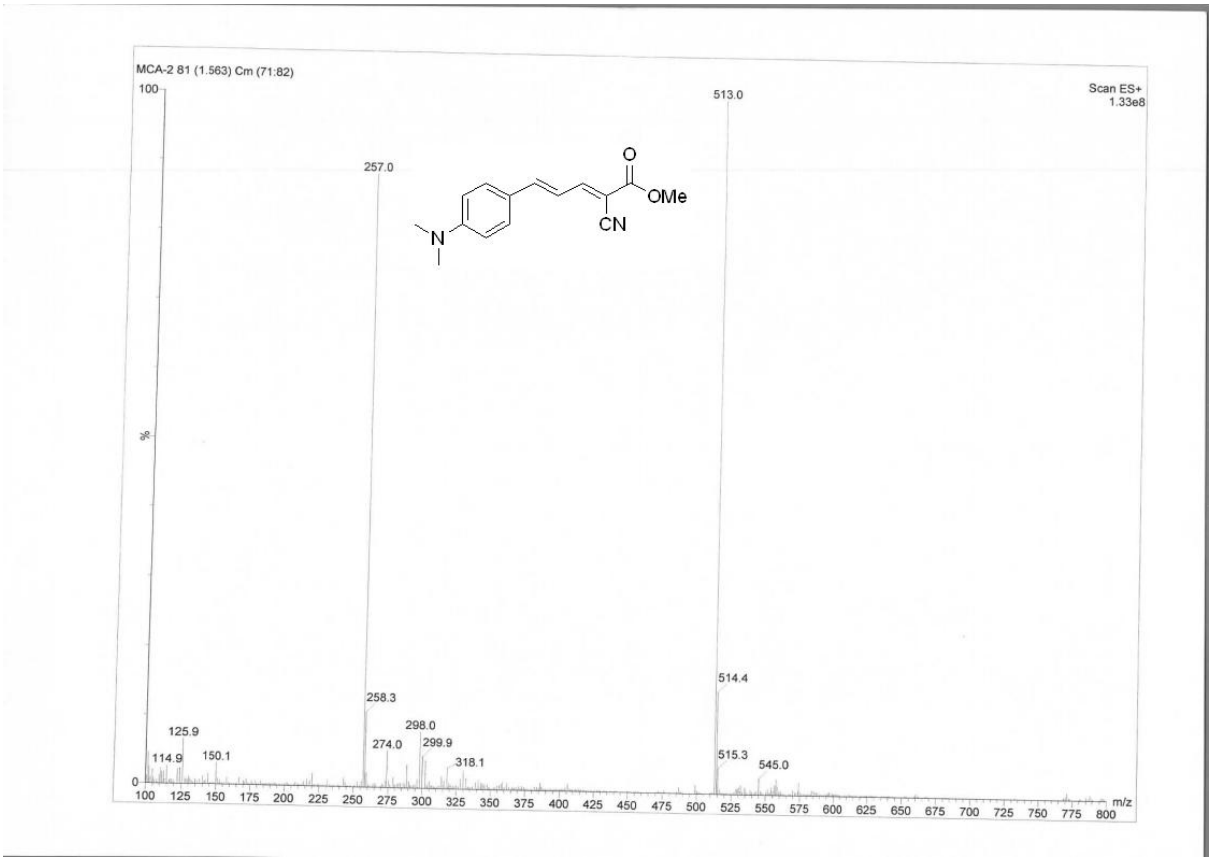
MCA-2 81 (1.563) Cm (71:82)
Scan ES+
1.33e8
100
%
0
513.0
257.0
514.4
258.3
298.0
274.0
299.9
318.1
515.3
545.0
125.9
114.9
150.1
O
OMe
CN
N
100 125 150 175 200 225 250 275 300 325 350 375 400 425 450 475 500 525 550 575 600 625 650 675 700 725 750 775 800
m/z

Elemental Composition Report

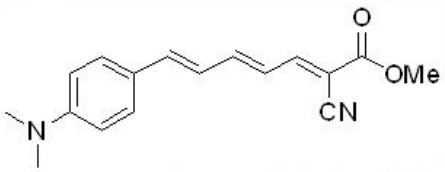

Single Mass Analysis
Tolerance = 5.0 PPM / DBE: min = -1.5, max = 50.0
Element prediction: Off
Number of isotope peaks used for i-FIT = 3

Monoisotopic Mass, Even Electron Ions
96 formula(e) evaluated with 1 results within limits (up to 50 closest results for each mass)
Elements Used:
C: 0-30 H: 0-30 N: 0-5 O: 0-5
FHL-MCA-3 1028 (17.501)
TOF MS ES+ 3.33e+003

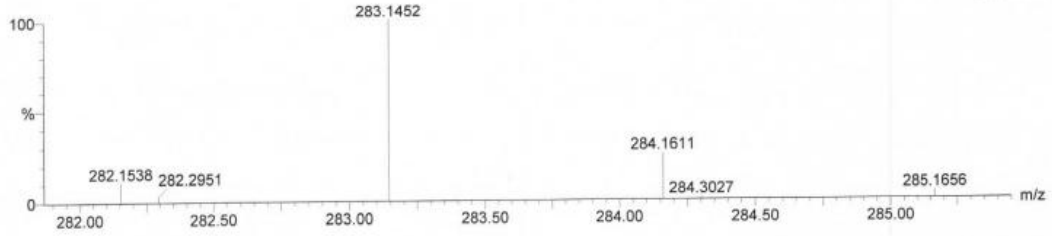

Minimum:		5.0	5.0	-1.5		
Maximum:				50.0		
Mass	Calc. Mass	mDa	PPM	DBE	i-FIT	Formula
283.1452	283.1447	0.5	1.8	9.5	29.4	C17 H19 N2 O2

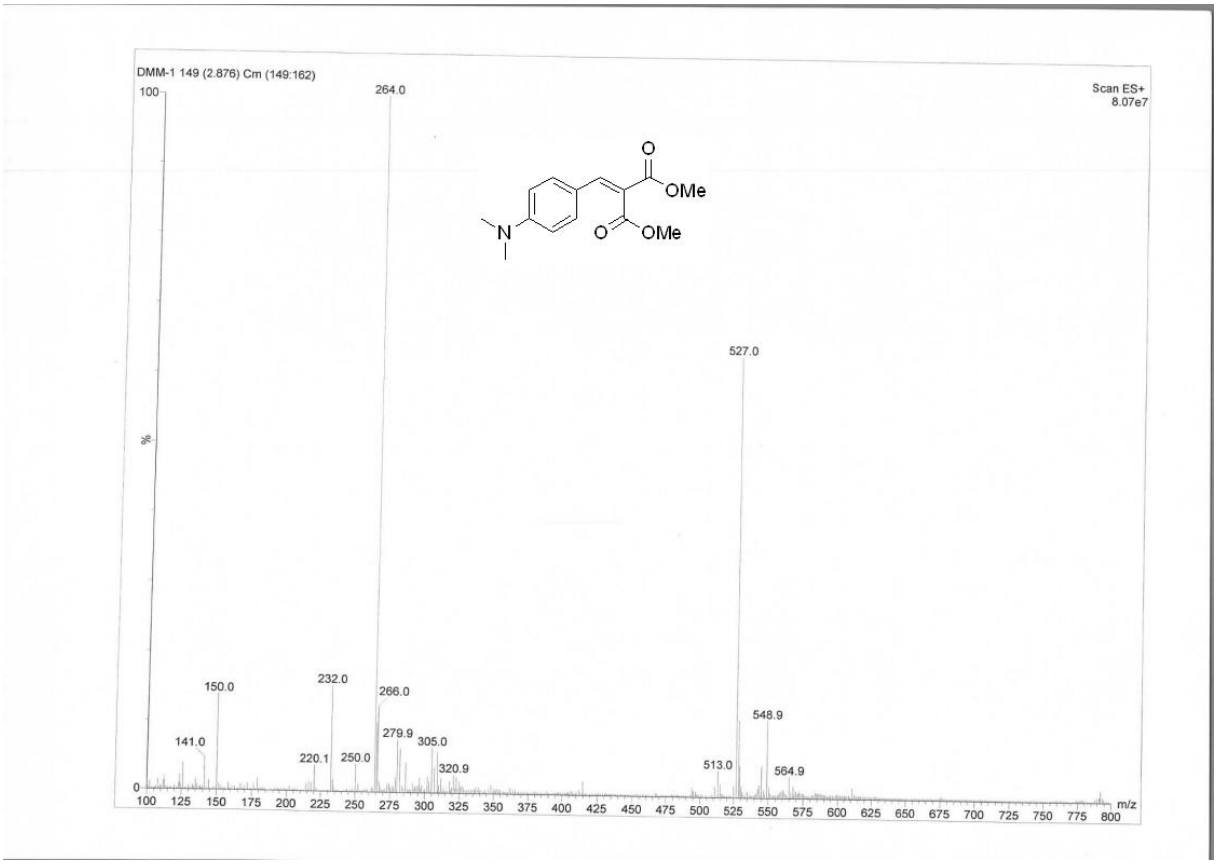

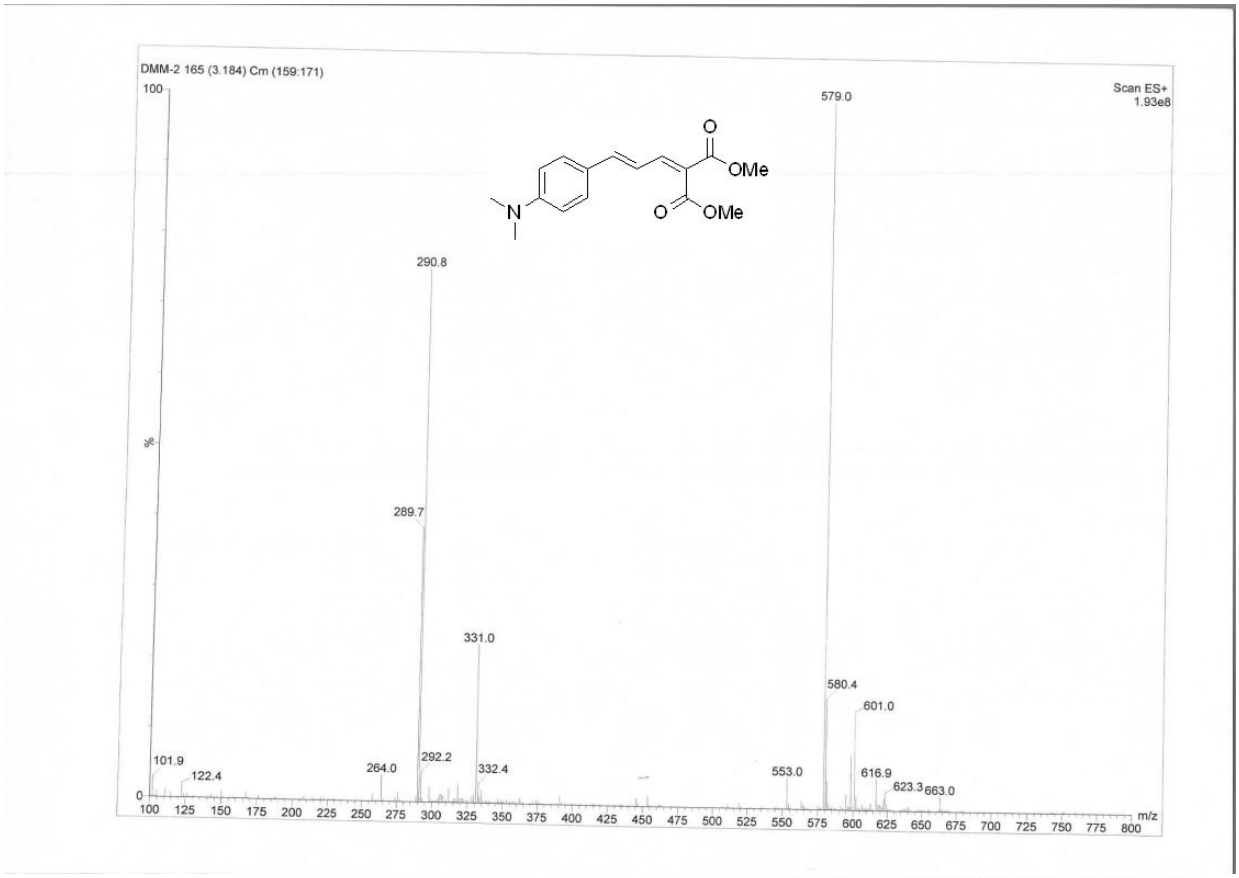

Elemental Composition Report

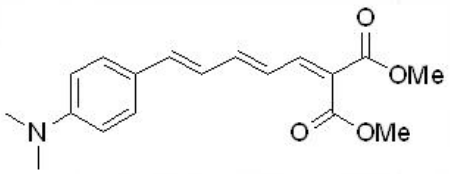

Single Mass Analysis
Tolerance = 5.0 PPM / DBE: min = -1.5, max = 50.0
Element prediction: Off
Number of isotope peaks used for i-FIT = 3

Monoisotopic Mass, Even Electron Ions
96 formula(e) evaluated with 2 results within limits (up to 50 closest results for each mass)
Elements Used:
C: 0-30 H: 0-30 N: 0-5 O: 0-5
FHL-DMM-3 153 (2.612)
TOF MS ES+

4.86e+002

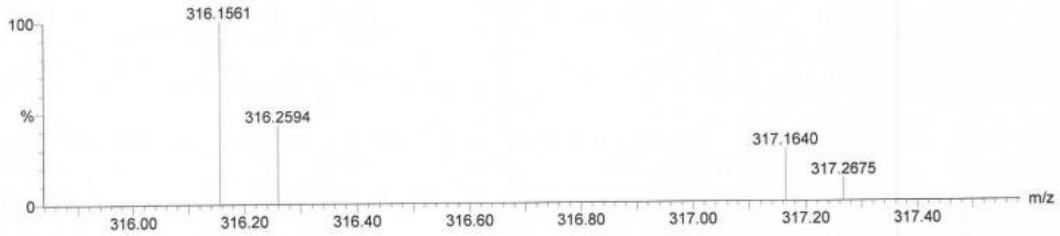

Minimum:				-1.5		
Maximum:		5.0	5.0	50.0		
Mass	Calc. Mass	mDa	PPM	DBE	i-FIT	Formula
316.1561	316.1562	-0.1	-0.3	13.5	n/a	C19 H18 N5
	316.1549	1.2	3.8	8.5	n/a	C18 H22 N O4

References

1 Z. Li, M. Cui, J. Dai, X. Wang, P. Yu, Y. Yang, J. Jia, H. Fu, M. Ono, H. Jia, H. Saji and B. Liu, *J. Med. Chem.*, 2013, **56**, 471.

2 J. Olmsted, *J. Phys. Chem.*, 1979, **83**, 2581.

3 A. Petric, S. A. Johnson, H. V. Pham, Y. Li, S. Ceh, A. Golobic, E. D. Agdeppa, G. Timbol, J. Liu, G. Keum, N. Satyamurthy, V. Kepe, K. N. Houk and J. R. Barrio, *Proc. Natl. Acad. Sci. U. S. A.*, 2012, **109**, 16492.

4 M. Hintersteiner, A. Enz, P. Frey, A.-L. Jaton, W. Kinzy, R. Kneuer, U. Neumann, M. Rudin, M. Staufenbiel, M. Stoeckli, K.-H. Wiederhold and H.-U. Gremlich, *Nat. Biotech.*, 2005, **23**, 577.

5 E. E. Nesterov, J. Skoch, B. T. Hyman, W. E. Klunk, B. J. Bacskai and T. M. Swager, *Angew. Chem.*, 2005, **44**, 5452.

6 Z.-P. Zhuang, M.-P. Kung, A. Wilson, C.-W. Lee, K. Plössl, C. Hou, D. M. Holtzman and H. F. Kung, *J. Med. Chem.*, 2002, **46**, 237.

7 Y. Cheng and W. H. Prusoff, *Biochem. Pharmacol.*, 1973, **22**, 3099.

8 M. Ono, H. Watanabe, H. Kimura and H. Saji, *ACS Chem. Neurosci.*, 2012, **3**, 319.

9 (a) A. D. Becke, *J. Chem. Phys.*, 1993, **98**, 5648; (b) K. D. Dobbs and W. J. Hehre, *J. Comput. Chem.*, 1987, **8**, 880; (c) P. J. Stephens, F. J. Devlin, C. F. Chabalowski and M. J. Frisch, *J. Phys. Chem.*, 1994, **98**, 11623.

10 M. J. Frisch, G. W. Trucks, H. B. Schlegel, G. E. Scuseria, M. A. Robb, J. R. Cheeseman, G. Scalmani, V. Barone, B. Mennucci, G. A. Petersson, H. Nakatsuji, M. Caricato, X. Li, H. P. Hratchian, A. F. Izmaylov, J. Bloino, G. Zheng, J. L. Sonnenberg, M. Hada, M. Ehara, K. Toyota, R. Fukuda, J. Hasegawa, M. Ishida, T. Nakajima, Y. Honda, O. Kitao, H. Nakai, T. Vreven, J. A. Montgomery, Jr., J. E. Peralta, F. Ogliaro, M. Bearpark, J. J. Heyd, E. Brothers, K. N. Kudin, V. N. Staroverov, R. Kobayashi, J. Normand, K. Raghavachari, A. Rendell, J. C. Burant, S. S. Iyengar, J. Tomasi, M. Cossi, N. Rega, J. M. Millam, M. Klene, J. E. Knox, J. B. Cross, V. Bakken, C. Adamo, J. Jaramillo, R. Gomperts, R. E. Stratmann, O. Yazyev, A. J. Austin, R. Cammi, C. Pomelli, J. W. Ochterski, R. L. Martin, K. Morokuma, V. G. Zakrzewski, G. A. Voth, P. Salvador, J. J. Dannenberg, S. Dapprich, A. D. Daniels, Ö. Farkas, J. B. Foresman, J. V. Ortiz, J. Cioslowski, and D. J. Fox, Gaussian 09, Revision D.01, Gaussian, Inc., Wallingford CT, 2009.

11 G. M. Morris, D. S. Goodsell, R. S. Halliday, R. Huey, W. E. Hart, R. K. Belew and A. J. Olson, *J. Comput. Chem.*, 1998, **19**, 1639.

12 (a) S. Cosconati, S. Forli, A. L. Perryman, R. Harris, D. S. Goodsell and A. J. Olson, *Expert Opin. Drug Discovery*, 2010, **5**, 597; (b) S. Forli and A. J. Olson, *J. Med. Chem.*, 2012, **55**, 623; (c) G. M. Morris, R. Huey, W. Lindstrom, M. F. Sanner, R. K. Belew, D. S. Goodsell and A. J. Olson, *J. Comput. Chem.*, 2009, **30**, 2785.

13 M. F. Sanner, *J. Mol. Graphics Modell.*, 1999, **17**, 57.

14 (a) N. P. Cook, M. Ozbil, C. Katsampes, R. Prabhakar and A. A. Marti, *J. Am. Chem. Soc.*, 2013, **135**, 10810; (b) A. T. Petkova, Y. Ishii, J. J. Balbach, O. N. Antzutkin, R. D. Leapman, F. Delaglio and R. Tycko, *Proc. Natl. Acad. Sci. U. S. A.*, 2002, **99**, 16742.

15 W. Humphrey, A. Dalke and K. Schulten, *J. Mol. Graph.*, 1996, **14**, 33.

16 *Physical Chemistry for the Life Sciences*. Atkins, Peter and Julio de Paula. Oxford, UK: Oxford University Press. 2006. 95.